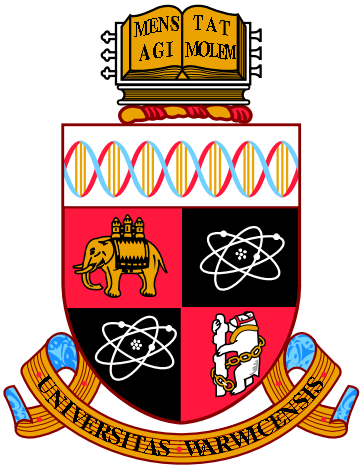

Structure and Dynamics of Protein in the Permeation and Gating of Potassium Ion Channels: Identifying Molecular Determinants and Developing Coarse-Grained Approaches

by

Salvatore Mario Cosseddu

Thesis

Submitted to the University of Warwick

for the degree of

Doctor of Philosophy

School of Engineering

November 2013

THE UNIVERSITY OF WARWICK

Contents

List of Figures

Acknowledgments

I would like to thank:

- My supervisors Dr. Igor Khovanov, Prof. Mike Allen and Prof Mark Rodger, for their important guidance and support.
- Diletta Cordeschi, which has made this possible.
- My family, for their strong support.
- All my collegues, Aaron Finney, Julia Choe, Jasmine Desmond, Domenico Caruso, Chimie Gamot.

This thesis was typeset with LaTeX 2$_\varepsilon$[1] by the author.

[1] LaTeX 2$_\varepsilon$ is an extension of LaTeX. LaTeX is a collection of macros for TeX. TeX is a trademark of the American Mathematical Society. The style package *warwickthesis* was used.

Declarations

This thesis has been composed by myself, and all work herein is my own work, excepted where otherwise stated.

Material reported in chapter 3 has been published in Cosseddu et al.[40].

Fig. 1.3 is ©Zhou et al., 2001. Originally published in *Nature* (doi:10.1038/35102009, licensed content of Nature Publishing Group, license number 3356501082913).

Fig. 1.2 is ©Chakrapani et al., 2007. Originally published in *Journal of General Physiology* (doi:10.1085/jgp.200709844, licensed content of The Rockefeller University Press, no permission is required for noncommercial purposes).

Abstract

Ion channels are transmembrane proteins which allow small ions to flow across the membrane downhill along the electrochemical gradient, with high efficiency and selectivity over the different ion species, and which play crucial roles in a wide range of vital physiological functions. Research on the channels selective for potassium ions have attracted a great deal of attention over the past decade. This is because of the availability of three dimensional microscopical structures and because they provide a paradigm for the study of the complex superposition of the permeation of the ions and structural rearrangements which is responsible for the regulation of the current in ion channels.

In the present work a thorough study of the strong coupling between permeation and the dynamics of the protein in the potassium ion channel KcsA is presented, based on Molecular Dynamics and Metadynamics calculations, which reveals the clear links between the function and the structure of the protein. The molecular determinants for the conformational changes of the pore region have been identified and described in details. The relationship between these rearrangements and the gating process known as "C-type inactivation", found in a variety of potassium ion channels, have been investigated and a mechanism has been proposed for the process. The knowledge acquired from these investigations is finally applied to unveil the driving forces and energetics associated with the permeation and selectivity properties of KcsA channel.

Chapter 1

Introduction

Cells are surrounded by membranes consisting of a phospholipid bilayer impermeable to charged compounds. Permeability is conferred by different classes of proteins and, among them, *channels* enable ions to flow rapidly in the downhill direction.[16,64] The latter catalyse ion permeation with extremely high efficiency, resulting in overall high conductivities, with additional features of selective permeability and gating according to some specific stimuli, such as a membrane potential change, a neurotransmitter, or a mechanical deformation.[64] Ion channels have primary responsibility for vital physiological functions such as the regulation of osmotic pressure and cell volume, and for electrical activity and signal transduction as they are involved in a variety of processes such as nerve impulses, muscle relaxation, cognition, sensory transduction, regulation of blood pressure, and cell proliferation.[10] Because of their fundamental roles, ion channels are among the most important drug targets and have been linked to diverse diseases including cardiac disorders, neurological indications, kidney failure, the perception of pain, and blindness.[10,75,124] Moreover, artificial analogues have also been found to have applications in engineering in the construction of biosensors, in interfacing biological surfaces with semi-conductors, and in organic-inorganic hybrid membranes synthesis for fuel cells. There is a great diversity among ion channels.[64] Typically they consist of different protein domains which span across the membrane, creating a water filled pore. Most of the ion channels possess a specific region that functions as a filter in the selection of the different ion species.[10,64] Diffuse families of ion channels are selective for K^+, Na^+, Ca^{2+} and Cl^-.[64] Selectivity is so efficient that Na^+ current is practically undetectable in K^+ ion channels except under very specific conditions.[110]

Although strong structural and functional similarities can be recognised,[64,70,132] wide differences are found even within the same family of ion

channels, which can differ in kinetics, mechanisms and modulation of gating. For instance, a mix of many K^+ channel sub-types characterised by different gating kinetics cooperates in each excitable membrane.[64]

Investigation of microscopic features and properties of ion channels is a complicated task. For a long time their three dimensional microscopic structures had been unknown because of the difficulties in isolation and crystallisation outside of their natural environment and because of the complexity of the experimental techniques required to solve protein structures.[64] Thus all the knowledge was derived from electrophysiology experiments. The first three dimensional molecular structure was determined only in 1998 by MacKinnon and co-workers,[46] for the K^+ ion channel KcsA from the *Streptomyces lividans* bacteria, in a work that was awarded the Nobel prize for Chemistry in 2003. Since then, structures of other K^+ ion channels have been determined (see for instance[73,74,81,84,94,95]) and, more recently, a Na^+ ion channel.[118]

Because of their fundamental roles in a wide range of physiological processes and the availability of three dimensional microscopical structures, K^+ ion channels continue to attract a great deal of attention from researchers and provide a paradigm for the study of ion channels.[64,132] Theoretical methods have been widely employed in exploring the most intimate mechanisms that govern these complex systems, particularly MD simulations and free-energy calculations (the subject has been reviewed several times, i.g. see[101,129,132]). The limitations imposed by experimental techniques, in which the complex dynamics occurring on molecular spatial and time scales are averaged, providing static images of a channel, can be overcome using these methods.[132] Thus the simulation area, with application to ion channels, is a rapidly growing field able to provide theoretical models and tools to better understand and interpret experimental data.[129]

1.1 KcsA

Potassium ion channels are found in several families such as voltage-dependent K^+ channels, in which the current is regulated by the transmembrane voltage, and inward rectifier K^+ channels, characterised by a higher conductance for inward current rather than outward current. However, they all share similarities in overall organisation and sequence.[64,70,132] The bacterial channel KcsA, found in *Streptomyces lividans* has been widely used as a model in the understanding of structural and functional features of these proteins, and it still continues to attract a great deal of attention. This is in part due to its sequence similarity to eukaryotic K^+ chan-

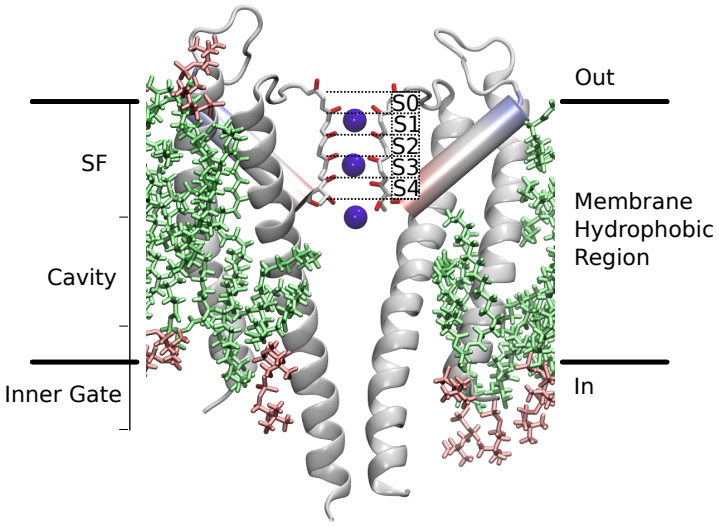

Figure 1.1: KcsA potassium ion channel. Different regions of the pore are denoted: Selectivity filter (SF), cavity, inner gate. Five binding sites for potassium, S0...S4, can be recognised in the SF. The P-helix is coloured according to an electrostatic calculation performed using the Particle Mesh Ewald (PME) method implemented in the program VMD[67], in order to show its dipolar nature (red and blue colours correspond to negative and positive charge, respectively).

nels, and in part because of its role as an archetype for ion permeation, selectivity and for the complex interplay of gating and activation that is commonly found in the K^+ channel superfamily.[64,128] It is a tetrameric protein in which each subunit is formed by two transmembrane helices (TM1 and TM2) connected by a P-loop. The P-loop is made up of a short polarised helix (*P-helix*) and an amino acid *signature sequence*, TXXTXGYGD, that represent a motif conserved across most of K^+ channels.[31,37,46,64,85]

In common with most of K^+ ions channels, the whole quaternary structure of KcsA is divided into three functional regions: the selectivity filter (SF), the cavity, and the inner gate (Fig. 1.1). The SF is the narrowest part of the pore, formed by the backbone carbonyl oxygens of the TXGYG sequences, part of the signature sequence, of the four subunits, i.e. residues from 75 to 79 with a valine in position 76 which results in the sequence TVGYG. The cavity is a wider water-filled region (~ 5 Å radius) that creates a hydrophilic environment for the ions in the hydrophobic region of the membrane. The inner gate is accompanied by large movements in the helical transmembrane segment TM2 which creates a restriction or relieves the ion flow.[62,119,138,140,147]

The SF is widely considered as being fundamental for permeation and selectivity, since backbone oxygen atoms of VGYG sequences and T74 side chains,

arranged in rings, create well-defined binding sites for the K^+ ions, which force the permeation to occur in a single file fashion. Although the initial X-ray experiments (resolution 3.2 Å) suggested the presence of four binding sites (named S1 to S4), more refined structures (resolution 2.0 Å) revealed the presence of five sites in the SF (S0 to S4) and an additional one, relatively weak, on the extracellular side (S_{ext}), confirmed by theoretical calculations.[18,157]

1.1.1 Gating

Current in K^+ ion channels is regulated by different types of "gates" which are crucial for physiological functions.[66] Experimental studies demonstrated that current is initiated by the opening of the inner gate, referred to as *activation gating*, and is further regulated by smaller structural rearrangements in the SF region.[29,37,119,157] In KcsA, activation opening is regulated by intracellular pH, with maximal open probability at acidic pH.[62,119,138,140] The proton sensors can be identified in two glutamate residues at the C-terminus of TM2 (E118 and E120) and a histidine at the N-terminus of TM1 (H25).

Once the inner gate is opened, conformational changes in the SF are responsible for slow inactivation (*C-type inactivation*) and modal-gating. The single-channel behaviour of KcsA is characterised by very low "open" probability (p_o). Although inactivation can be coupled to the activation process,[42] continuous recordings of single-channel currents demonstrated a certain degree of independence. Measurements under steady-state conditions at maximal activation (pH 3.0) showed very long silent periods ($\tau > 25$s) interrupted by very fast bursts of opening.[29,35] Bursts are characterised by three gating modes: high-p_o, low-p_o and a high-frequency flicker mode, all differing in their mean open times (Fig. 1.2). C-type inactivation, frequently found in K^+ ion channels, is responsible for the long silent periods and reveals a dependence on the voltage in KcsA, particularly on the inversion of the direction of the current. It is furthermore affected by the extracellular concentration of K^+.[34–37,66]

The overall regulation of the current is thus believe to arise from a complex dynamics among the different states reported in the scheme 1.3, which involve transition of the inner gate and subsequent rearrangements of the filter region. Detailed understanding of these fine regulations occurring at the level of the SF remains elusive. In KcsA the conductive state of the SF is intrinsically unstable.[28,29,35] A structure solved in the presence of a low concentration of K^+ revealed a constriction in the central region of the SF, often referred to as "collapsed" state, which was proposed as a putative inactive state.[157] Crystallographic studies on a constitutively

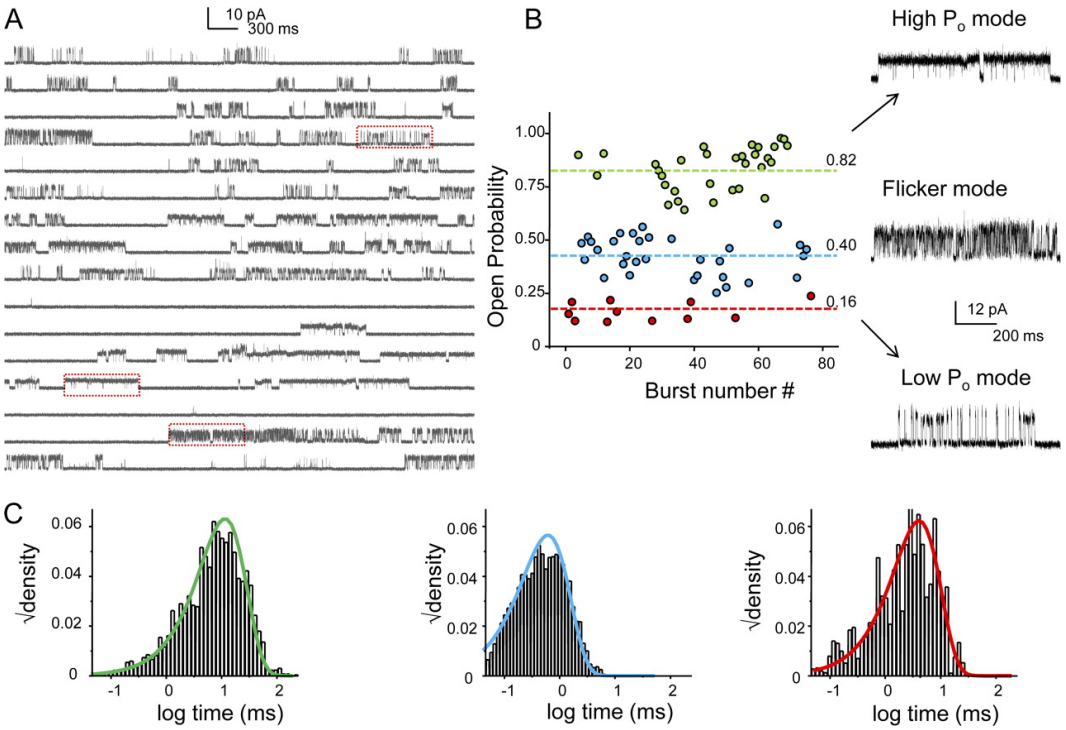

Figure 1.2: Modal behaviour of KcsA. (A) A continuous single-channel recording of KcsA under steady-state conditions at pH 3.0 (maximal activation) with membrane potential at +100 mV. (B) the highly variable kinetic behaviour of KcsA arises from a combination of three distinct modes of channels activity: the low-p_o, high-p_o, and the flicker mode (p_o is reported as P_o in the figure). These modes occur with random frequency. (C) The open-state lifetimes within the modes are described by single exponentials. ©Chakrapani et al., 2007. Originally published in *Journal of General Physiology* (doi:10.1085/jgp.200709844)

open mutant channel (tKcsA-OM) showed systematic variations in the structure of the SF associated with the diameter of the intracellular gate, which suggested they provided a mechanism for the C-type inactivation. Within this mechanism, the existence of an intermediate state was suggested in which the K^+ pathway is slightly narrowed by the movements of the glycine residues in position 77 (G77) before the complete collapse of the pore is finally reached. However, this mechanism remains conjectural since a dynamical pathway is still lacking, as well as a detailed description of the molecular determinants and evidence of a dynamical equilibrium between active and inactive states once the intracellular gate is opened.[35,68] At the same time, experimental evidence supports the idea that different non-conductive states exist and different hypothesis for C-type inactivation, such as pore dilation, have been proposed as the reason for this.[66]

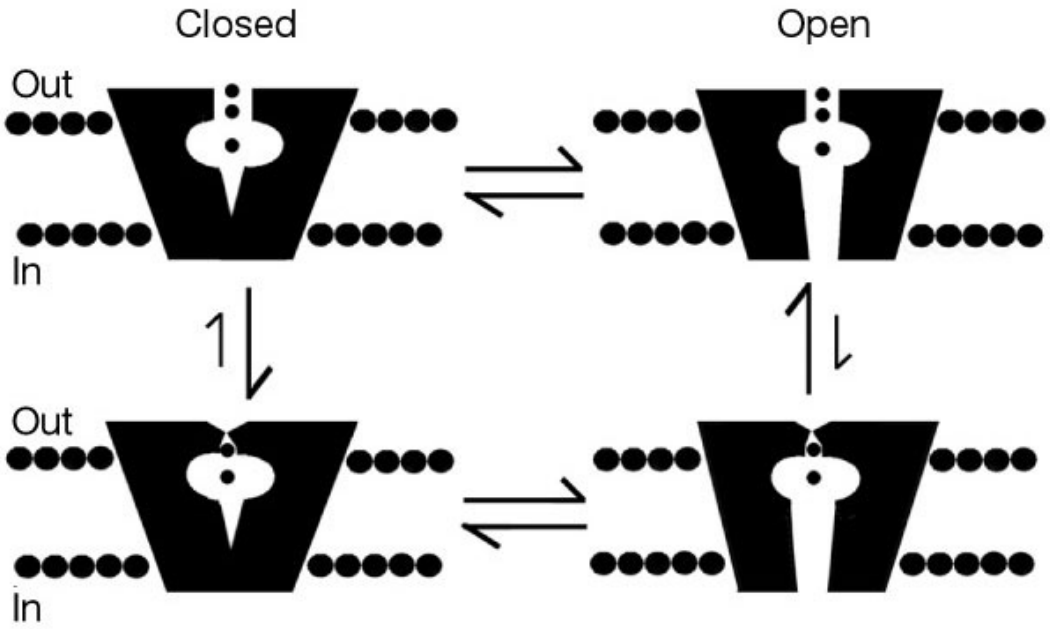

Figure 1.3: Scheme of the structural transitions from which the current regulation is believed to arise in many K^+ ion channels. Transitions between conductive and collapsed structures of the filter (upper and lower) should correspond to C-type inactivation and recovery from inactivation in single channel records. ©Zhou et al., 2001. Originally published in *Nature* (doi:10.1038/35102009, licensed content of Nature Publishing Group, license number 3356501082913)

Different experiments suggested the important role played by the region that surrounds the SF in determining inactivation probability. A key role in selectivity filter conformational changes was identified for the E71–D80 hydrogen bond by

means of current measurements, crystal structure determination, and radioactive flux studies, with the E71A mutant (in which this hydrogen bond cannot exit, Fig. 1.4) being resistant to the collapse of the selectivity filter, even at low K^+ concentrations.[29,30,32,35,38] Furthermore, dependence of inactivation on voltage was suppressed by the neutralisation of E71.[34] Either the breaking or the strengthening of E71–D80 bridge was suggested as being related to C-type inactivation.[30,32,34–37] The mutation of E71 with histidine (E71H) generated a non-conductive channel. Molecular dynamics simulations showed the creation in this protein of an hydrogen bond between D80 and H71, which caused a lowering of the backbone distance $C_\alpha - C_\alpha$ between positions 71 and 80 as well as the disruption of the conductive state. Using this finding as the starting point, Cordero-Morales et al.[36] compared inactivation probabilities of different mutants in position 71, and the backbone distance $C_\alpha - C_\alpha$ between positions 71 and 80 was found to be directly linked to the inactivation process. The authors then proposed the strengthening of E71–D80 bridge as a possible cause of the inactivation. The residue E71 and D80 are two acidic residues, and their carboxyl groups are distant ~ 2.6 Å in the putative conductive structure of KcsA.[157] The existence of a carboxyl-carboxylate linkage has been widely studied.[19,22,24] It is believed that the two residues share a proton, with a preference for E71.[24] A mechanism for the lowering of the distance between D80 C_α and E71 C_α in the wild type (WT) is still unknown.

Several mutants proved the influence on inactivation process of other residues located in the region behind the SF. Among these, residues R64, Y82 and W67 demonstrated the most dramatic effects:[35,37,105] macroscopic currents from rapid pH jumps showed a sharp reduction of inactivation for R64A and an enhancement of the rate and extent of inactivation for Y82A (Fig. 1.4), while inactivation was suppressed for W67Y. Furthermore, a cooperation between the two neighbouring arginines R64 and R89 was proved to be influencing the inactivation process.[105] These results suggest inactivation in K^+ channels a result of cooperation among different residues. In this direction Cordero-Morales et al.[37] proposed that C-type inactivation in KcsA is governed by a multipoint hydrogen-bond network formed by the triad E71-D80-W67. However, fundamental questions remain regarding the molecular determinants on the mechanism, which originate the C-type inactivation, and on the structural definition of the inactive state of the channel.

1.1.2 Permeation

The most determinant region of the protein for permeation and selectivity is the SF,[7,64] that is often referred as the real pore. The carbonyls' dipoles pointed toward

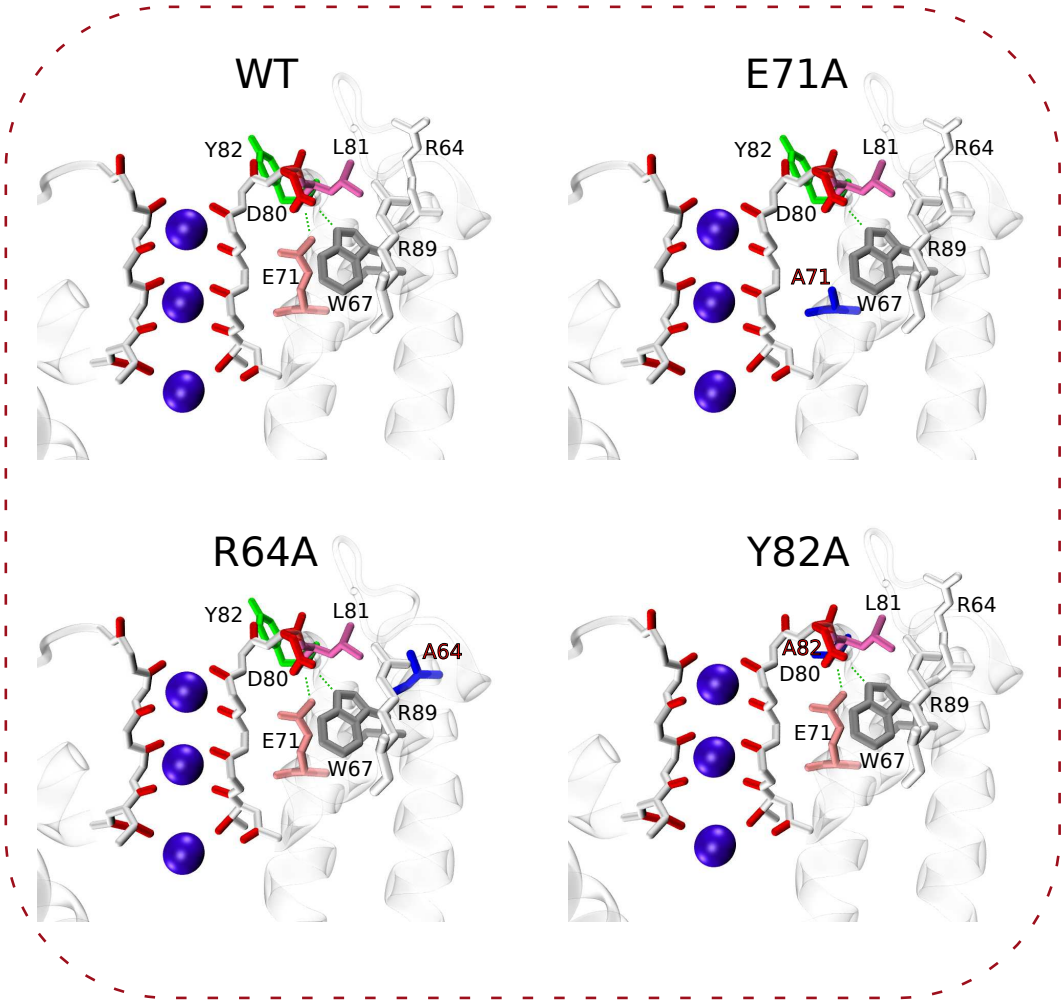

Figure 1.4: Structures of the region of the selectivity filter in the different proteins studied in this work: i) wild type (WT, pdb code 1K4C[157]), ii) E71A, iii) R64A, and iv) Y82A. The latter three mutants were created in-silico from starting from the structure of the WT. Relevant residues are showed in the pictures.

the channel axis are able to repel anions while attracting cations and catalyse their dehydration.[46,60,64] Different lines of evidence suggest that ions and water molecules in the SF are arranged in a single file, in order to have two or three K^+ ions in the selectivity filter.[17,18,44,46,72,107,107,154,156] High resolution X-ray experiments at high [K^+] suggested the four sites S1 to S4 on average are equally occupied. This is consistent with a high permeation rate for K^+ ions.[154,156]

Current experimental techniques are not able to distinguish between the fine details of permeation and selectivity. In consequence, a huge number of theoretical models have been developed for the purpose of trying to catch the complex behaviour of the microscopic current.[9,64,101,129] Issues in modelling ion channels originate from the intrinsic complexity of the systems. These have often been described too simplistically for capturing the relationship between structure and function. For example, traditional models consider ions as point charges, water as a continuous dielectric, and protein as a dielectric with rigid walls, although ion size, hydration, and interactions with protein are also known to play crucial roles. Thus atomistic models, such as Molecular Dynamics (MD), have been widely used in recent years because of their ability to provide detailed descriptions of the processes involved, often in combination with free energy methods, mainly the so-called Umbrella Sampling (the topic has been reviewed in detail in[9,64,101,129,132]).

Permeation is believed to occur according to the hypothesis of a "knock-on" conduction mechanism, firstly proposed by Hodgkin and Keynes[65], in which an incoming ion "knocks-on" the ions already in the SF.[18,39,72,107] Based on MD simulations, Berneche and Roux[18] proposed that concerted motions of ions within the pore are purely diffusive, with barriers contained within 2 and 3 kcal/mol. In any event, the process is not completely clear owing to the *inherent complexities* associated with inactivation and the conformational flexibility of the pore which make calculations very difficult, as recently reported in a paper of one of the authors of the previously-cited work (see Li, Andersen, and Roux[92]). Moreover, the occurrence and the role of vacancies within this mechanism, proposed by Hodgkin and Keynes[65] in the same work in which "knock-on" was described, is still under debate.[54,71,72]

1.1.3 Selectivity

Selectivity in potassium ion channels has been the focus for decades of ion-channel research but remains an open question. The ability to select K^+ over smaller ions, especially Na^+, is crucial for physiological function. A number of different hypotheses have been proposed (see Andersen[7] and reference within) that can be grouped into two main classes: i) kinetically driven, initially proposed by Bezanilla[21] and

determined by the entrance rates of the different ion species in the SF; and ii) thermodynamically driven, derived from Mullins[108], which is based on the ion-pore interactions being able to better compensate for the energetic cost of dehydration for K^+ than for Na^+. The classic textbook explanation is the so-called "snug fit" hypothesis and belongs to the latter class: selectivity occurs before the SF because the small Na^+ ions are not coordinated as well as the K^+ ions within the pore.[64]

When the microscopic structures of the channels became available these hypotheses were tested against the dynamical properties of the protein in numerous studies.[7,110,130] The geometry of the filter is consistent with the "snug fit" hypothesis, since the eight oxygen ligands that constitute the sites are optimally placed to interact with a K^+ (radius 1.33 Å) more than with the smaller Na^+ (radius 0.95 Å).[8,43] Some authors proposed alternative mechanisms based on a more flexible interpretation of the filter. The site S2, located at the centre of the pore, was proposed as being responsible for a thermodynamically driven selectivity.[18,48,130] Other studies proposed that the binding of Na^+ inside the filter to be not thermodynamically unfavourable and the existence of different binding sites, called B sites, for Na^+, has been suggested.[78,110,135,141] This led to kinetically based hypotheses for selectivity which occurs before the SF.[78,110,141]

A coupling between selectivity and gating was proved by experimental studies. Intracellular Na^+ was found to decrease the open probability of the channel, causing a slow "gating effect" mostly noticeable at high voltages and affecting the K^+ current with a fast block.[110,111,141,157] The two effects are believed to occur according to different mechanisms that have yet to be fully understood.[110]

Despite the long-lasting research and the available experimental data, the debate is still continuing and a definitive answer for selectivity and its associated processes is not available.

1.2 Aim of the work

Macroscopic current in potassium ion channels arises from a complicated interdependence between ions-protein interactions and fine structural rearrangements of the protein which is responsible for complex behaviours of the single-channel current.[28,29] Selectivity appears to be coupled with the same mechanisms as those which underlay current regulation.[66,110] The understanding of the physiological behaviours of K^+ channels requires the investigation of the atomic resolution dynamics. Available experimental techniques are unable to provide directly a similar dynamical picture. Theoretical approaches have therefore been, and continue to be, widely used

in studying ion channels. Molecular dynamics simulations are an excellent tool for this purpose since they are able to deliver a detailed description of the microscopic scales. A wide research on empirical force fields for biological systems[79,98] and great developments of the computational resources have permitted a wide application of this method which has been used in many relevant works on ion channels over the last few years.[9,64,101,129,132]

The success of molecular dynamics simulations lies in the possibility of determining free energies, fundamental information to define directions, rates, and the driving forces of biological processes. The advantage with respect to different methods derives from the dynamical nature of molecular dynamics, which allows the explicit consideration of the entropic contribution to free energy, which is essential in biological systems. Methods commonly used to compute free energy from molecular dynamics simulations on biological systems take advantage of modified Hamiltonians, which are biased on selected subsets of degrees of freedom. These order parameters, usually referred as collective variables (CVs), are chosen to provide an adequate description of the investigated process. There is no general, simple approach for this selection, which primarily depends on chemical intuition and on the experience of the researchers.[86] The Boltzmann distribution and free-energy are then recovered, as a function of the CVs, from the exact knowledge of the bias potential added to the original Hamiltonian. The high complexity of the these systems makes free-energy calculations a challenging task. The dimensional reduction derived from the projection of the free-energy onto the CVs can be extremely difficult, reflecting the fact that proteins are highly correlated systems having a wide range of time scales involved in their dynamics. This is the case for ion channels. In a recent paper from the B. Roux Group, which has worked for long time in ion channel research, the authors stated:

> "However, while MD simulations of K^+ channels of ever-increasing complexity are possible, issues of permeation and selectivity are partly obscured by the inherent complexities associated with inactivation and conformational flexibility of the pore."[92]

In the present work a wide investigation on the strong coupling between permeation and the dynamics of the pore region in the potassium ion channel KcsA is presented. The study was performed using Molecular Dynamics simulations combined with free-energy methods, in particular well-tempered Metadynamics, and statistical analysis. The network of residues and the dynamics responsible for the regulation of the channel activity was defined in details. The long-lasting question of the control of the current at the filter was addressed, and a mechanism for C-type

inactivation has been proposed based on conformational changes of the network of residues located behind the selectivity filter of the channel. Finally, these results allowed a more transparent investigations of permeation and selectivity than that provided in previous works, revealing driving forces and mechanisms, by means of the suppression of the conformational equilibria associated with inactivation, which are widely known to obscure similar analysis. From this work one paper was published,[40] while three papers are in preparation.

In Chapter 3, in which part of the results published in Cosseddu et al. [40] are reported, the dynamics of the channel was investigated from the MD trajectories in order to validate the applicability of the methods commonly used to compute free energies and to determine the relevant time scales involved in the dynamics of the system. In Chapter 4, the existence of a highly-correlated network of residues behind the SF was revealed, centred on a highly-conserved aspartic acid residue located on the pore entryway (D80). This network was proved to be able to influence the state of the filter and the dynamics of the permeating ions. In Chapter 5, possible mechanisms for C-type inactivation are proposed based on conformational changes of the network of residues, which further confirmed the key role of the aspartic acid D80 and its neighbouring hydrogen-bond donors in determining the state of the pore. In Chapter 6, studies on permeation and selectivity are presented, having been performed on a truly conductive state of the channel, the equilibrium conductive/non-conductive states being transparently suppressed. These studies unveiled the driving forces and energetics associated with the two processes, including energies involved in the dehydration of the ions.

Chapter 2

Methods

2.1 Molecular Dynamics

Molecular Dynamics represents the most detailed approach to study complex biomolecular systems. With the availability of empirical force fields able to describe proteins and lipids, molecular dynamics have been used extensively to create realistic atomic models of complex biological systems, including many types of ion channel.[129]

Molecular dynamics (MD) is the term used to describe the *solution* of the classical equations of motion (Newton's equations) for a set of molecules[2], and it provides a *direct route* from the microscopic details of a system to macroscopic properties of experimental interest. It is based on the possibility, within the Born-Oppheneimer approximation, to express the Hamiltonian of the system as a function of the nuclear variables, the motion of the electrons having been averaged out. Given the sets of coordinates $\boldsymbol{q}_i$ and momenta $\boldsymbol{p}_i$ of each molecule i:

$$\boldsymbol{q} = (\boldsymbol{q}_1, \boldsymbol{q}_2, \boldsymbol{q}_3, \ldots, \boldsymbol{q}_N) \tag{2.1a}$$

$$\boldsymbol{p} = (\boldsymbol{p}_1, \boldsymbol{p}_2, \boldsymbol{p}_3, \ldots, \boldsymbol{p}_N) \tag{2.1b}$$

the Hamiltonian can be written as a sum of kinetic, $\mathcal{K}$, and potential, $\mathcal{V}$, energy terms

$$\mathcal{H}(\boldsymbol{q}, \boldsymbol{p}) = \mathcal{K}(\boldsymbol{p}) + \mathcal{V}(\boldsymbol{q}). \tag{2.2}$$

Usually $\mathcal{K}$ take the form

$$\mathcal{K} = \sum_{i=1}^{N} \sum_{\alpha} \frac{p_{i\alpha}^2}{2m_i} \tag{2.3}$$

where m_i is the mass of the ith atom, and α runs over x, y, z, the components of

its momentum. The term $\mathcal{V}$ is the potential function of the system and contains the force acting on the i^{th} atom

$$\boldsymbol{f}_i = -\nabla_i \mathcal{V} \tag{2.4}$$

where ∇_i is the gradient operator on the coordinates of the i^{th} atom. For Cartesian coordinates, Eqs. (2.2) to (2.4) become[56]

$$\dot{\boldsymbol{r}}_i = \boldsymbol{p}_i / m_i \tag{2.5a}$$

$$\dot{\boldsymbol{p}}_i = -\nabla_i \mathcal{V} \tag{2.5b}$$

where m_i and $\boldsymbol{r}_i$, are the mass and position of the ith atom respectively and the dot denotes the time derivative. Eqs (2.5) describe a state in the phase space $\mathbb{R}^6$, corresponding to $6N$ equations for a system of N atoms. The trajectories of the system in the phase space are generated integrating numerically Eq. (2.5), since an analytical solution is not achievable due to the continuous changes in the forces as the particles move.

In common biological simulations Eq.(2.5) is computed for millions of integration steps on many thousands of atoms. Although this might appear as an excessive effort, given the highly correlated nature of the investigated system this is most of the time necessary. For instance, in the case of ion channels, experimental evidence has shown that the filter is directly affected by mutations in remote positions.[41] Decreasing the size of the simulated system to *bare essentials* could in many cases lead to loss of significance, because many important microscopic factors would be likely altered or even cut off.[129] Computations are made more efficient representing the potential energy $\mathcal{V}$ in Eq. (2.5b) using quite simple functions, including relatively simple mathematical terms to describe the physical interactions and empirical parameters fitted to accurately reproduce experimental and quantum mechanical energetic data.[98] The combination of the functional forms and the associated parameter set is called a *Force Field* (FF). The fitting is not trivial and a proper balance between solvent-solvent, solvent-solute, and solute-solute interactions is very important to have the right partitioning of molecules or parts of molecules in different environments. It means making compromises among best fitted parameters in different conditions. Furthermore FF most commonly used in biological simulations does not account for the phenomenon of electronic polarization, with the aim of simulate bigger systems for longer times.[158] This lack is usually compensated scaling the parameters for polar molecules by a factor derived from a quantum mechanical calculations, where the polarization effect is represented, which is chosen to better reproduce condensed-phase properties at the expense of agreement with gas-phase

data.[99,158] It is important to note that the potential function incorporates the greatest assumptions of molecular dynamics,[2] and it is fundamental to the success of the method.

In a real multi-particle system, the term $\mathcal{V}$ should be:[2]

$$\mathcal{V}_i = \sum_i v_1(\boldsymbol{r}_i) + \sum_i \sum_{j>i} v_2(\boldsymbol{r}_i, \boldsymbol{r}_j) + \sum_i \sum_{j>i} \sum_{k>j>i} v_3(\boldsymbol{r}_i, \boldsymbol{r}_j, \boldsymbol{r}_k) + \dots \tag{2.6}$$

where $v_1(\boldsymbol{r}_i)$ represents the effect of an external field and v_n $(n = 2, 3, \dots)$ are the potential terms between pairs, triplets, etc. The pair potential is the most important, and in the practical implementation of molecular dynamics *pairwise approximation* is used defining an *effective* pair potential in which the upper terms are, in principle, included as ensemble averages. Then Eq.(2.6) is rewritten in the form:

$$\mathcal{V}_i \approx \sum_i v_1(\boldsymbol{r}_i) + \sum_i \sum_{j>i} v_2^{\text{eff}}(r) \tag{2.7}$$

where $r = r_{ij} = |\boldsymbol{r}_i - \boldsymbol{r}_j|$. The presence of any external field is usually neglected, although electric fields have been considered in modeling ion channels. However their implementation is not always straightforward and the effect of the finite sizes of the system is still under debate.[127] For molecular systems, intramolecular potential terms are added to model the geometries that are generally referred as "bonded interactions".

Several different force fields and set of parameters have been developed over the past years. The most known and used for biological systems are CHARMM, AMBER, GROMOS and OPLS. The calculation of the present work were performed employing all-atom CHARMM force field.[79,99,100] The intramolecular potential includes terms for bond stretching, angle bending, Urey-Bradley 1,3 interaction, torsional rotation, and out-of-plane (improper) motion and has the form

$$\begin{aligned} V_{\text{bonded}}(r) = &\sum_{bonds} K_b(b - b_0)^2 + \sum_{angles} K_\theta(\theta - \theta_0)^2 + \\ &\sum_{Urey-Bradley} K_u(u - u_0)^2 + \sum_{dihedrals} K_\phi[1 + cos(n\phi - \phi_0)] + \\ &\sum_{impropers} K_\psi(\psi - \psi_0)^2 \end{aligned} \tag{2.8}$$

where K_b, K_θ, K_u, K_ϕ and K_ψ are the bond, bond angle, Urey- Bradley, dihedral angle, and improper dihedral angle force constants, respectively; b, θ, u, ϕ and ψ are the bond length, bond angle, Urey- Bradley 1,3 distance, dihedral torsion angle,

and improper dihedral angle, respectively, with the subscript zero representing the equilibrium values for the individual terms. The Urey-Bradley term is a harmonic term in the distance between atoms that are bonded to a common third atom of some of the angle terms important for the in-plane deformations as well as separating symmetric and asymmetric bond stretching modes.[100]

Pairwise potential, usually referred as "non-bonded" because it is computed between atoms that are not covalently bonded, assumes the form

$$V(r) = \sum_{i,j} 4\epsilon_{ij} \left[\left(\frac{\sigma_{ij}}{r_{ij}} \right)^{12} - \left(\frac{\sigma_{ij}}{r_{ij}} \right)^{6} \right] + \sum_{i,j} \frac{q_i q_j}{\epsilon_D r_{ij}} \tag{2.9}$$

where i, j are non-bonded pairs and q_i, q_j are their charges. Non-bonded, non-electrostatic Van der Waals forces are represented by a Lennard-Jones 12-6, in which the first term represents repulsions due to the Pauli principle and the second attractions due to small instantaneous dipoles generated by the electronic motions. It is characterised by a minimum of depth ϵ, where the two terms are balanced, and the curve crosses the x-axis when the distance is σ. The final term of Eq. (2.9) represents the coulumbic interactions. Consistent with CHARMM parametrisation, non-bonded interactions have been computed also for the atoms within the same molecules, excluding the bonded atoms and all pairs of atoms that are bonded to a common third atom. In this work grid-based correction CMAP was used, which improves distributions of the dihedral angles of the protein backbone.[25]

Boundary conditions are crucial to overcome the problem of surface effects that arises in the small simulated systems. Periodic boundary conditions were used in this work, and they are also the most commonly used in molecular dynamics. The system is virtually replicated in the three dimensions to create an infinite lattice of identical cells, and each atom interacts, according to the force field, with all other atom in this infinite periodic lattice, those in the box and their replica, included his own copy.[53] There is, in principle, an infinite number of terms. To avoid this, the *minimum image convention* is used: each atom lies in the centre of a region of the same size and shape as the basic simulation box, and it can directly interact only the atoms inside this region. On top of this, cutoffs on Van der Waals forces are employed to reduce the amount of computation.

Solution of the Hamiltonian equations The Hamiltonian equations are solved by a step-by-step procedure. The most used methods of integration are the *Verlet-style* algorithms.[53] They are simple, allow to use large time step and give a very good energy conservation over long times. The most common is the so-called *Velocity*

Verlet

$$\boldsymbol{r}(t+\delta t) = \boldsymbol{r}(t) + \mathbf{v}(t)\delta t + \frac{1}{2}\boldsymbol{a}(t)\delta t^2 \tag{2.10a}$$

$$\mathbf{v}(t+\delta t) = \mathbf{v}(t) + \frac{1}{2}\left[\boldsymbol{a}(t) + \boldsymbol{a}(t+\delta t)\right]\delta t. \tag{2.10b}$$

with $\boldsymbol{r}$, $\mathbf{v}$, $\boldsymbol{a}$ the sets of Cartesian coordinates, velocities and accelerations. The algorithm implemented to advance the configuration of the system over a time-step δt is the following:

$$\mathbf{v}(t+\frac{1}{2}\delta t) = \mathbf{v}(t) + \frac{1}{2}\boldsymbol{a}(t)\delta t \tag{2.11a}$$

$$\boldsymbol{r}(t+\delta t) = \boldsymbol{r}(t) + \mathbf{v}(t+\frac{1}{2}\delta t)\delta t \tag{2.11b}$$

$$\boldsymbol{a}(t+\delta t) = \frac{-\nabla\mathcal{V}(\boldsymbol{r}(t+\delta t))}{m} \tag{2.11c}$$

$$\mathbf{v}(t+\delta t) = \mathbf{v}(t+\frac{1}{2}\delta t) + \frac{1}{2}\boldsymbol{a}(t+\delta t)\delta t. \tag{2.11d}$$

2.2 Free energies Methods

2.2.1 Free energies and MD

MD simulations are based on performing a sampling on a statistical ensemble such as microcanonical (NVE), canonical (NVT), or isothermal-isobaric (NpT). Free energies are equilibrium properties and they can be retrieved by applying statistical-mechanics equations. Free energies related to a process of interest are conveniently defined with respect to a small subset of n degrees of freedom, generally referred as collective variables, *CVs*. They can be easily defined as functions of the Cartesian coordinates of the N atoms of the system $S(\boldsymbol{r}) = (S_1(\boldsymbol{r}), S_2(\boldsymbol{r}), \ldots, S_n(\boldsymbol{r}))$, $\boldsymbol{r} = (x_j, y_j, z_j)$ with $0 < j < N$. This dimensional reduction is crucial to allow any understanding of events that involve a large number of atoms. CVs are usually selected to be representative of a given process, and typical examples are distances, angles, coordination numbers, etc. Let's define the potential energy $\mathcal{V}(\boldsymbol{r})$, $\beta = 1/k_B T$ where k_B and T are respectively Boltzmann's constant and the temperature, and $\delta_s = \delta\left(S(\boldsymbol{r}) - \boldsymbol{s}\right)$ is the bin in the the histogram of the CVs for the n dimensional vector of values $(s_1, \ldots, s_n)$. Following Roux [126], at equilibrium the probability distribution function (*pdf*) of the CVs is, according to the Boltzmann distribution,

$$\mathcal{P}(S) = \langle\delta_s\rangle = \frac{\int d\boldsymbol{r}\, e^{-\beta\mathcal{H}(\boldsymbol{r})}\delta_s}{\int d\boldsymbol{r}\, e^{-\beta\mathcal{H}(\boldsymbol{r})}}. \tag{2.12}$$

where $\int d\boldsymbol{r}\, e^{-\beta\mathcal{H}(\boldsymbol{r})}$ is the partition function of the system. This probability is clearly equal to one on the space of the CVs,

$$\int ds\, \mathcal{P}(s) = 1. \tag{2.13}$$

From statistical mechanics, the free energy, G, can be written as function of S, within an immaterial constant C[86]

$$G(S) = -k_B T\, \ln\left(\mathcal{P}(S)\right) + C. \tag{2.14}$$

From the definition of MD and within the assumption of ergodicity, the pdf in Eq. (2.12) is retrieved from the histogram of the CVs[13]

$$N(S,t) = \int_0^t dt'\, \delta\left(S(\boldsymbol{r},t') - \boldsymbol{s}\right) \tag{2.15}$$

in the limit of a complete sampling

$$\mathcal{P}(S) = \lim_{t\to\infty} \frac{N(S,t)}{\int ds\, N(s,t)}. \tag{2.16}$$

In big systems, especially in the biological ones, it is very difficult to obtain a good convergence of Eq. (2.16), due to limits of computational resources. As mentioned in previous sections, MD requires significant computational efforts, which become unrealistic when dealing with very complex free energy landscapes, characterised by large barriers.[86] To overcome these limitations, several methods to perform non-Boltzmann sampling have been developed.

2.2.2 Umbrella sampling

Umbrella sampling is probably the most known of among the non-Boltzmann sampling methods. It belongs to a category of method where the MD is performed on modified Hamiltonians where an extra potential energy term $\mathcal{W}(S)$ is added to *bias* the calculation

$$\mathcal{H}^*(\boldsymbol{r},\boldsymbol{p}) = \mathcal{K}(\boldsymbol{p}) + \mathcal{V}_i(\boldsymbol{r}) + \mathcal{W}(S(\boldsymbol{r})). \tag{2.17}$$

Thus this class of methods are generally referred as *biased* simulations.

In umbrella sampling the bias potential is fixed and used to enhance the sampling in a particular region of the CVs phase space. Since only a small piece of the FES is computed with sufficient accuracy, several calculations (*windows*) are performed, moving the centre of the bias potential on different values of $S(\boldsymbol{r})$. The

most common choice is to use harmonic bias potentials, that, for the case of a single CV, takes the form of

$$\mathcal{W}_i(S) = \frac{1}{2} K \left(S(\boldsymbol{r}) - s_i\right)^2 \tag{2.18}$$

where s_i are the centres of the different n windows.[126] The different pieces of the FES obtained from the different calculations are finally combined to obtained the FES over the whole range of interest of $S(\boldsymbol{r})$.

Following Eq. (2.12), the biased distribution for the single window is

$$\begin{aligned} \mathcal{P}_{\mathcal{W}_i}(S) &= \frac{\int d\boldsymbol{r}\, e^{-\beta \mathcal{V}(\boldsymbol{r})} e^{-\beta \mathcal{W}_i(S)} \delta_s}{\int d\boldsymbol{r}\, e^{-\beta \mathcal{V}(\boldsymbol{r})} e^{-\beta \mathcal{W}_i(S)}} \\ &= \frac{e^{-\beta \mathcal{W}_i(S)} \mathcal{P}(S)}{\int d\boldsymbol{r}\, e^{-\beta \mathcal{W}_i(S)}}. \end{aligned} \tag{2.19}$$

From Eq. (2.14), the free-energy can be written[126]

$$G(S) = -k_B T \ln\left(\mathcal{P}_{\mathcal{W}}(S)\right) - \mathcal{W}(S) + F \tag{2.20}$$

where $F = \int d\boldsymbol{r}\, e^{-\beta \mathcal{W}_i(S)} + C$ is an unknown constant. The absolute value of this constant is not required for practical purposes, but it is adjusted at the moment of the reconstruction of the FES for the whole range of interest.

In general the unbiasing procedure granted by Eq. (2.20) is made difficult by many statistical errors, mainly in the overlapping region between two windows.[126] Different methods have been proposed to solve the equation

$$\mathcal{P}(S) = \sum_{i=1}^{n} \mathcal{C}_i(S) \mathcal{P}_i(S) \tag{2.21}$$

were $\mathcal{C}_i(S)$ is the appropriate weight of the unbiased distributions $\mathcal{P}_i(S)$ computed for the i-th window. Weighted histogram analysis method (WHAM), first proposed by Kumar et al.[82], is one of the most in use and it was employed in this work via the implementation by.Grossfield[58] The complete description of the method is out of the scope of this work (see Roux[126] and references therein for details).

2.2.3 Metadynamics

Metadynamics (metaD) is a computational method that can be used either to reconstruct free energy surfaces (FES) or to force the system to escape from energy minima.[13,86–88,137] It is based on a bias history-dependent potential created as a sum of Gaussians centred along the trajectory of the CVs. It is sometimes referred

as a self-learning adaptive umbrella sampling because previous extensive knowledge of the investigated process is not strictly required, adapting the bias potential to the underlying free-energy. Several implementations of the metaD algorithm have been successfully used in the past. In the present paper, we used the so-called well-tempered metaD for the productive runs which allow a better convergence to the true free energies, and the both well-tempered and standard implementations for the preliminary test calculations.

The biasing potential for metaD, with respect of the previously defined set of CVs $S = (S_1(\boldsymbol{r}), S_2(\boldsymbol{r}), \ldots, S_n(\boldsymbol{r}))$, is given by

$$\mathcal{V}_{\mathrm{B}}(S) = \sum_{t'=\tau_{\mathrm{G}},2\tau_{\mathrm{G}},\ldots} w \prod_{i=1}^{n} e^{\left(-\frac{(S_i(\boldsymbol{r}_i) - S_i(\boldsymbol{r}_i, t'))^2}{2\sigma^2}\right)} \tag{2.22}$$

where w is the Gaussian height, τ_{G} is the time interval between the deposition of the Gaussians, 2σ the Gaussian width along the each CV.[87] For well-tempered metaD the height w is history-dependent as well

$$w = w_0 e^{\frac{\mathcal{V}_{\mathrm{B}}(S,t)}{k_B \Delta T}} \tag{2.23}$$

where w_0 is the initial Gaussian height and ΔT a parameter with the dimension of a temperature.[13] In this case the biasing potential generates a flat distribution, the FES can be easily retrieved from the biased potential for standard implementation of metaD

$$G(S) = -\mathcal{V}_{\mathrm{B}}(S) \tag{2.24}$$

or via a scaling factor in well-tempered metaD

$$G(S) = -\frac{T + \Delta T}{\Delta T} \mathcal{V}_{\mathrm{B}}(S). \tag{2.25}$$

In well-tempered metaD the scaling factor in Eq. (2.23) theoretically guarantees the convergence to the real free energy. The function $G(S)$ is often referred as potential of mean force, PMF, and we will use the term as synonymous of FES.

2.2.4 MetaD parameters

Free-energy surfaces computed via biased methods derives from the projections of the full distribution function for the system onto the reduced set of n CVs, S, via non-Boltzmann sampling. This is obtained by integrating over the remaining variables

with appropriate weights. However a particular care is required to obtain meaningful distributions, that, in the practice, can be very challenging. As in any biased method, the choice of CVs is crucial for a good implementation of metaD and it would ideally be the smaller possible set of CVs which are able to deliver the best description of the process under investigation. There are also practical difficulties in the calculation, because an optimal sampling of the CVs is obtained for the bias potential's slow growths, in the limit of $w/\tau_G \rightarrow 0$.[87,88] In the practical implementation of the method this limit cannot be reached and, as a result, there is a risk of overfilling some minima by generating hysteresis. This issue are alleviated by the use of history-dependent heights of the Gaussians as implemented in well-tempered metaD and can be solved explicitly considering within the set of CVs, and thereby bias, the degrees of freedom that most contribute in generating similar effects.[86,88]

The success of the free energy reconstruction in well-tempered metaD relies on the parameters i) ΔT and ii) $\omega = w_0/\tau_G$, the initial deposition rate.[13] A fine choice of ΔT allows both a quicker convergence and a confinement within a relevant region of the CVs space. It is worth noting that although important from a practical perspective, the computed FES will eventually converge to the real one irrespective of the particular choice of ΔT.[13] Initial deposition rate $\omega = w_0/\tau_G$ affects relaxation over the orthogonal degrees of freedom.[13] The choice of w_0 was not trivial in our case and, as will be discussed in details in Chap. 6, low values (0.005 Kcal/mol) produced the best outcome resulting in a smoother filling of the biasing potential. The deposition times (τ_G) was selected 400 fs for the one dimensional calculations and 200 fs for multidimensional, but these different choices did not appear to affect the final results.

2.3 Simulation set up

The simulations presented in this work were performed using NAMD 2.8 and NAMD 2.9[120] in the NpT ensemble with pressure 1.01 bar (Langevin piston implemented via Nose-Hoover method[120]), temperature 310 K (Langevin thermostat[120]) and electrostatic forces were computed using the smooth particle-mesh Ewald method (SPME).[49] Metadyanamics calculations were performed using the built-in "colvar" module.[50] A multiple-timestep algorithm was used[59,145] and different integration steps according to the scope of the simulations:

- 1 fs for unbiased simulations, bonded interactions computed every time step, non-bonded non-electrostatic forces computed every 2 time step and electrostatic forces every 4 time step;

- 2 fs for biased simulations, bonded and non-bonded non-electrostatic forces computed every time step and electrostatic forces computed every 3 time step;

Using longer integration steps (2 fs) is a common choice for biased simulations, since it allows longer sampling[18,20,36,54,78,92,131,131] The CHARMM27 force field (FF) was used for the protein, with a modification in the Lennard-Jones term to represent the interaction between K^+ and the carbonyl oxygens of the protein, CHARMM36 for the lipids and TIP3P for water.[79,99,112]

2.3.1 Embedding protein in the membrane

The system was prepared from the X-ray structure of KcsA solved at 2 Å resolution.[157] The protein conformation is widely considered as a closed conductive state, i.e. the inner gate is closed, while the SF is in a conductive conformation. The single monomer reported in the original file obtained from the protein data bank (pdb code 1K4C) was replicated according to the transformation matrix provided by the authors to create the tetramer and embedded in a membrane patch of 1-palmitoyl-2-oleoylphosphatidylcholin (POPC) using the VMD 1.8.6 membrane plug-in, modified in order to work with CHARMM36 (Fig. 2.1). Two K^+ ions were placed in the SF and one K^+ in the cavity. The system was solvated inserting the protein into a pre-equilibrated water box with VMD solvate plug-in. To avoid the creation of unphysical gaps close to the protein surface, this step had been preceded by a preliminary salvation using the Solvate program by Grubmüller (www.mpibpc.mpg.de/home/grubmueller/downloads/solvate), which creates an irregularly-shaped solvent volume around the protein according to steric criteria. Many water molecules inside the cavity were not resolved by the X-ray experiments, and have been inserted using the DOWSER program.[152] The missing parameters for K^+ necessary for DOWSER have been taken from the GROMOS87 FF for consistency.[115] MD free energy sampling, and quantum mechanical/molecular mechanical (QM/MM) calculations suggest that, in the conductive state, the E71/D80 pair are linked by an hydrogen bond (H-bond) where one residue is ionised, and the proton exchanges with a preference for E71.[19,24] Consistent with conventional MD force fields, this has been mimicked in this work by assigning the proton to E71 in every protein where E71-D80 bridge is present (WT, R64A, Y82A). R52, R64, R89 were modelled as protonated, and E51 as deprotonated, as appropriate for a pH range 4–8.[29,35,157] The potassium concentration in the aqueous phase was 0.2 M, equal to bulk concentration used in many experiments.[29,34–36,46,157]

The system was relaxed before the productive runs in three steps. (i) A 2 ns

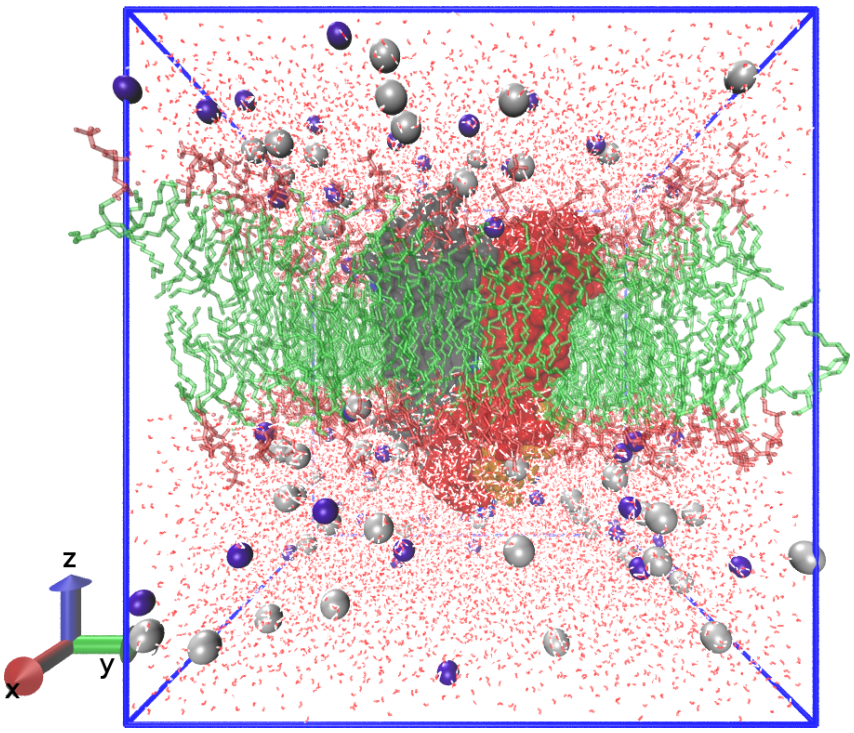

Figure 2.1: Simulated protein, prepared from the X-ray structure of KcsA solved at 2 Å resolution (pdb code 1K4C, 6284 atoms),[157] embedded in a membrane patch of 1-palmitoyl-2-oleoylphosphatidylcholin (POPC, 222 molecules and 29748 atoms), solvated by 17740 water molecules (53220 atoms), with 75 Cl^- ions and 63 K^+ ions. The final size of the system was $\approx 95 \times 95 \times 100$ Å and the total number of atoms was 89390. The different sizes of the atoms in the figure are chosen only for visualisation purposes and do not have any physical meaning, while the colours are chosen as follow: i) a different colour is used for each protein domain; ii) lipid tails are in green; iii) lipid heads in red; iv) K^+ ions in purple; v) Cl^- ions in grey; vi) water molecules are in red (oxygen atoms) and white (hydrogen atoms).

MD simulation in which the protein, water, ions and lipids headgroups were frozen; this ensured melting of the lipid tails. (ii) A further 2 ns MD simulation in which the protein (only) was restrained with harmonic tethers. (iii) A 1 ns MD simulation in which all atoms were unrestrained.

2.4 General analysis

2.4.1 Order parameters or Collective variables

In the present work conformational changes in the region of the selectivity filter of potassium ion channel KcsA are investigated. Within these dynamics, it will be shown that an aspartic acid residue located in the external entryway of the channel

(D80) plays a key role. Consequently several analyses have been focused on the rearrangements of D80 with respect of its neighbouring residues. Few sets of order parameters which will be used throughout the text are defined below.

The first set corresponds to distances between D80 side chain, defined by C_γ atom (the carbon of the carboxyl group), and an atom used to describe a second residue's side chain. The distances are simply labelled by "d", appending the position of the second residue, i.e. d71 is the distance between D80 and E71 side chains. The following residues have been considered as second residues: (i) E71 ("d71"), its side chain defined by the H-bond donor oxygen belonging to the carboxyl group; (ii) arginines R64 ("d64") and (iii) R89 ("d89"), their side chains defined by the carbon atoms of the guanidino group (C_ζ); and (iv) W67 ("d67"), its side chain defined by the H-bond donor $N_{\epsilon 1}$.

A second set defines distances between D80 side chain and the backbone C_α atom of a second residue and they are labelled by appending "CA". In this case two residues have been considered as second residues, the residue in position 71, glutamic acid for WT, Y82A, R64A and alanine for E71A ("d71CA") ; ii) the alanine in position 73 ("d73CA"). The distance between D80 and E71 C_α atoms is named "E71CA-D80CA".

A third set corresponds to distances from the SF of the side chains of relevant residues. Again the side chains are defined by representative atoms, and the SF by the center of mass (COM) of the C, N, $C_\alpha$atoms of the residues in position 74 to 78 of each subunit. These distances are labelled by "C" followed by the number of the considered residue, i.e. C64 and C89 are, respectively, the distance from the SF COM of the C_ζ atoms of the arginines in position 64 and 89.

A forth set defines dihedral angles of different residues. Their names are formed by appending the position of the residue in the sequence to the name of the Greek letter that defines the dihedral within the residue itself, ignoring incremental numbers if exists. For instance $\chi 1$ dihedral angle of residue L81 is labelled chi81, *psi* of residue V76 is psi76.

Labels for the ions bound to the SF and in the cavity are formed by the symbol of the element and an increasing number starting from the outermost in the SF, i.e. two K^+ ions in the SF and one in the cavity are labelled respectively K1, K2 and K3.

2.4.2 Projection of the computed FES onto lower dimensional surfaces

In this work, the computed FES have been projected into lower dimensional surfaces in several cases. The projections onto a subset of the CVs, $A \subset S$, were computed from the unbiased distribution, integrating over the j CVs that does not belong to A, $S - A$:

$$G(A) = \int_{S_k \in S-A} \mathrm{d}S_k \, e^{-\frac{G(S_i)}{k_b T}} \tag{2.26}$$

where the terms $G(S_i)$ were obtained via Eq. (2.25) for $S_i \in S$. Eq. (2.26) was implemented using R language.[122]

2.4.3 Statistical analysis

The statistical analysis were performed using R language and vmd 1.9.[67,122] Several packages for R were used in addition to the core functions: bio3d, ggplot2, car, fields.[1,52,55,57,148] Many functions and packages have been written both for R and VMD for the purpose of this study that have a more general applicability. Most of the analysis have been performed on the whole simulated trajectories with the coordinates stored either every 5 or 2 ps, ignoring an initial equilibration period.

Chapter 3

Dynamics of the ions and free-energy calculations

KscA is a potassium ion channel from *Streptomyces lividans* bacteria, which has an amino acid sequence closely similar to that of vertebrate and invertebrate voltage-dependent potassium channels[46]. The detailed molecular structure of KcsA has been known since 1998[46]. Since that time it has been actively studied through the use of molecular dynamics (MD) simulations for verifying and testing a variety of hypotheses related to the conductivity and selectivity of the channel. The extremely high dimensions of the corresponding model (see Sec. 2.1) represents one of the most difficult aspects in the analysis.[27,144]

A MD model is a Hamiltonian, non-linear, high-dimensional, dynamical system which typically shows multi-scale behaviour in both space and time. A direct way to reduce the dimension is to assume ergodicity and mixing in the systems, that is to consider Brownian Dynamics model. These assumptions allow each atom to be considered as a particle moving in some potential under the action of a stochastic source, resulting in a low-dimensional dissipative stochastic non-linear system. Thus, a simple way to think of the permeation of ions through the channel is by focusing on the properties of a selected part of the system: the permeating ions. In this way the ions can be described by a generalised Langevin Equation (GLE) of the form[80]:

$$m_i \dot{\mathbf{v}}_i(t) = -\frac{\partial G(\mathbf{r}_i)}{\partial \mathbf{r}_i} - \int_0^t \mathbf{M}(t-\tau)\mathbf{v}_i(\tau)d\tau + \mathbf{R}(t), \tag{3.1}$$

where $\mathbf{v}_i$ is the ion's velocity ($\mathbf{v}_i = \mathbf{p}_i/m_i$); $G(\mathbf{r}_i)$ is the so-called potential of mean force (PMF) and corresponds to the free energy (Sec. 2.2); and the term $\mathbf{M}(t)$ is an appropriate memory function connected to the random force $\mathbf{R}(t)$ acting on the ion

via the second fluctuation-dissipation theorem:

$$\mathbf{M}(t) = \frac{1}{k_B T}\langle \mathbf{R}(0)\mathbf{R}(t)\rangle. \tag{3.2}$$

The picture is typically further simplified by making the assumption that ionic motion corresponds to overdamped Markovian diffusion[17,126], resulting in the overdamped Langevin equation[123]

$$\dot{\mathbf{r}}_i = -\frac{1}{m_i\gamma(\mathbf{r}_i)}\frac{\partial G(\mathbf{r}_i)}{\partial \mathbf{r}_i} + \sqrt{\frac{2k_BT}{m_i\gamma(\mathbf{r}_i)}}\boldsymbol{\xi}(t), \tag{3.3}$$

where $\gamma(\mathbf{r}_i)$ specifies the damping and $\boldsymbol{\xi}(t) = (\xi_x(t), \xi_y(t), \xi_z(t))$ is a vector of Gaussian white noises. The parameter γ can be calculated from the diffusion coefficient D, if known, using the relation $D = k_BT/\gamma$. Diffusion coefficients can sometimes be estimated experimentally, otherwise from coordinate and velocity time-series (see Mamonov et al.[103] for details).

Within this framework the identification of $G(\mathbf{r}_i)$ is a key task, since it is determinant in the definition of the process. However, this identification is generally very complicated. It is possible to retrieve $G(\mathbf{r}_i)$ in Eq. (3.3) directly from the MD trajectories (see Sec. 2.2 and[126]). This is extremely expensive in computational resources and in many cases unachievable. Therefore, common techniques for calculating free-energies are based on the introduction of a known additional deterministic term in the Hamiltonian $\mathcal{H}$ (Eq. (2.2)) for a subset of degrees of freedom of the system S, generally referred to as "order parameters" or "collective variables" (CVs), which are defined as functions of $\mathbf{r}_i$. This additional force enables the retrieval of the theoretically true Boltzmann distribution for $S(\mathbf{r}_i)$ from a non-Boltzmann sampling thus reducing the computational efforts.[126] The most frequently-applied technique is the so-called Umbrella Sampling (US) method (Sec. 2.2.2), which has been widely used to investigate ion channel properties.[18,20,54,78,121,126,131] However the assumption that the diffusion process can be fully described by an overdamped equation (3.3) instead of a GLE (3.1) must be validated. This can be achieved by means of time-series analysis of the trajectories obtained from MD simulations. Additionally this analysis would provide more general information on dynamical and statistical properties of the system, and in particular of the ions in channels.

In this chapter, ionic dynamics are considered in the selectivity filter of the KcsA channel using MD simulations and the common assumptions employed in the description of ion channels and in the derivation of free energies for describing ions' motion are discussed. The applicability of the overdamped model is verified by

analysing the statistical and dynamic properties of the system. Moreover, statistical errors derived from the MD approach are investigated. The results presented here are published in Cosseddu, Khovanov, Allen, Rodger, Luchinsky, and McClintock [40].

3.1 Methods

A set of MD simulations was performed. The dynamics of the ions were analysed, in particular in the the three sites S2, S1 and S0. Two configurations were selected for MD simulations. One of these was C1 with two K^+ ions in the cavity, a water molecule in S4, a K^+ in S3, a water molecule in S2 and an K^+ in S1. The other configuration, referred to as C2, corresponded to a K^+ in S4, a water molecule in S3, a K^+ in S2, a water molecule in S1, and a K^+ in S0.

The coordinates $\mathbf{r} = (x, y, z)$ calculated relative to the centre of mass (COM) of the selectivity filter (referred to as CVs, units of Å), and corresponding velocities $\mathbf{v} = (v_x, v_y, v_z)$ (in units Å/ps) were stored for each integration step of 1 fs for different atoms. These atoms included: K^+ ions and water molecules inside the selectivity filter, K^+ ions in the cavity and in the bulk, as well as the oxygen atoms of the binding sites. A typical realisation consisted of 10^6 time steps (1 ns). During the simulations the lipids of the membrane were not constrained and the simulated piece of membrane slowly moved together with the channel protein. The centring on the CVs was applied to compensate for this slow motion, and the COM of the selectivity filter was defined as the backbone atoms of residues between 74 to 79 of the four subunits. It should be noted that slow time-scales of longer than about 10^5 ps were automatically removed from consideration.

3.2 Analysis of equilibrium dynamics

Atomic motions are assumed to be realisations of a stochastic process. The latter are characterised by the probability density functions (distributions) of positions and velocities $\mathcal{P}(\mathbf{r})$ and $\mathcal{P}(\mathbf{v})$, as well as by the power spectrum $P(f)$ and/or the auto-correlation coefficient $\rho(\tau)$ of the coordinates' or velocities' projections onto one of the Cartesian axes x, y or z, for the correlation time τ.[15] The resultant time-scales of the atomic dynamics can be revealed via $P(f)$ and/or $\rho(\tau)$. Although there are no analytic expressions for $P(f)$ and $\rho(\tau)$ for arbitrary forms of $G(S)$, a huge volume of results is nonetheless available for different stochastic non-linear equations similar to Eq. (3.3). They place limitations on the possible shapes of the power spectrum and the auto-correlation function. Thus, combining estimated distributions with power

spectra (or auto-correlation function), it is possible to verify the validity of the use of the overdamped Langevin dynamics for the ions in the selectivity filter. This is the assumption most widely used for analysing the properties of ions in the KcsA channel.[18,20,54,78,121,126,131]

Distributions of the coordinate and the velocity of a K^+ ion in different locations are shown in Fig. 3.1. The velocities have same distributions, regardless of the position of the ion: they are almost perfectly Gaussian, consistent with the Maxwell-Boltzmann distribution. Accordingly, the value of temperature T_s can properly be estimated on the basis of $\mathcal{P}(v_s)$. Coordinates x, y and z show similar distributions and are close to Gaussian for coordinates x and y, but they differ significantly from Gaussian for the z coordinate, as illustrated in Fig. 3.1a. This depends on the cylindrical geometry of the channel, with the main symmetry axis (channel axis) being approximately parallel to z in the simulation set-up. The current understanding is that the permeation process occurs along the channel axis through a concerted sequence of jumps performed by the ions between the different sites.[18,39,65,72,107] Hence the PMF along z is multistable and non-parabolic. Analyses of the distributions $\mathcal{P}(z)$ for different steady-state positions demonstrated that the PMF was close to being harmonic (parabolic) in the vicinity of each stable/meta-stable state but that its shape deviated from parabolicity at large displacements from that state. The overall picture, parabolic PMF and linear (3.3) and (3.1) in (x, y), multistable PMF along z, demonstrated the particularly good coordination offered by the SF to K^+, confirming a design specialised in catalyse K^+ flow.

The power spectra in each of the positions considered are very similar, and Fig. 3.2 shows a representative example. The spectra for all coordinates have a part characterised by $1/f$ scaling, which for the velocity spectra transforms to $\propto f$ scaling because $P_v(f) = P_r(f)f^2$. The existence of this scaling region is reflected in the behaviour of the auto-correlation coefficients $\rho(\tau)$ (Fig. 3.3) for each coordinate, which decay slowly towards zero. This picture is typical of processes with long-range correlation. However, the auto-correlation for velocity does not support the presence of any long range correlation and $\rho(\tau)$ decays exponentially to zero, but in an oscillatory manner. This latter feature demonstrates that the motion of the atoms is not overdamped.

The $1/f$ scaling is observed for the low frequency range only, which suggests that a possible origin of $1/f$ scaling lies in the relatively slow changes in the protein dynamics. This can be illustrated by the spectral coherence function $\psi(f)$ (Fig. 3.2b) which estimates the linear correlation between atoms for a given frequency.[15] It can be seen that for any atomic location the coherence is maximal in the low frequency

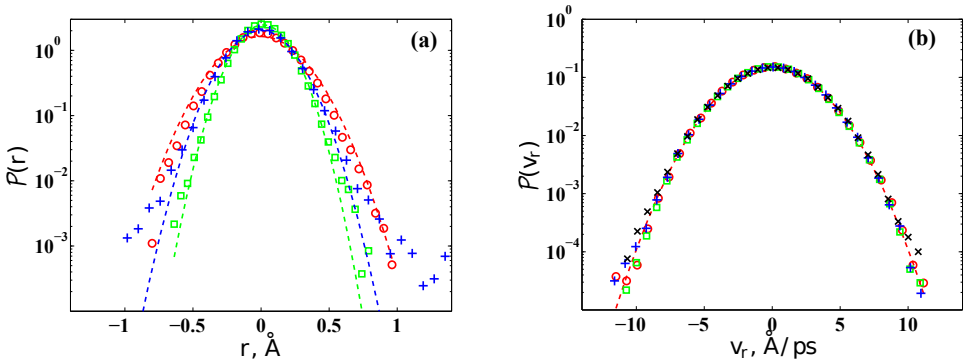

Figure 3.1: Distributions (log scale) of (a) coordinate $\mathcal{P}(r)$ and (b) velocity $\mathcal{P}(v_r)$ of ions for different locations are shown by markers: $\circ$ (red colour) corresponds to the coordinate x and velocity v_x of an ion in the site S1, $\square$ (green colour) corresponds to the coordinate y and velocity v_y of an ion in the site S2, $+$ (blue colour) corresponds to the coordinate z and velocity v_z of an ion in the site S0; and $\times$ (black colour) corresponds to the velocity v_z of an ion in the bulk (the distribution of the coordinate is not shown in this case since it is time-dependent). The coordinate distributions $\mathcal{P}(r)$ are centred with respect to the mean value, that is $\langle r \rangle = 0$. Dashed lines correspond to fits of Gaussian distributions with mean values and the variances estimated from the corresponding time-series.

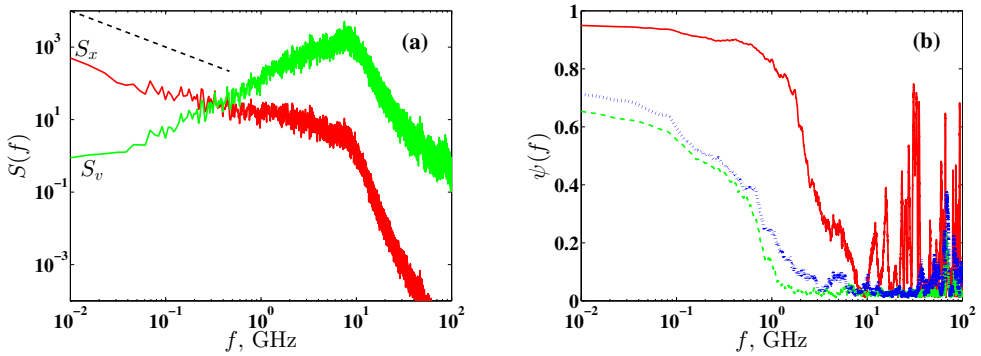

Figure 3.2: (a) The power spectra P_x of coordinate x (red colour) and P_v velocity v_x (green colour) of the ion in the site S1. The dashed line indicates $1/f$ scaling. Both axis scales are logarithmic. (b) The spectral coherence $\psi(f)$ between the z coordinate of an oxygen atom at the bottom of the site S1 and the z coordinates of three different atoms: the solid (red) line corresponds to an oxygen atom located on the same sub-unit at the top of the site S1; the dashed (green) line corresponds to an oxygen atom located on a different sub-unit at the bottom of the site S1; and the dotted (blue) line corresponds to an ion located in the site S1. The x-axis is logarithmic.

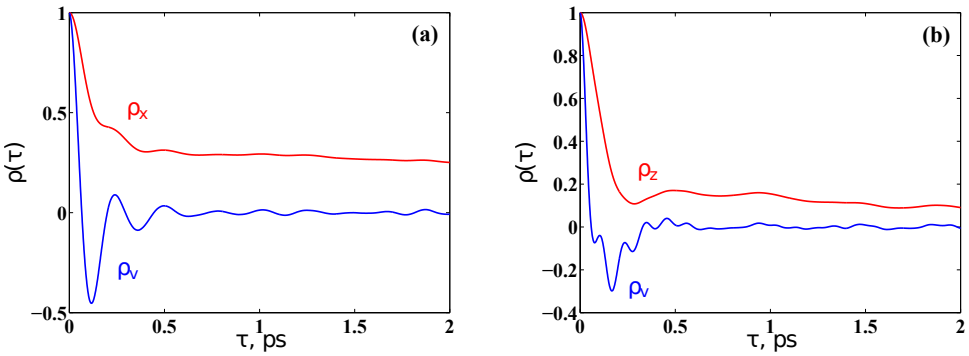

Figure 3.3: The auto-correlation coefficient of: (a) the coordinate x (red line) and velocity p_x (blue line) of the ion in the site S1; and (b) the coordinate z (red line) and velocity p_z (blue line) of the ion in the site S0.

part of the coherence function $\psi(f)$. However the coherence is not complete and there is a significant stochastic component in the low-frequency range.

$1/f$ noise or flicker noise is an ubiquitous phenomenon in nature, extensively studied in many physical systems[47], and it was recently observed in single ionic conductance.[139] In solid physics, it has been explained as a superposition of independent noise sources induced by generation-recombination processes.[47]. In biological system a general consensus exists that $1/f$ noise indicates a complex multi-scale dynamics, although a debate is still continuing.[11] Only trajectories in which ions and the filter were in meta-stable configurations have been considered in this work, therefore we suggest that the $1/f$ noise is related to the more general variability of the protein.

It is noted that the presence of the $1/f$ scaling affects the retrieval of the PMF from MD trajectories, which is accompanied by an undetermined error. This error originates from the large energy contribution from the $1/f$ noise which leads statistical measurements such as probability distributions to converge slowly. Considering the representative case of a K^+ ion a meta-stable state (site S0), mean values and variances show significant variations as functions of the time interval used to calculate them (Fig. 3.4). However, these dependences can be overcame by longer sampling, since mean values and variances eventually converge toward plateaus, as shown in Fig. 3.4, which have their roots in the definition of the CVs, i.e. in the centring of the coordinates with respect of the filter, which effectively removes the slower time-scales.

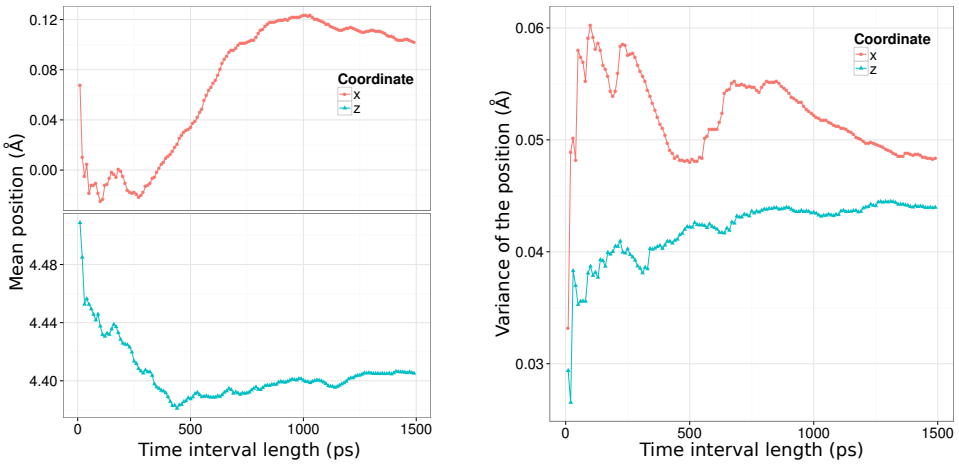

Figure 3.4: Mean values and variances of the positions of a K^+ ion in the site S0 as a function of the time interval used to calculate them (coordinates x and z centred with respect of the COM of the selectivity filter are reported). An instability is demonstrated for small lengths of the time interval which is proposed being originated from the $1/f$ noise. This instability can be overcome by means of longer sampling, because the use of longer time intervals reveals that the examined values eventually converge toward plateaus thanks to the centring of the coordinates with respect of the COM of the filter, which effectively removes the slower time-scales.

3.3 Conclusions

The conventional assumption of over-damped dynamics for the permeating ions cannot completely explain the process. Accordingly, a role for inertia should be considered. The dynamics of the selectivity filter and of the atoms bound to it (ions and water molecules) include a $1/f$ component. Although this $1/f$ component is unimportant for activated events occurring on a relatively fast time-scale, among which permeation is an example, the presence of the $1/f$ scaling leads to biased calculations of free energies. A convergence can be reached using longer sampling, with errors derived from the $1/f$ component being included in the outcomes. However, this inclusion eventually leads to overestimates of the free energies and to a loss of accuracy. A similar result is consistent with various published studies on different narrow ion channels in which the barriers obtained by MD simulations were considered overestimated.[3,51,54] An attempt to explain these unexpected barriers has been done by attributing the errors to the lack of an explicit consideration of electronic polarisation in the current implementation of the empirical force field.Patel et al.[117] Although this latter might indeed represent an additional source of error, the present work demonstrates that the presence of $1/f$ noise in K^+ ion channel can explain an overestimation of the free energies using MD models. This means that a calculation

properly performed is able to reliably deliver a qualitative picture of the PMF, whilst quantitative analysis would be associated with an uncertainty which it is difficult to determine.

Time-series analysis of MD trajectories indicates the presence of complex multi-scale dynamics of the pore which are unknown. In the next chapter the investigation will focus on the investigation of some relevant molecular factors in the region of the protein that surrounds the pore which are proposed being determinant in these dynamics.

Chapter 4

Identification of the network of residues affecting SF dynamics

4.1 Introduction

Initial studies of ion channels treated the pore as a rigid structure which were considered as being independent from the dynamics of the rest of the protein.[129] This idea has been abandoned over the past decades when it became clear that conduction, selectivity and gating are in reality closely linked to each other with structural rearrangements of the channel. The recent availability of microscopic structures has opened the way to vast research on the mechanisms underlying these linkages.[30,35,37,68,85,93,119,141,151,157] It has been found that a relevant part of the regulation of the channel activity occurs because of small rearrangements in the filter region which are responsible for C-type inactivation and modal-gating.[66,85] Although structures of putative inactive states have been proposed and a set of residues near to the pore were identified as affecting inactivation of the channel, there is still no complete understanding of mechanisms and determinants.[66,85] This is mainly due to the limitations of the available experimental tools used to investigate the phenomena, which so far are only able to provide static pictures and miss the actual dynamics of the processes.[132] Theoretical approaches have been recently employed with the aim of overcoming these limitations, in particular MD and free-energy methods.[9,64,101,129,132] Although they have proved to be a powerful tool in the exploration of the dynamics of protein and ions from an atomistic perspective, a comprehensive description has not yet been drawn, mainly because of the inherent complexities associated with the conformational variability of the pore.[20,92]

In the previous chapter these complexities were proved and it was shown that

they affect any permeation analysis of potassium ion channels, such as KcsA, because of the presence of a $1/f$ component in the dynamics of the ions. This is the result of the multi-stable dynamics of the protein governed by a complex energy landscape, which further determines the dynamics of the ions governing the equilibrium between the conductive and non-conductive states of the channel. It is worth noting that this is not the limit of the theoretical descriptions used to perform the analysis, but it arises from intrinsic features of ion channels that are, at the same time, the origins of some of the most important macroscopic properties of the current. Therefore, a deep understanding of the dynamics of the pore region becomes a fundamental prerequisite in the study of both the permeation and gating processes. This is even more important when considering that for KcsA multiple lines of evidences suggest that the conductive state is not favoured but is intrinsically unstable.[29,35]

Several experimental studies have revealed the existence in the protein sequence of molecular determinants for permeation, selectivity, and inactivation.[28–32,34–37,105] Few residues located in the region near to the pore were found to have a strong influence on the modes of the current burst, on the inactivation probability, and on the dependence of inactivation on the voltage. Among them E71, Y82, R64 and W67 were recognised as having a great impact (Fig. 1.4).[34–37] Cordero-Morales et al.[37] recently suggested the existence of a network of hydrogen bonds behind the SF formed by the triad E71-D80-W67 which is capable of stabilising the conductive conformation. Additionally, within the dynamics of the SF, a rotation which involves the peptide group linking V76 and G77 (generally referred as V76 flipping) was proposed as possibly being responsible for non-conductive states of the channel.[17,20,30] However, there is no complete picture and the mechanisms behind the strong influences of some residues revealed by the experiments are mostly unknown.

In this chapter, it will be shown that the dynamics of the pore cannot be considered to be independent from the rest of protein. Small rearrangements of a highly coupled network of residues which surround the pore induce structural rearrangements along the permeation path. The most relevant elements of this network are identified, and the central role of the aspartic acid D80, the main hub, is demonstrated. This aspartic acid residue is located at the outer entrance to the channel and acts as a *handle* of the filter. It should be noted that this residue belongs to the signature sequence motif conserved across most of the K^+ channels, suggesting a more general importance of the results.

The investigation was carried out by means of unbiased MD simulations and metaD free-energy calculations on four proteins: i) the wild type of KcsA (WT, pdb

code 1K4C[157]), and three mutants created in silico ii) Y82A which experimentally showed an enhanced probability of inactivation; iii) R64A which showed a sharp reduction of inactivation; and iv) E71A, which was resistant to inactivation and is often referred to as behaving similarly to the most conductive mode of WT.[29,35] Analysis on E71A, a system less complicated to investigate than the other proteins, revealed that rearrangements in the SF can be caused by wider structural dynamics and proved that flipping of V76 does not hinder the K^+ current by itself. The results were confirmed by the comparison of the behaviours of WT, R64A and Y82A, which made it possible to define the main elements of the highly-correlated network located behind the pore.

4.2 Results

The mutations on the simulated proteins involve the region behind the pore (Fig. 1.4). In the mutant E71A, the substitution in position 71 of a glutamic acid with an alanine residue suppresses the possibility of a direct electrostatic interaction with the aspartate in position 80. A non-inactivating protein is generated which is resistant to the collapse of the SF even at low K^+ concentrations.[30,32,35,36,125]

Two opposite effects on inactivation are generated by the mutations of residues Y82 and R64 with alanine (Fig. 1.4), respectively enhancing and reducing the probability of its occurrence. The reason behind such different behaviours is unknown. As shown in the pictures, Y82 and R64 are located relatively close to each other in the quaternary structure, with R64 directly interacting with the Y82 neighbour residue L81.

Initial simulations commenced from an observed crystal structure of the WT[157] (pdb code 1K4C, widely considered to be a closed conductive state) inserted into a POPC bilayer, with the potassium concentration in the aqueous phase 0.2 M equal to bulk concentration used in many experiments.[29,34–36,46,157] Mutants were obtained from the same crystal structure, as described in the chapter "Methods", and simulations started from an identical set-up. The KcsA channel has a tetrameric structure and the four subunits of the KcsA are referred to using capital letters A, B, C, D. The SF is described as a five-site pore[46,64] (Fig. 1.1), where ions and water move in a single-file fashion. Standard notation of the sites will be maintained: S0 to S4 starting from the outer site. The ion configurations in the SF are described in this chapter by five digits using a binary formalism (from S0 to S4, 1 will represent the potassium ion, 0 a water molecule) separated from the number of the K^+ ions in the cavity by a "+", e.g. 01010+1 means the presence of K^+ in

S1, S3 and in the cavity. All the simulations started from a 01010+1 arrangement of the K^+ ions.

Several simulations for WT were performed. The longest was $\sim$ 38 ns long, and this will be simply referred to as WT. The others will be described within the text when encountered. One main simulation was performed for each of the considered mutants: Y82A was simulated for $\sim$ 28.5 ns, R64A for $\sim$ 23 ns and E71A for $\sim$ 24 ns. None of the protein showed dramatic conformational changes, with the RMSD for the backbone from the original X-ray structure of the WT reaching a limiting value of $\sim$ 1.8 Å.

In the WT, V76 flipped temporarily few times at the beginning of the simulation until transitions of the ions 01010+1 $\longrightarrow$ 01011+0 $\longrightarrow$ 10101+0 led to the final stable conformation without any V76 residue in a flipped conformation. The most external K^+ left the SF briefly when in S0, being substituted soon after by another K^+ from the bulk. A vacancy was created in site S3, occupied by neither an ion nor a water molecule in the configurations 10101+0 and 00101+0, as observed in similar previous works.[72] Analogous sequences of events were found in other simulations for the WT, and for just one of them ($\sim$ 18 ns long) the V76 flipped conformation was found to be meta-stable for a relatively long time ($>$ 10 ns).

4.3 Analysis of E71A dynamics

When considering the SF, E71A showed a variability similar to or slightly greater than the WT, with RMSD of the SF backbone atoms from the X-ray structure lying within 1 Å for both the proteins. Interestingly, V76 flipped in subunit B of E71A ($\sim$ 9 ns) and it stabilised until the end of the simulation ($\sim$ 24 ns). From single-channel recording open probability of E71A has been proved being closer to 1 once the inner gate is opened, i.e. the SF can be considered as always being in a conductive conformation.[29,32,35]

In E71A the residues behind the pore demonstrated a clearly enhanced mobility and this was particularly so for D80 because of the absence of the E71–D80 H-bond. This enhanced variability mainly resulted in wide fluctuations of the D80 side chain towards the extracellular region, which was further promoted by the close interactions of D80 side chains (negatively charged) with the positively charged guanidino groups belonging to nearby arginines (R89 and R64). In the simulation presented in this section, strong hydrogen-bonds (*H-bond*) with D80 were created mainly with R89, while later in the text different calculations will demonstrate that R64 can interact in a similar way, both in E71A and in the remaining proteins.

Comparison of time series for the position of the D80 side chain between E71A and WT proves this enhanced mobility. These positions are reported in Fig. 4.1 using a convenient order parameter, *d73CA*, defined as the distance C_γ atom of D80 (representative for the side chain) with respect to the C_α atom of A73 (Fig. 4.2). The latter was chosen as a relatively stable reference point since T72, A73 and T75 revealed the lowest fluctuations from the RMSD of the backbone atoms of each residue from the X-ray structure of the WT. Standard deviation of d73CA for E71A, 0.86 Å, was higher than the WT, 0.22 Å, considering all the four subunits. Notably, the value d73CA $\sim$ 13.5 Å, which was very close to the value obtained by means of X-ray experiments on the WT ($\sim$ 13.3 Å), was found to be a metastable state. This suggests that the conformation of D80 found in the X-ray experiment on WT is favoured by the protein conductive structure and that the E71–D80 H-bond brings an additional strong stabilisation.

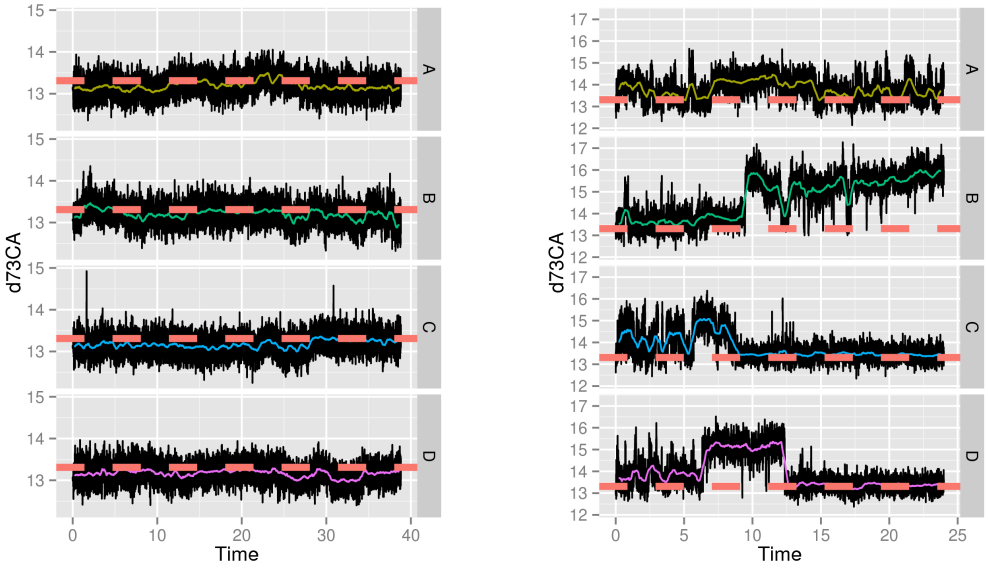

(a) Time series of d73CA for WT.

(b) Time series of d73CA for E71A.

Figure 4.1: Time series (reported in ns) of the state of D80 side chain, defined as the distance from the C_α atom of residue 73 used as a reference (d73CA, measured in Å). Dotted lines indicate the value of d73CA obtained X-ray experiments (pdb code 1K4C[157]).

The side chain of D80 showed the greatest variability in subunit B, finally stabilised to d73CA $\sim$ 16 Å. The simulation demonstrated a clear link between the motions of D80 and conformational changes of the filter, which was mainly associated with V76 flipping. This motions of D80 were found to be closely correlated with the

dynamics of the neighbouring H-bond donor residues and in particular with the creation of a H-bond with the nearby arginine R89. Statistical analyses and time series are presented in which the flipping of V76 was studied by means of the ψ dihedral angle of V76 (*psi76*), and the interactions between the D80 and R89 side chains were investigated by means of the order parameter *d89* (see sec. 2.4.1), which represents the distance between the carboxyl group of D80 and guanidino group of the closest R89. Additionally, rotation around the ψ dihedral angle of D80 (*psi80*) was considered, as well as correlations with the outermost ion (K1) in the SF, represented by means of its z coordinates centred with respect to the centre of mass of the SF (simply referred in the figures as "K1", and the SF defined as backbone atoms of residue 74 to 78).

Analysis revealed highly-correlated dynamics. The time series for d73CA, psi76, d89, D80psi and K1 of subunit B are shown in Fig. 4.3, while Fig. 4.2 reports the superposition of relevant snapshots from the simulation and the description of the order parameters. The noise obscured the trends in some cases, especially for d73CA, therefore only the smoothed trajectories are shown (moving averages procedure was applied with windows length = 77 ps). The part of the simulation before the flipping of V76 (the first ns have been ignored as relaxation) was subdivided into three sections : i) *before the creation of D80-R89*, up to 2.5 ns and values of d89 $\sim$ 6.5 Å (Fig. 4.3, blue rectangles); ii) *creation of D80-R89*, between 2.5 and 5.9 ns and fluctuations of d89 towards lower values; and iii) *after the creation of D80-R89* and before V76 flipping, between 5.9 and 9 ns with d89 $\sim$ 4.7 Å and D80-R89 H-bond length $\sim$ 3 Å (Fig. 4.3, green rectangles). The presence of the H-bond caused a small drift in the mean value of d73CA, from $\sim$ 13.5 to $\sim$ 13.8 Å, which was clearer from comparison of the distributions of d73CA in the sections *before* and *after* its creation (Fig. 4.4, two-sample Kolmogorov-Smirnov test's p-value $< 2.2 \cdot 10^{-16}$). The final strengthening of the H-bond was accompanied by a slight distortion of the TYGVG backbone structure (Fig. 4.2, green to coloured), mainly characterised by a rotation of $\sim$ 50 degrees of psi76 which can be defined as a *partial flipping* of V76. This appears to be a key event driven by the tendency to form the D80–R89 H-bond. Interestingly, the partial flipping was soon followed by a small inward movement of K1 to a position between the sites S1 and S2 (Figs. 4.3 and 4.2), accompanied by an adjustment of the water molecule in S2. A similar sequence, a change in the state of D80 side chain that caused a transition of an ion in the SF, reveals an important feature of KcsA to which we will return in this work: the existence of a strong link between the permeating ions and the residues behind the pore.

Similar conclusions were obtained from the three and four-dimensional scatter

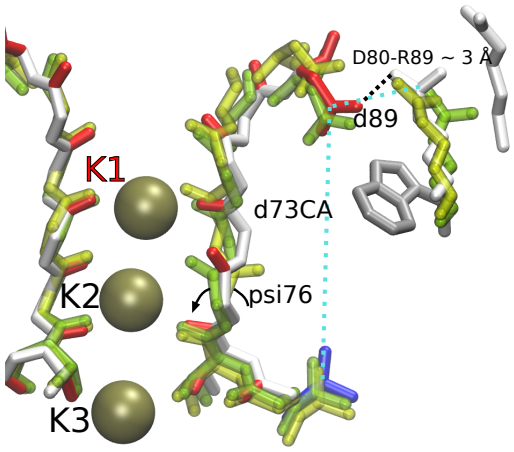

Figure 4.2: Superposition of relevant snapshots from the simulation of E71A which shows the link between the creation of the D80-R89 H-bond and rearrangements in the filter structure, which include the flipping of V76. The green drawing is the initial configuration after 1 ns of relaxation; the coloured drawing is a snapshot of the structure with D80-R89 H-bond formed and V76 in the partially flipped state; the yellow drawing is the final configuration with V76 in the flipped conformation. The relevant order parameters used in the statistical analyses are defined as follow: i) d73CA, the position of D80 side chain with respect of the C_α atom of residue 73 used as a stable reference; ii) d89, the distance between D80 and R89 side chains defined by the C_γ and C_ζ atoms respectively; iii) psi80, the *psi* dihedral angle of residue D80; iv) K1, the "z" component of the position of the outermost ion bound to the SF, centred with respect of the COM of the SF.

plots of the transitions. The third and fourth dimensions are the time, represented by means of a colour gradient (from blue to red, Fig. 4.5). These analyses allowed us to partially overcome the loss of information derived from the smoothing procedure applied to the time series. For the sake of clarity only the region prior to the V76 flipping is shown in the scatter plot of d89 against d73CA. As expected, the position of the D80 side chain was uncorrelated to R89 fluctuations *before* the creation of the D80–R89 H-bond, as demonstrated by the d89-d73CA scatter plot (blue clouds). Correlations arose as the time advanced (light blue) *during* the creation of D80-R89 (Fig. 4.5 A). In this period, D80 and R89 side chains intermittently approached, fluctuating between the presence and the absence of the D80–R89 H-bond, i.e. d89 between $\sim$ 4.7 Å and $\sim$ 6.5 Å and d73CA between $\sim$ 13.5 and $\sim$ 13.8 Å. These fluctuations are mostly suppressed by the smoothing procedure in the time series. The strengthening of D80–R89 H-bond was allowed by the partial flipping of V76 (Fig. 4.5 B) which appears in the scatter plots as a small cloud for psi76 $\sim 0°$ (light

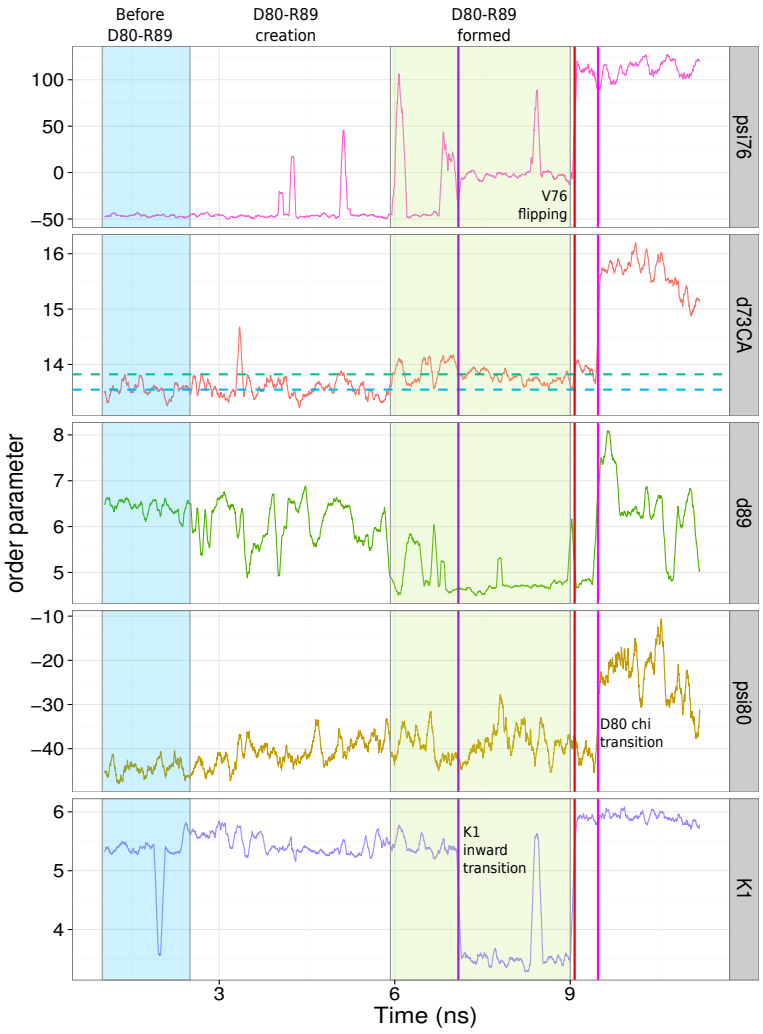

Figure 4.3: Time series for the influence of the dynamics of D80 and R89 on the selectivity filter and the dynamics of the permeating ions in E71A. Time series for subunit B are reported. The coloured lines represent the smoothed trajectories (moving average procedure applied, with windows 0.25 ns long). The definition of the order parameters are described in Fig. 4.2, the units for d73CA, d89 are K1 are Å, the units for psi76 and psi80 are degrees. The reported sequence demonstrates that the creation of a D80–R89 H-bond can generate a stress on the backbone of the TVGYGD sequence that results in small conformational rearrangements. These backbone rearrangements are showed only for the residues V76 (initially a partial flipping, followed by a complete flipping) and for D80. The latter caused the breaking of D80-R89 removing the stress on the filter structure.

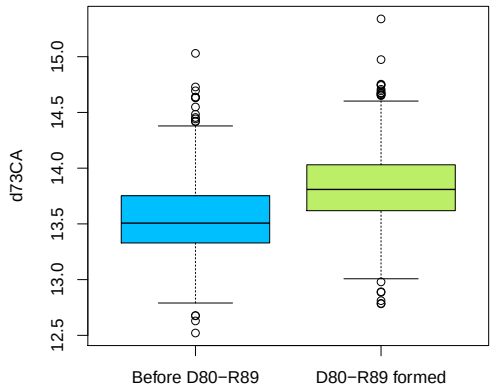

Figure 4.4: Distributions of d73CA (Å) in E71A depending on the state of D80–R89 H-bond: before D80-R89 H-bond is formed (between 1 and 3.5 ns) and just after its formation (between 6.5 to 9 ns). The first distribution is positively skewed because interactions were noticeable between the two side chains quite soon after the simulation started. The analysis demonstrates that the creation of the bond change the state of D80 side chain, which is proposed as the cause of a stress on filter structure which led to structural rearrangements.

green). Both time series and scatter plot reveal the instability of the conformation characterised by D80–R89 H-bond, a partial flipping of V76 and K1 located between S1 and S2, which resulted in a short life-time. The system soon reacted with a complete flipping of V76 (red vertical line in the time series, Fig. 4.3, and Fig. 4.5 C), stabilised by the water molecule in S2 H-bound to the amino group of G77. Substituting the oxygen of V76 backbone, this water molecule re-established the square anti-prism geometry of the coordination sphere of K1, which moved back to its original position S1. Hence, correlated motions of D80 and R89 side chains associated with the creation of a strong H-bond resulted in transitions in the central region of the pore, being the rearrangements delivered by the rigid structure of the SF backbone. It is important to note that the path described for a meta-stable V76 flipped configuration in E71A must not be considered as unique, but just one among many available.

The movement of the D80 side chain towards the extracellular side finally broke the H-bond (Fig. 4.2, coloured to yellow), thereby restoring the initial uncorrelated motions of the D80 and R89 side chains. The outward transition of D80 was characterised by a rotation of ψ dihedral angle of D80, psi80, from ~ -43 to $\sim -22°$. Scatter plots do not show this additional degree of freedom but reveal in-

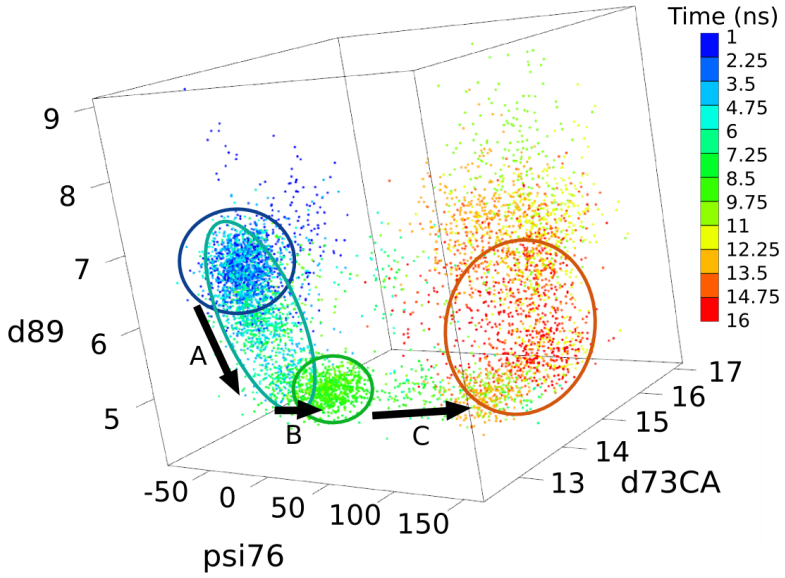

Figure 4.5: The creation of D80–R89 H-bond was related to structural rearrangements of the SF, associated with the flipping of V76, in the simulation of E71A. This is showed by means of a four dimensional scatter plot in which the extra dimension is the time, represented as a colour gradient. The three order parameters represent: i) the position of D80 side chain with respect of the C_α atom of residue 73 used as a stable reference, both the residues belonging to subunit B (d73CA, Å); ii) the distance between the side chain of D80 from the subunit B and the side chain of R89 from the neighbouring subunit C (d89, Å, defined by the C_γ and C_ζ atoms respectively); iii) the *psi* dihedral angle of residue V76 of subunit C (psi76, degrees). Three main step can be recognised: A) the creation of D80–R89 H-bond: a correlation arose between the movements of D80 and R89 side chains because the intermittently approached forming and disrupting the H-bond. B) The partial flipping accompanied the temporarily stabilisation of the D80–R89 H-bond. C) The complete flipping of V76, as a consequence of the stress induced by the D80-R89 H-bond on the backbone of the TVGYGD sequence.

stead the uncorrelated motion of D80 and R89 in the last part of the simulation (red cloud). Summarising, interactions between the D80 and R89 side chain generated a structural instability in the pore region which caused complicated sequences of small rearrangements until new stable state was reached. These rearrangements involved the filter and the ions bound to it.

Flipping of V76 was also temporarily observed in subunits A and C during the simulation, but without the concurrent formation of the D80–R89 H-bond and the associated rearrangements, the configurations obtained did not demonstrate high stability and had only a brief existence (< 2 ns). This apparent asymmetry in the behaviour of the different subunits can be explained by considering the protein as a whole with its own global motions. These induce slow fluctuations in relative positions of the neighbouring D80 and R89 side chains, which themselves belong to different protein domains. The coupling between these slow motions and the faster variability of the side chains can create the temporary asymmetry noticeable among the subunits.

4.4 Permeation test on V76 flipped conformation

The flipping of V76 has been reported in several published works[17,20,30,45,121] and it has been suggested as being able to generate a non-conductive conformation responsible for the inactivation of the filter (C-type inactivation) or for modal-gating (flicker mode).[20,30] Any conformation in which the G77-V76 peptide group is rotated with respect to the putative conductive X-ray structure has been referred to as "V76 flipped". A structure of E71A in which D80 is completely exposed to the bulk, usually referred to as "E71A D80-flipped", was determined and was found associated with various structural rearrangements of the filter structure with include V76 in the flipped state.[35] Our simulations demonstrated that in reality V76 flipped states are easily reached in the E71A. According to single-channel current measurements, open probability of E71A is close to 1,[29] and this leads to the hypothesis that the flipping of V76 is unable to generate non-conductive closed states compatible with C-type inactivation or even flicker mode unless stabilised by additional more general rearrangements, because they involve closed states with duration on the ms time scale[29]). The conductivity of the V76 flipped conformation for WT and E71A were tested by means of MD simulations to confirm this hypothesis.

Simulations were initiated from the last configurations obtained from simulations of WT and E71A in which V76 flipped appeared as meta-stable states with life time longer than 10 ns. Outward transitions were induced by swapping the position

of a K^+ ion from the bulk with a water molecule in the cavity. In this way, because of the closed state of the channel, the electrostatic repulsion of the two ions in the cavity was capable of promote the permeation. Simulations were preceded by 10^5 steps of minimisation. Two simulations were performed for the WT with different initial velocities and one for E71A.

Both E71A and WT proved to be conductive and the flipped state of V76 to be reversible within few ns in the presence of a permeation. We suggest, and will demonstrate in the following chapters, that reversibility of V76 flipping depends on rearrangements in the region behind the pore. The analysis additionally confirmed the possible occurrence of vacancy during permeation. The topic will be discussed in more in detail in Chap. 6.

4.5 Comparison of WT, Y82A and R64A

Investigations of E71A showed that correlated motions in the region behind the pore are capable of inducing structural rearrangements along the permeation path affecting the dynamics of the ions. At the same time they revealed that flipping V76 is not sufficient to generate long-lasting non-conductive states in KcsA. Similar mechanisms are demonstrated more generally by means of simulations on channels that show a greater variability in the current than E71A, including the WT. The other two proteins that were investigated were the deep-inactivating Y82A and R64A, which is characterised by a reduced inactivation probability.

4.5.1 Analysis of dynamics of R64A and Y82A

None of the simulated proteins WT, R64A, Y82A showed dramatic transitions compatible with inactivation. In the putative conductive structure of KcsA, the triad E71-D80-W67 is linked by H-bonds,[37] which has been suggested as stabilising the conductive state.Cordero-Morales et al.[37] During the simulations these linkages were broken in different subunits of all the proteins: i) a few brief disruptions in two neighbouring subunits (B and C) in the WT; ii) a temporary but relatively long ($\sim$ 10 ns) break for one subunit in R64A; and iii) several breaks in two neighbouring subunits (A and C) of Y82A. The simulation of the latter protein ended with the linkages stably broken in those two subunits, while the simulation of WT ended with the linkages broken in one subunit (Fig. 4.7). The fact that the E71–D80 H-bond broke in all the simulated proteins suggests that this simple event is not sufficient to inactivate the channel.

Linkages behind the SF demonstrated a clearly enhanced variability in Y82A.

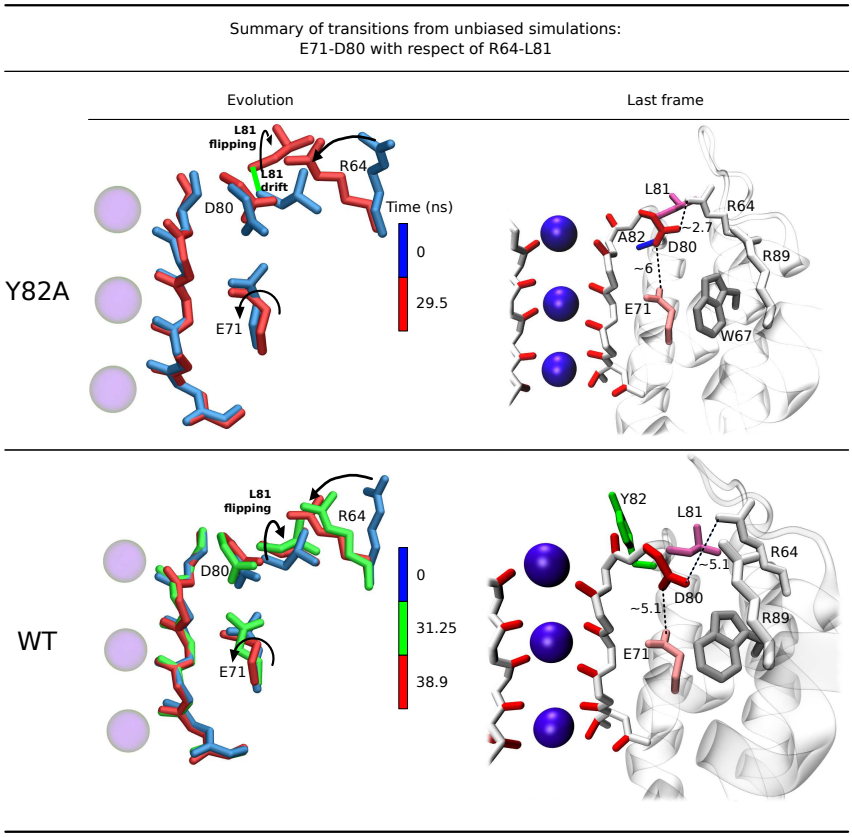

Figure 4.6: Relevant snapshots from the simulations of WT and Y82A. The conformations are superimposed with respect of the SF (the backbone atoms of resides 74 to 78). The figures reveal the interconnection between the dynamics of L81 and the possible arising of strong interactions between D80 and R64. These interactions, which can eventually evolve into strong H-bonds, are able to cause the disruption of the linkages between the E71-D80-W71 triad.

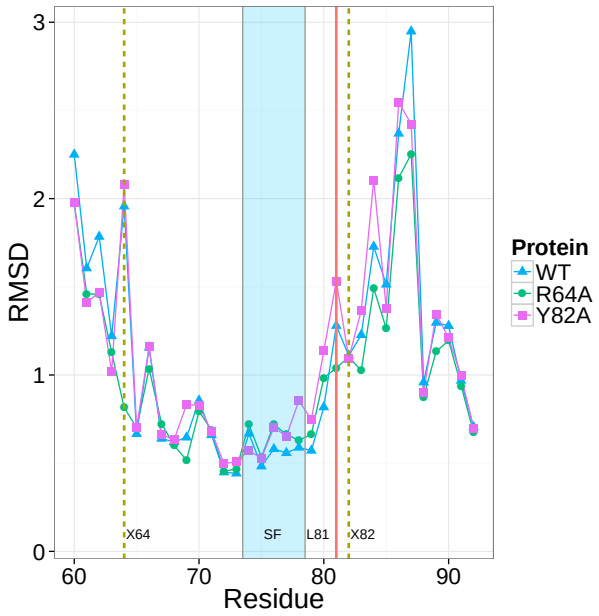

Figure 4.7: Root mean square displacement (RMSD, Å) computed for the residues in the region of the SF (residue from 60 to 92), from the X-ray structure of the WT (pdb code 1K4C).

The main cause for this was identified in the strong interactions between the D80 and R64 side chains that eventually lead to the creation of strong H-bonds (length $\sim$ 2.7 Å, Fig. 4.6). Similar to the process which involved D80 and R89 seen in E71A, the guanidino group of the arginine R64 started by approaching the D80 carboxyl group in Y82A, finally creating tight H-bonds. These strong R64–D80 interactions eventually promote transitions in the state of the D80 side-chain which cause the E71–D80 and W67–D80 H-bonds to break. This process was observed in two subunits, both in WT and in Y82A (Fig. 4.6, evolution), but in the latter case it occurred with fastest kinetics. Breaks of the E71–D80 H-bond caused by interactions between R64 and D80 were preceded by a rotation of the E71 side chain in WT (Fig. 4.6, evolution, green), which was not seen in Y82A, and was accompanied in both proteins by the bending of the same side chain, which pointed towards the centre of the SF (Fig. 4.6, evolution, red). This sequence of events is not possible in R64A, where R64 is substituted by an alanine.

An additional transition of D80 was observed in Y82A associated with the enhanced conformational variability of the region behind the pore. This involved the partial rotation of the side chain around the $\chi 1$ dihedral angle, a *partial flipping* (Fig. 4.8). This enhanced D80 mobility distinguished the deep-inactivating mutant Y82A from WT and R64A.

Configurations of the SF with V76 flipped were seen transiently during all the simulations, in some cases associated with the rearrangements in the region behind the pore. However, they were transient and outwards transitions of the ions were seen in all the proteins despite the variability of V76. This further supports the idea previously discussed that the flipping of V76 needs further stabilisation to create non-conductive states of the channel.

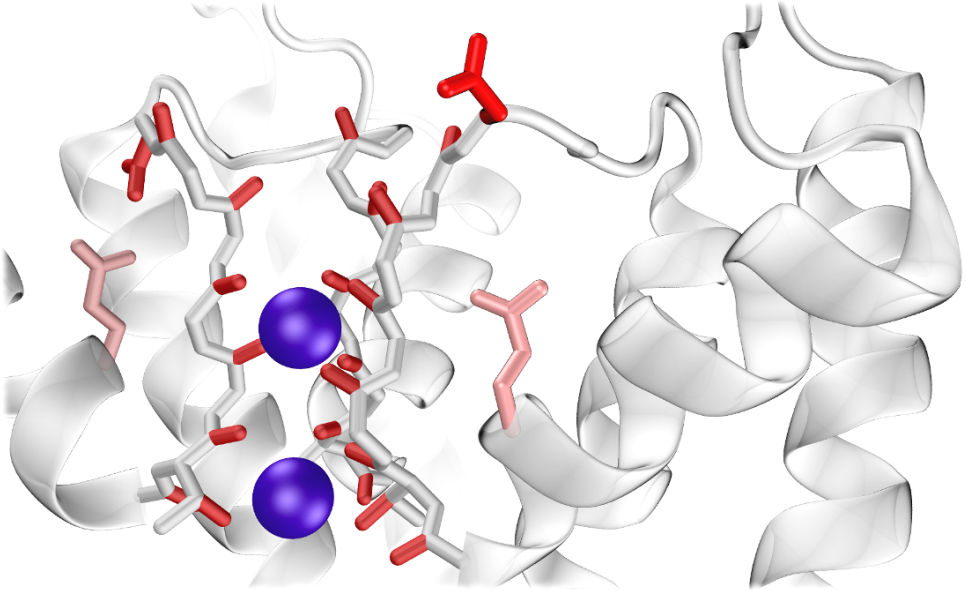

Figure 4.8: Flipping of D80 side chain observed in the simulation of Y82A.

Although R89 arginine is believed to induce analogous transitions, its influence appeared strongly reduced in WT, R64A and Y82A with respect to E71A because of the presence of the strong E71–D80 bridge that limits the mobility of D80. In this case, the arginine R64 demonstrated a more evident influence on the dynamics of the pore region than R89.

4.5.2 R64-L81 interplay

An explanation for the different kinetics of the R64 motions in the WT and Y82A can be derived from the interplay between R64 and the leucine in position 81 (L81). L81 is adjacent to R64 in the quaternary structure and it precedes the mutated residue X82 in the amino acid sequence. Simulations demonstrated that conformational changes of L81 are able to hinder or facilitate the creation of a D80-R64 H-bond (Fig. 4.6). This change can be described as a *flipping* of its side chain, i.e. a rotation around the $\chi 1$ dihedral angle. In Y82A, the presence of the non-bulky alanine neighbouring L81 allows small readjustments in the region that facilitates L81 motions,

including the flipping of its side chain. In the WT, these additional readjustments are strongly reduced because of the presence of the bulky Y82 side-chain, leading to higher barriers for correlated transitions of L81 and R64.

The L81/R64 interplay can be easily seen by means of the relevant configurations assumed by Y82A and WT during the simulations reported in Fig. 4.6 (evolution). The structures of the protein are superimposed with respect to the heavy atoms of the SF. In addition to the side chain flipping, the whole L81 residue slides slightly laterally in Y82A and this movement, which involves the protein backbone, facilitates R64 and D80 approaching. A similar backbone movement was far less prominent in the WT, and the flipping of L81 appeared as the main variation associated with the R64 variability. Additionally, coupled transitions involving L81 and R64 were so fast in Y82A that intermediate conformations could not be distinguished, whereas a defined intermediate state was identified for the WT (green in the figure), characterised E71 $\chi 1$ angle flipped ~ 120 degrees.

Analysis of the root mean square displacements (RMSDs) further help to understand the complicated behaviour of the pore region. The RMSDs were computed for each residue and averaged over the whole trajectory for each protein, using the X-ray structure of the WT as reference. This analysis gives a quantitative comparison of the deviation of each residue from the structure of the WT used to construct the system. Fig. 4.7 reports the RMSD for the residues from 60 to 92. Deviations are generally relatively low, especially in the SF region, with the exception of W87 and its neighbouring residues. The residue W87 is in direct contact with the lipid bilayer and plays a role in the stabilisation of the protein in the membrane, thus its fluctuations directly depend on the slow diffusion of the lipid molecules.[102,142] Residues in position 64 showed similar RMSD for WT and Y82A that was dramatically reduced when the arginine was substituted by alanine (R64A). We can safely interpret the result with the existence of a strong variability of the arginine side chain. At the same time an increment in the extent of L81 deviations is noticeable moving across the proteins: R64A $>$ WT $>$ Y82A. Low RMSD in R64A suggests a coupling between R64 and L81 variability, the latter being enhanced by the R64 motions via sterical interactions. On the other hand, the difference between WT and Y82A are related to the backbone movements previously described. Motions of R64 and L81 side chains induce readjustments in the amino acid sequence L81-X82-P83-V84 which can be roughly described as pivoting around the residue in position 82 (tyrosine in the WT, alanine in Y82A). These readjustments are wider in Y82A than WT, where they are limited by the bulky tyrosine, and the pivoting is the origin of the invariant RMSD for X82 among the proteins opposed to the clear changes of the

surrounding residues that follow the inactivation probabilities R64A > WT > Y82A.

In any event, even allowing for sightly increased readjustments involved in the dynamics of Y82A, L81 flipping is the main event associated with the creation of D80-R64 interactions. Transitions of P83 and V84, further away from the region of interest, appear as secondary adjustments to transitions of L81. We noted that the dynamics that involve the backbone of the sequence L81-X82-P83-V84 may also directly affect D80, mainly in Y82A, representing an additional element which is able to affect the stability of the linkages among the triad E71-D80-W67.

An additional residue showed an interesting RMSD trend across the proteins: S69. A hypothesis about the origin of a such behaviour is that S69 belongs to the same helix as R64, and can therefore be affected by its motions. However, as yet a complete explanation remains unclear.

4.6 Energetics of the arginine motions

Free-energies underlying motions of the arginines R64 and R89 were computed in order to identify the most probable states and investigate the origins of the apparent different kinetics of L81/R64 interplay in Y82A and WT.

4.6.1 FES for R64 dynamics

A FES for L81/R64 interplay were estimated as functions of two CVs: i) *C64*, i.e. the distance of the R64 guanidino group (defined by its C_ζ atom) from the centre of mass of the filter (atoms N, C_α, and C of residues from 74 to 78) and ii) *chi81*, i.e. $\chi 1$ dihedral angle of L81 residue. The former CV was chosen because the arginine side chain forms strong H-bonds with D80 the closer it gets to the filter.

Y82A

In the simulation of Y82A, R64 and L81 performed several transitions. Therefore an estimation of the FES was directly computed from the sampled distributions, as described in Sec. 2.2.1 Sampling was improved by combining the data from all four subunits, which corresponds to $\sim$ 114 ns. The FES thus obtained is not likely to be completely accurate and will be biased toward the initial configuration (the configuration of the X-ray structure of WT used to build the mutant) because of insufficient sampling. In any event, it was considered satisfactory for the scope of this work in order to obtain approximate heights of the barriers and identify the location of the relevant minima. The FES is reported in Fig. 4.9.

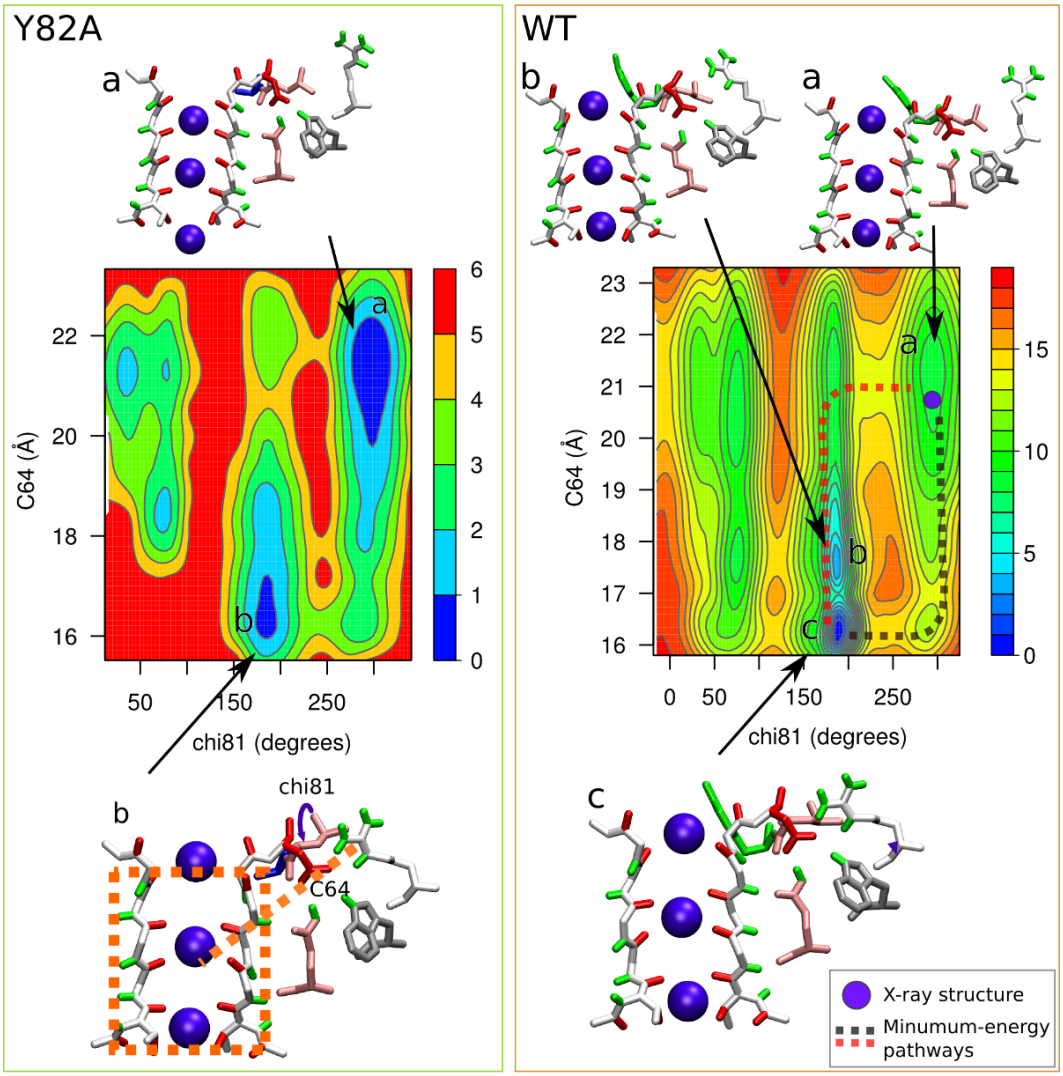

Figure 4.9: Estimate of the FES for the interplay between R64 and L81 and representative conformations of the protein in: i) Y82A, computed from unbiased simulation, and ii) WT computed via well-tempered MetaD approach. The CVs, showed in the figure, are: i) C64, the distance of the R64 guanidino group (defined by its C_ζ atom) from the centre of mass of the filter (atoms N, C_α, and C of residues from 74 to 78) and ii) chi81, the $\chi 1$ dihedral angle of L81 residue. Energy in kcal/mol, distances in Å, lines in the contour plots are drawn every 1 kcal/mol.

Two main minima are noticeable: the broad minimum "a", corresponding to the configurations closest to the initial configuration and the X-ray structure of the conductive state (C64 $\sim$ 21.5 Å and chi81 $\sim$ 298°); and the smaller minimum "b", corresponding to the L81 side chain in the flipped conformation and the R64 guanidino group located close to the SF and D80 (C64 $\sim$ 16 Å and chi81 $\sim$ 185°). The existence of these two minima confirms the analysis of the trajectories and the role of L81, which acts as a gate capable of obstructing the path for R64 leading towards D80 and the creation of H-bonds.

WT

The estimate of the FES for L81/R64 interplay in the WT from the simulated trajectories was poorer than in Y82A, because the slower kinetics of the process resulted in fewer transitions of R64 and L81. This was overcome by using well-tempered metaD to estimate the FES (Sec. 2.2.3, $\Delta T = 1200$ K and integration step 2 fs for a total sampling of $\sim$ 122 ns). The initial configuration was obtained from the unbiased simulation WT ($>$ 25 ns of relaxation) with K^+ ions arranged 10101+0 in the SF and a vacancy in S3. During the sampling transitions of no K^+ ions were seen in the SF.

The computed FES is reported in Fig. 4.9. The main differences are the heights of the barriers, higher in the WT than in Y82A, and this can explain the slower motions of R64 observed in the simulations of the WT.

The position of the minima confirms that the conformation of the L81 side chain determines the stability of the different configurations of R64: *non-flipped* conformation favours states for R64 that are far from D80 and close to the one found in the X-ray experiments (minimum "a", chi81 $\sim$ 295°), while *flipped* conformation promote the R64's approach towards D80 (chi81 $\sim$ 185°). Two minima ("b" and "c") are found in this region: the absolute minimum of the FES, which corresponds to R64 H-bound to D80 (minimum "c", C64 between 16 and 17 Å) and a neighbouring small minimum, which corresponds to the intermediate state towards the creation of the D80–R64 H-bond described in Sec. 4.5.2, which was observed in the unbiased simulations (minimum "b", C64 between 17 and 18 Å). The presence of this additional minimum with respect to the Y82A's FES probably depends on the lower mobility of sequence L81-X82-P83-V84 in the WT.

The interplay between R64 and L81 mainly follows two low-energy paths "a $\leftrightarrows$ b" according to the FES. The first path is highlighted by a magenta dotted line in the figure and consists of an initial flipping of the L81 side chain (chi81 $\sim$ 298° $\rightleftarrows\sim$ 185°), followed by subsequent transitions of R64 along a downward

gradient towards the SF. The second path is highlighted by a black dotted line and involves the initial creation of a relatively unstable D80–R64 H-bond which is finally stabilised by the flipping of the L81 side chain. Both paths require similar energies of between 5 and 7 kcal/mol, even if the second path appears to be more accessible because of the presence of an intermediate state that makes the higher barrier $4-5$ kcal/mol.

Interestingly, the absolute minimum of the FES did not contain the conformation obtained by X-ray experiments. Analogous result was also obtained for R89, which is described later. At this point, it is useful to bear in mind that arginines are charged residues which are exposed to the ions from the bulk. Radial distribution functions (RDF) for Cl^- ions from the atom C_ζ of R64 and R89 reveal the strong interactions between the arginines and the negatively charged elements in the outer bulk (Fig. 4.10). Variations in the concentration of these elements can possibly modify relative depths of the minima. In our simulations the ion concentration was chosen to reproduce a common experimental set-up for the ionic concentration in the bulk ($[K^+] = 0.2$ M).[29,34–36,46,157] It is very difficult to determine the actual ionic strength close to the membrane in the real system, particularly when an electrochemical gradient across the membrane is present. Different ionic strengths from those considered in the simulations may eventually lead to the stabilisation of the X-ray configuration for R89 and R64. In any event, the main feature of the cooperative motions between the R64 and L81 residues will be retained.

4.6.2 FES for R89 dynamics

The dynamics of the arginine R89 was investigated in the WT. The FES was directly computed from the trajectories as a function of the CV *C89*, i.e. the distance between the C_ζ atom of R89 guanidino group and the centre of mass (COM) of the SF. The data from all the four subunits from two different simulations were used yielding a total sampling of 224 ns.

The analysis confirmed that in a similar manner to R64, the side chain of R89 creates a strong H-bond with D80 (length ~ 2.7 Å) when closer to the filter. The barrier for the process was found to be relatively low (~ 1 kcal/mol), hence the estimation of FES was considered to be satisfactory. Additionally, the analysis revealed a dependence of the FES on the position of the K^+ ions in the filter. Fig. 4.11 shows sections of the FES for three relevant ion configurations 00101, 01010, 10101. The two minima corresponding to the presence and the absence of the D80–R89 H-bond are clearly recognisable, respectively at C89 ~ 15.7 Å and C89 ~ 17.1 Å. The probability of the H-bond forming is increased when the outermost sites are

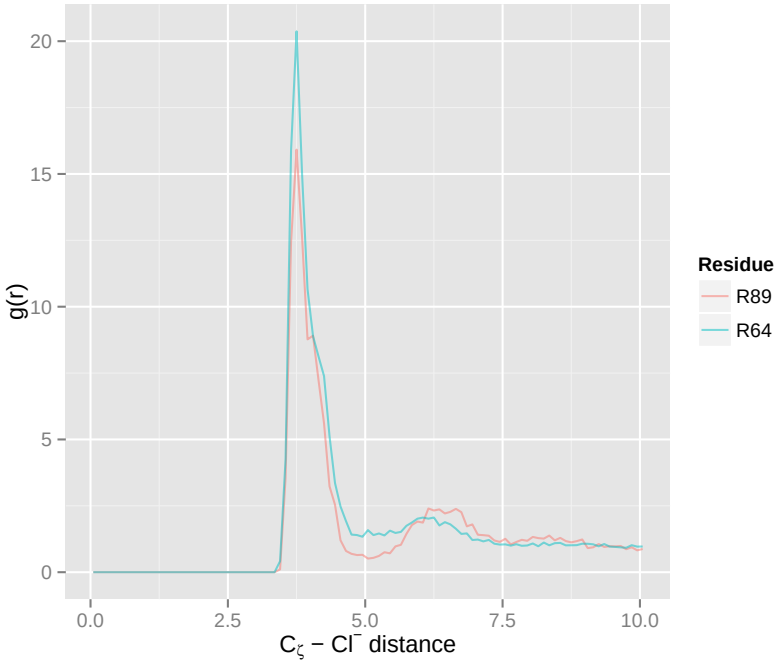

Figure 4.10: Radial distribution functions (RDF) for Cl^- ions from the atom C_ζ of the arginines R64 and R89, computed from an unbiased simulation of WT.

not occupied by any K^+ ions, with a maximum for the occupancy of the SF 00101. Similar configurations, and thus R89–D80 H-bonds, must have a higher probability in the case of a low concentration of K^+ in the bulk, which is the condition when the inactivation probability is higher. Further in this work it will be shown that a more general dependence exists between the conformation of the region which surrounds the pore and the position of the K^+ ions in the filter.

The double-well free-energy profile which depends on the ion occupancy controlling the dynamics of R89 suggests that the arginine may play an additional role in the destabilisation of the SF through the interaction with D80. However, the low barriers also suggest that the destabilisation delivered by the only R89 might not have a dramatic impact in the WT. It is suggested that R89 has a more relevant role in collaborative processes with R64, as will be demonstrated in the following sections and as proved by experimental evidence.[105]

4.7 1d FESs for d71

The role of arginines in the destabilisation of the triad E71-D80-W67 was further investigated by also considering the influence of the position of the K^+ ions in the

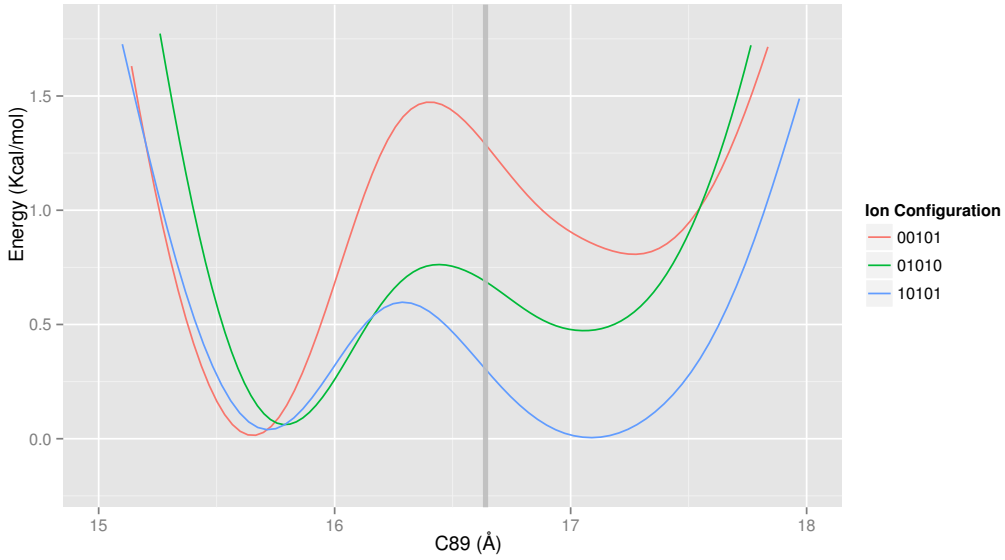

Figure 4.11: Estimate of the FES for the dynamics of R89 in the WT, computed as a function of the distance C89 (the distance between C_ζ atom of R89 and the centre of mass of the SF) for the different conformations of the K^+ ions in the SF. Energy in kcal/mol, distances in Å. The vertical grey line show the value of C89 obtained from the X-ray experiments.[157]

filter. Our simulations suggest that the E71–D80 H-bond is the key element of the triad. This linkage has been suggested by different authors as having the key role in the stabilisation of the conductive structure and as being linked to the inactivation process.[30,32,35,37,119] Free energies that govern this strong interaction were computed by means of well-tempered metaD as a function of the distance between D80 and E71 side chains (*d71*), defined by the distance of the C_γ atom of D80 (the carbon of the carboxyl group) and the hydrogen bond (H-bond) donor oxygen belonging to the E71 carboxyl group (see sec. 2.4.1). The relevant parameters for the calculations were chosen as follow: i) $\Delta T = 1500$ K, ii) $w_0 = 0.005$ Kcal/mol (see Sec 2.2.4). The influence of R64 and occupancy of the SF were taken into account by explicit sections of the FES being computed by varying the L81 side chain conformation, which determines the most favourable state for R64, and the positions of the K^+ ions. R89 and W67 were not specifically considered even if they participate in defining the free-energy, their influences having been averaged over the course of the sampling.

All the starting configurations were obtained from the long unbiased simulation previously described. Configurations of L81 were restrained with harmonic potentials ($K_{spring} = 5$ kcal/mol degree^2) centred in two positions according to

the FES reported in Fig. 4.9: i) *L81 non-flipped*, chi81$_0$ = 297.6°; ii) *L81 flipped*, chi81$_0$ = 185°. Side chain of R64 fluctuated far from D80 in the case of the L81 non-flipped conformation, whereas it could be found in two meta-stable positions, "b" and "c" in Fig. 4.9, when L81 is flipped. From preliminary extensive tests R64 in the former position "c" was seen to be having the greatest effect on the D80 state.

The conformations of K^+ ions in the SF were chosen in order to avoid additional restraints that might affect the dynamics of the pore. Two were selected: 10101+0 and 00101+0, both having a vacancy in S3. These two were found to be the most stable (meta-stable) on long simulations, reducing the probability of undergoing transitions. During our biased test simulations, conformations 01010+1, 00101+1 and 01011+0 always evolved into 10101+0, with a vacancy in S3.

Four sections of the FES were computed and they are shown in Fig. 4.12. The energy required to break the E71-D80 H-bond is strongly dependent on the position of the R64 side chain. Its influence greatly increased the probability of the H-bond breaking, producing low barriers up to 2.5 Kcal/mol (L81 flipped and 00101+0 SF occupancy), even 5 Kcal/mol lower than the case when R64 was not involved. The configuration of the ions had less dramatic effects on the height of the barriers, but it strongly affected the presence and the shape of the minima once the bond was broken (d71 $\geq$ 4.5 Å).

Barriers for reverse transitions were found to be low, suggesting that long-lived non-conductive states require additional rearrangements than the simple breaking of the E71–D80 H-bond.

4.8 D80 state and the dynamics of the SF and the ions

The dynamics of the region behind the pore were further investigated in order to demonstrate the direct influence on the permeation path. Simulation on E71A demonstrated that the rearrangements of the aspartic acid D80 can be delivered to the TVGYG sequence. A targeted simulation was developed to demonstrate that this is also valid for the WT. In the latter case, the state of D80 was shown as being influenced by arginines R64, which are capable of promote relatively wide transitions. The simulation was performed on a protein conformation in which the probability of these events occurring was enhanced by the maximisation of D80–R64 interactions. This conformation was obtained based on the FES shown in Fig. 4.9. An equilibrated conformation ($\sim$ 6 ns) was relaxed for 20 ps, restraining every L81 residue in the flipped conformation (harmonic potential with a spring constant of 24 kcal/mol degree^2 and centred on 185°). An additional restraint on χ1 dihedral angles of R64

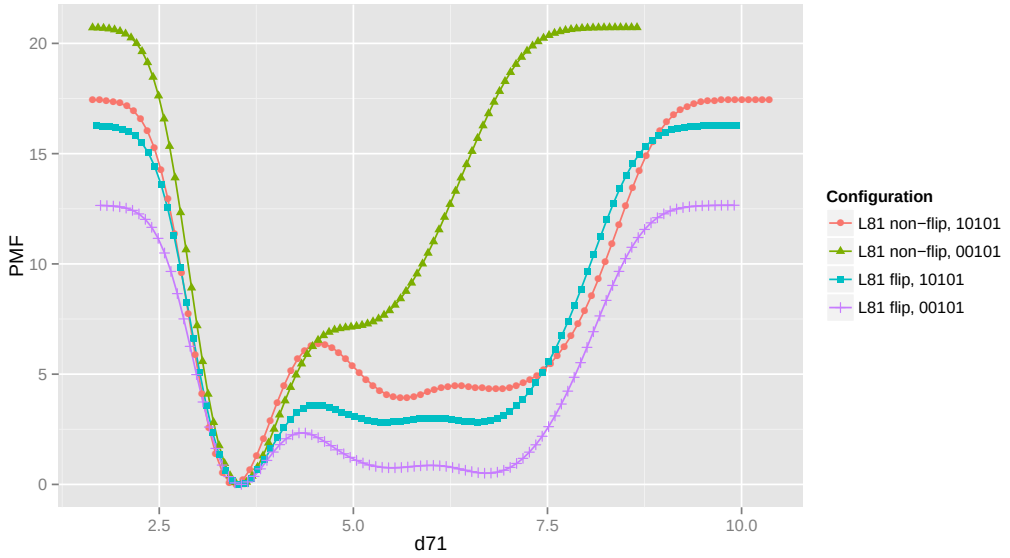

Figure 4.12: Estimate of the free-energy as a function of the distance d71 (FES), the distance between side chains of D80 (defined by the C_γ atom) and E71 (defined by the H-bond donor oxygen belonging to the carboxyl group). Different FESs are computed with respect of different conformations of the K^+ ions in the SF, 10101+0 and 00101+0, and conformations of the residue L81, flipped and non-flipped. Energy in kcal/mol, distances in Å.

residues was applied to speed up the process (spring constant 20 kcal/mol degree^2 centred on $-160°$), even if a few tests showed that this was not strictly necessary. Further 25 ps of relaxation were performed without any restraint. The R64 guanidino groups moved towards D80, approaching the closest minimum "b" in the FES (Fig. 4.13b). The total length of the productive sampling was $\sim$ 45 ns.

From the beginning SF showed an increased variability with respect to the calculations originating from the X-ray structure. The R64 influence promoted long breaks of linkages between E71-D80-W67 ($\sim$ 17 ns) for subunit C and brief disruptions in all the remaining subunits. The long break involved a large number of small rearrangements but can be summarised as: the initial break promoted by R64 caused an outward movement of D80 toward the extracellular side (Fig. 4.13b) which was accompanied by the stretching of the TVGYG sequence and the flipping of V76.

Scatter plot in Fig. 4.13b shows for subunit C the evolution of the system in the conformational space in the first 22.5 ns, the period of time in which most of the relevant transition occurred. Three order parameters were considered: i) d73CA, the position of D80 side chain (see sec. 2.4.1); ii) psi76, the *psi* dihedral angle of residue V76 (see sec. 2.4.1); and iii) the length of the TVGYG (*SF length* in the figure) measured as the distance of the C_α atoms of the residue T75 and G79. The time is

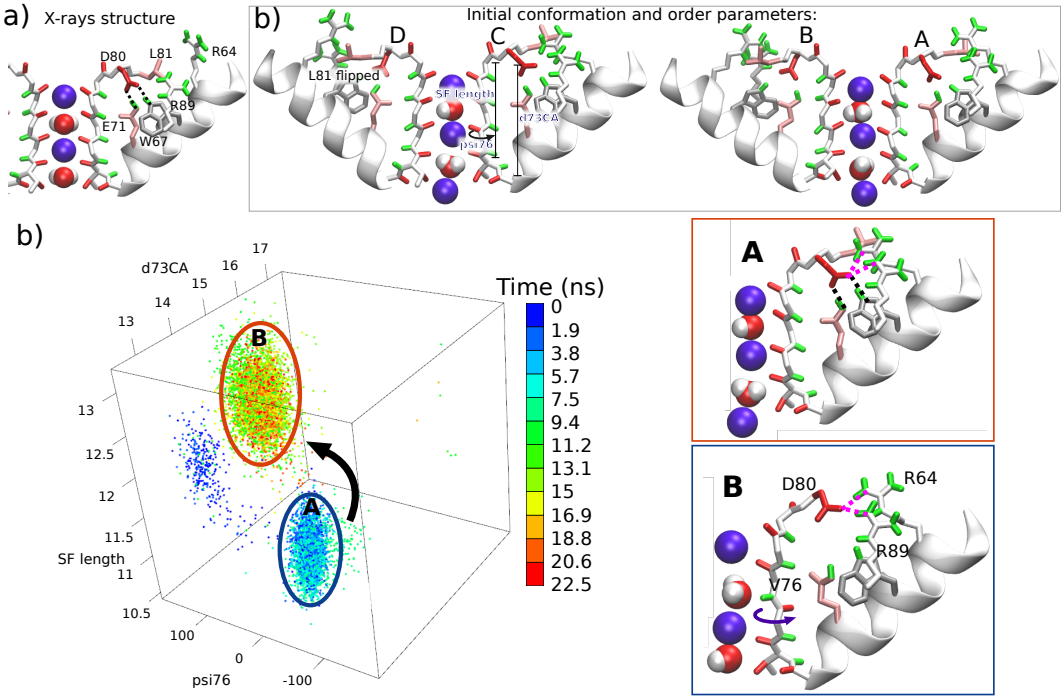

Figure 4.13: Dynamics of the filter and the nearby residues during a simulation started from a conformation in which the R64-D80 interactions were maximised (b). The L81 residues in the flipped state are the reason for the maximised R64-D80 interactions. The simulation was preceded by 20 ps of relaxation in which the state of every L81 residue was restrained in the flipped conformation (harmonic potential with a spring constant of 24 kcal/mol degree^2 and centred on 185°) as well as the $\chi 1$ dihedral angles of R64 residues (spring constant 20 kcal/mol degree^2 centred on −160°). Further 25 ps of relaxation were performed without any restraint. Panel (a) shows, for comparison, the configuration of the network of residues behind in the X-ray structure used to build the system (pdb code 1K4C[157]). c) Evolution of the SF region for the subunit C in the first 22.5 ns of simulation represented in a convenient conformational space in which the three dimension are: i) the position of D80 side chain with respect of the C_α atom of residue 73 used as a stable reference (d73CA, Å); ii) the length of the TVGYG sequence defined as the distance between the C_α atoms of the residue T75 and G79 (SF length, Å); iii) the ψ dihedral angle of residue V76 (psi76, degrees). The extra dimension is the time, represented as a colour gradient. Additionally, two representative snapshots for the two main states of the system within this conformational space are reported. The figures demonstrate that the interactions with R64 can promote the breaking of the E71-D80-W67 linkages (black dotted lines) and the outward movement of D80 side chain, which is further stabilised by R89 (magenta dotted lines). This movement, in turn, induces a stretching of the TVGYG sequence which causes structural rearrangements in the filter. These rearrangements primarily involve the V76, which was found practically always in the flipped state for bigger values of d73CA.

represented by a colour gradient. The figure shows very brief initial transitions of V76 (psi76 from $\sim -50°$ to $\sim 145°$) which demonstrate the inherent variability of the V76/G77 peptide group and the causes of which are difficult to determine. After 5 ns the interactions between D80 and R64 side chains promoted the breaking of E71-D80-W67 linkages and a clear drift in the position of D80 (d73CA from ~ 13.5 to ~ 15.5. This new state led to a stretching of TVGYG sequence which involved few small rearrangements which can be seen comparing the two relevant snapshots (A and B) from the simulation reported in Fig. 4.13b. Among these rearrangements, the flipping of V76 was the most noticeable, which was stabilised by the new state of D80 (Fig. 4.13b) until the E71-D80-W67 linkages were re-established. The snapshot "B" reported in Fig. 4.13b demonstrated that the new state after the breaking of the linkages was stabilised by H-bonds between D80 and both the arginines R64 and R89. This suggests a certain degree of cooperation between the two arginines in determining the state of the D80 side chain.

The rearrangements of D80 and surrounding residues strongly influenced the dynamics of the elements within the pore. Fig. 4.14 shows statistical analyses on K^+ ions bound to the SF (K1 and K2) in that part of the simulation when the E71–D80 H-bond was broken: scatter plots, distributions and correlations (Pearson's coefficients) for the z coordinates centred with respect to the COM of the SF (defined as previously described). A comparison is shown with the same analyses performed on part of a simulation characterised by an identical configuration of K^+ ions 01010+1 and commencing with the X-ray conformation. The complex dynamics of the region behind the pore, delivered through D80, caused rearrangements of TVGYG sequences which were able to disrupt the strong correlation between the K^+ ions, a feature of the conductive state,[134] with the Pearson's coefficients dropping from 0.74 to 0.06. This resulted in an increased variability of the ions leading to wider distributions and unexpected reverse transitions of the innermost ion K2 01010 $\rightleftarrows$ 01001. The re-establishment of the E71-D80-W67 linkages previously mentioned resumed the features of the conductive and was soon followed by outward transitions of the K^+ ions 01010+1 $\longrightarrow$ 01011+0 $\longrightarrow$ 10101+0.

4.9 Network centred on D80

The analyses performed in the present chapter provide a complex picture of the strong coupling between the structural dynamics of the pore region and permeation. A strong interconnection exists between small rearrangements in the region behind the SF and the dynamics of the permeating ions. The main elements involved in these

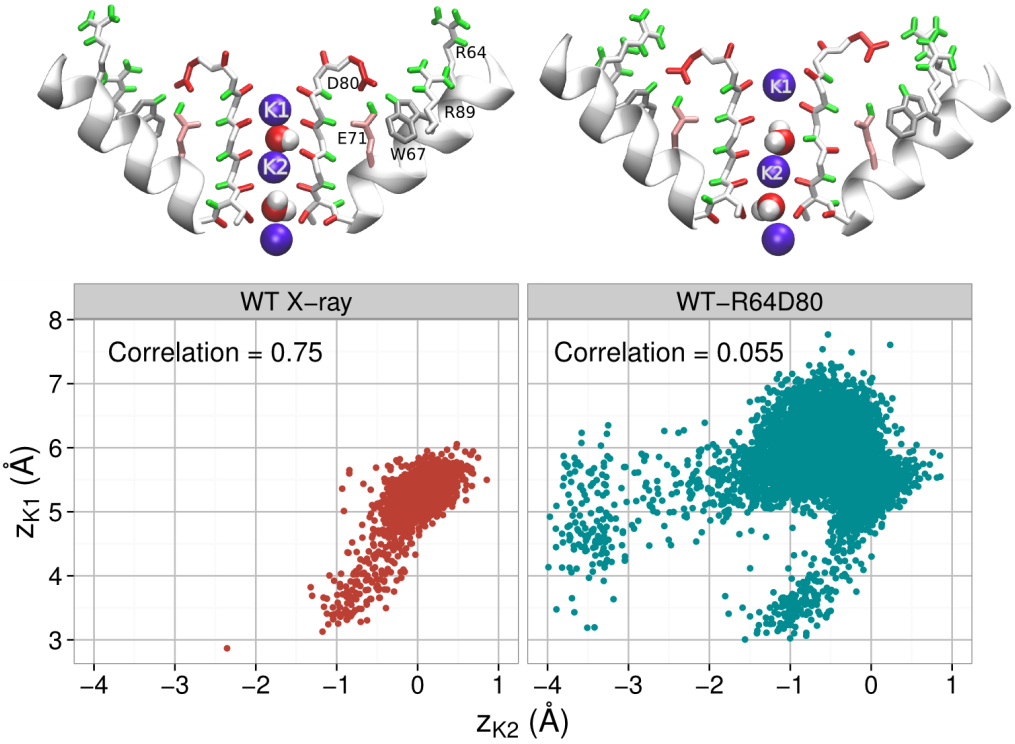

Figure 4.14: Correlations and scatter plots of two permeating ions (K1 and K2) for identical ion occupancy 01010+1. Two trajectories are compared: the first (left) obtained starting from the X-ray structure, with R64 relatively far away from D80; the second (right) was a portion of a trajectories when E71-D80 and D80-W67 H-bonds were broken as a consequence of D80-R64 interactions (WT-R64D80). The figures shows that the dynamics of the residues in the region behind the selectivity filter strongly influence the permeating K^+ ions: the strong correlated motion is lost (Pearson correlation coefficient drops from 0.75 to 0.055) and the two ions move over wider ranges, as a consequence of the distortions of the filter which lead the binding sites to be spatially more weakly defined.

rearrangements have been recognised and the existence of a network centred on the aspartic acid D80 is suggested as being able to determine the state of the permeation path. In the following chapters, this network is suggested as being responsible for the fine regulation of the K^+ current at the SF, which includes the inactivation of the channel.

Fig. 4.15 shows the network drawn following simple rules: i) blue dashed lines represent non-bonded electrostatic interactions that can eventually lead to strong H-bonds; ii) black lines represent connections through the backbone of the protein; iii) green dotted lines represent all the remaining non-bonded interactions, such as the steric interactions or repulsions between positive or partially-positive charged groups. The sizes of the nodes are weighted according to the number of edges connecting each node.

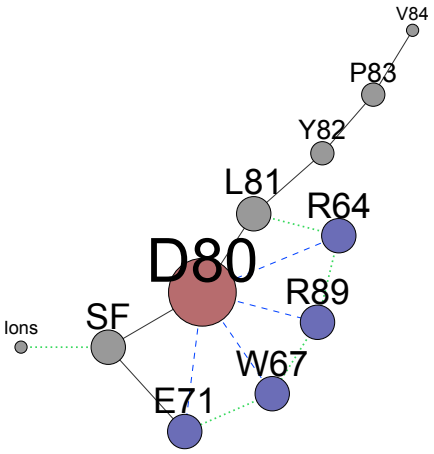

Figure 4.15: Network of residue that regulates the conductivity in KcsA. The figure was produced using gephi.[14]

The picture shows the central role of the residue D80, the main hub, which clearly arose from the calculations. Together with the surrounding H-bond donors, E71, W67, R64, R89, it creates the first level of the network (red and blue in figure). L81 belongs to a second level, comprised of the residues that play a relevant but secondary role. L81 shows a connectivity similar to the elements of the first level, but it is linked with D80 through the protein backbone. Its conformation in the WT mainly regulates the interactions between R64 and D80, while its direct influence on D80 is likely to be weaker than the elements of the first level. It is likely that additional elements belong to the second level which have not been discussed in this work. A third level can also be recognised in those residues, such as Y82, that are able to affect the behaviour of the first level without any direct contact with its element. The number of elements in the third level is also expected to be larger than

that shown in Fig. 4.15, and its existence, and the influence of its elements on the first and second levels could explain the behaviour of a number of different mutants with respect to conductivity and inactivation.

4.10 Conclusions

Different patterns of macroscopic currents in K^+ ion channels originate from the complicated behaviours which are governed by small structural rearrangements of the pore region once the inner gate is opened.[28,29,66] The pore region exhibits a complex variability which is mostly obscure and requires detailed mechanistic studies at a microscopic level in order to be understood. At the present time experimental techniques are unable to investigate these microscopic dynamics and theoretical approaches, such as MD, greatly help in their understanding.

In this work, comparisons of the behaviours of the KcsA WT and the mutants E71A, Y82A and R64A were performed by means of MD simulations, free-energy calculations (well-tempered metaD[13]) and statistical analyses. They provide a detailed description of the main elements involved in the rearrangements directly linked with the state of the filter, their different roles and the way they interact and collaborate in influencing the permeation path. A complex picture is delivered that demonstrates that the hydrogen-bond network between the triad E71-D80-W67 proposed by Cordero-morales et al.[36,37] is indeed a small part of a wider highly-coupled network of residues centred on the aspartic acid D80. The latter plays the main role in delivering to the selectivity filter structure the conformational changes that occur in the surrounding region, acting as a "filter handle". Modification in the state of D80 was found directly linked with the state of the SF and responsible for relevant structural rearrangements both in the mutant E71A and, most significantly, in the WT. The state of D80, in turn, was found strongly linked with the dynamics of the surrounding H-bond donors E71, W67, R64, R89. In particular the two arginines has been shown as being able to perturb the conductive conformation, promoting outward motions of the D80. In the WT R64 demonstrated to have the stronger influence, although a certain degree of cooperation between the two has been seen. Additionally the ability of R64 to interact with D80 and to influence the structure of the SF was found dependent on the conformation of the leucine in position 81 (L81). The L81 side chain behaves as a "gate" for R64 to approach D80.

These residues, proposed as being the principal molecular determinants for structural rearrangements of the permeation path, form a highly-correlated network. The main hub is D80 which form the main level of the network together with the

surrounding H-bond donors E71, W67, R64, R89. This result assumes a more general importance taking into account the fact that the aspartic acid D80 belongs to the signature sequence TXXTXGYGD, which is highly conserved among K^+ ion channels and is usually surrounded by different H-bond donors.[26,31,37,85] This suggests that the existence of similar complex networks may be a general feature of K^+ ion channels. L81 is suggested as belonging to a second level of the network constituted by the residues that have a secondary role which is relevant but only indirectly determines the state of the D80 side chain.

Moreover, the residue in position 82 was proved by free-energy calculations to be capable of influencing L81, and consequently R64 variability. In the following chapter this variability of R64 will be shown to be fundamental in order to explain the increased probability of inactivation reported in the literature for Y82A, which is strongly reduced when R64 is removed in R64A.

Additionally, the role of V76 flipping was investigated. In the published literature it was referred to as being capable to generate non-conductive states of the channel. In our simulations V76 was found to be adopting flipped states very easily in all the proteins, including the non-inactivating mutant E71A. Starting from V76 flipped states of the proteins E71A and WT, permeation was seen occurring in both accompanied by reverse transitions of V76. Although conformation of V76 influences the energetic involved in the permeation, as demonstrated in previous works[20], this result suggests that additional conformational readjustments are necessary in order to hinder K^+ permeation and generate long-lasting non-conductive states. Otherwise the effect is only temporary.

Chapter 5

Gating: C-type inactivation

5.1 Introduction

The K^+ ion channel KcsA continues to attract a great deal of attention because of its role as an archetype for the complex interplay of gating and activation that is commonly found in the K^+ channel superfamily. The result of experimental studies is a complicated time-dependence for current through the ion channel, which is generally accepted to arise from a superposition of the pH-sensitive opening of an inner gate formed from a helix bundle that spans the cytoplasm/membrane interface (activation opening) with conformational changes in the region of the selectivity filter (SF) that is located near the extracellular side of the membrane (C-type inactivation). The latter function also means that the SF has a dual role, both in ion selectivity and current modulation.[30,35,37,68,85,93,119,141,151,157]

Over the last few years, a number of experimental studies have begun to unravel the key features of the different states associated with KcsA. The opening of the intracellular gate is triggered by pH changes and is associated with changes to a whole network of hydrogen bonds and salt bridges within the KcsA helix bundle.[62,119,138,140,146,147] Residues E118, E120 and H25 play a key role in this process, but with a cooperativity that ensures no single residue is solely responsible for the activation opening.[68,140] Dynamical correlations have been observed between the protein domains of the tetrameric KcsA channel during activation opening[23] and structural correlations between the intracellular gate and the SF regions.[41,147] However, there is evidence of a conformational equilibrium between active and inactive states (associated with the C-type inactivation)[29,30,35,36,68,85,157] which suggests there should be a degree of independence between the conformational changes that occur in the intracellular gate and the SF.

Significant progress toward understanding the relationship between structure and function in the SF has emerged from X-ray experimental studies. Zhou et al.[157] solved a structure for KcsA, in the presence of a low concentration of K^+, with a constriction in the central region of the SF, often referred to as "collapsed", which was proposed as being the C-type inactive state.[157] More recently, in crystallising a constitutively open mutant channel (tKcsA-OM), Cuello et al.[42] managed to identify five conformer classes. When ordered according to the diameter of the intracellular gate, these conformer classes also showed systematic variations in the structure of the SF, from the putative conductive to the collapsed, which they suggested provided a mechanism for the C-type inactivation. However, without evidence of a dynamical pathway linking the conformer classes, and given the evidence of a dynamical equilibrium between active and inactive states once the intracellular gate opens, this mechanism remains conjectural. Using different theoretical approaches, Domene et al.[45] demonstrated that the presence of the K^+ ions in the central region of the SF is necessary to stabilise the conductive state. They observed that the collapse of the pore was caused when the ions vacate the central region with a maximum of two subunits assuming a collapsed conformation. The authors considered that two collapsed subunits are sufficient to hinder the K^+ current. Hypotheses about C-type inactivation alternative to pore constriction, such as pore dilation, were also put forward.[66]

Different inactive states of the pore exist, but their nature and mechanisms remain mostly obscure.[29,66,150] Among these, the existence of deeply non-conducting "defunct" states was recognised for different K^+ channels, likely characterised by denatured states of the pore.

Mutagenesis studies revealed that a number of different residues in the pore region are able to dramatically affect inactivation in KcsA.[30,35,36,105] A network of hydrogen bonds which links the residues E71, D80 and W67 was suggested as stabilising the the conductive state, and either the breaking or the strengthening of the E71–D80 bridge was suggested as being related to C-type inactivation.[30,32,34–37] Moreover, different studies deliver an overall picture for C-type inactivation which is further complicated by cooperation between subunits.[66,90,114,116,125] In the previous chapter, the hydrogen bond network between E71, D80 and W67 was demonstrated as belonging to a highly correlated network of residues responsible for the regulation of the state of the SF in KcsA. This network is centred on the residue D80, which is located on the outer entrance of the pore and belongs to the highly conserved motif TXXTXGYGD known as "signature sequence".[31,37,85] The first level of the network was recognised formed by D80 and the neighbouring H-bond donors which have a

relevant role in defining the state of the filter.

Further investigations of the dynamics of the network of residues behind the pore are presented in this chapter, which provide a dynamical interpretation for C-type inactivation. Atomistic simulations (molecular dynamics) were used, combined with free energy methods (metadynamics). An initial approach used a combination of protonating/deprotonating switches of the E71 with unbiased molecular dynamics (MD) simulations. In many K^+ ion channels, extracellular pH acts as a regulator for inactivation.[33,76,85,91] It is believed that this effect is very limited in KcsA.[29] Although this approach might indeed be representative of rare cases under physiological conditions, it provided important information about the mechanistic connection between different states towards C-type inactivation. A second approach involved a more detailed investigation into the dynamics and free energies of the pore that did not involved any proton exchange. Physiologically, this might be the most relevant case.

The conductive state of KcsA was proved to be fundamentally unstable and very sensitive to conformational changes of the network. Inactive states were reached and the most relevant free energies involved in the process were computed. Mechanisms for the C-type inactivation are suggested which are consistent with experimental findings and can explain the influence of different mutations on inactivation probabilities. The results demonstrate once again the key role of the aspartic acid D80 in the regulation of state of the pore. The nearby hydrogen bond donors residues, E71, R64, W64, R89, were proved to be determinant in defining the state of D80 and consequently induce the structural rearrangements of the pore associated with the inactivation. The positions of the K^+ ions bound to the SF greatly affected the energetics of the transitions associated with the network and this led to an explanation for the influence of the extracellular concentration of K^+ on the inactivation process. Our results were in agreement with the collapsed conformations of SF identified in different studies of crystal structure.[42,157]

The results obtained for the WT were compared with the free-energies computed on two mutants, Y82A and R64A, which, from alanine scanning, demonstrated respectively enhanced and reduced inactivation probability with respect of the WT.

5.2 Methods

As described in the Chap. 4, the four subunits of the KcsA are referred to by using capital letters A, B, C, D. The SF is described as a five-site pore using standard notation S0 to S4, starting from the outer site. The ion configurations in the SF are

described by five digits using a binary formalism (from S0 to S4, 1 will represent the potassium ion, 0 a water molecule) separated from the number corresponding to the K^+ ions in the cavity by a "+", e.g. 01010+1 means the presence of K^+ in S1, S3 and in the cavity.

Collective variables are labelled as described in Sec. 2.4.1. The distances between D80 and different side chains are labelled by "d" appending the position of the second residue , e.g. "d71" is the distance between D80 and E71 side chains. Distances between D80 side chain and the backbone (C_α) atom of a second residue are labelled appending "CA", i.e. "d71CA" is the distance between D80 and the C_α atom of the residue in position 71. Dihedral angles are labelled appending the position of the residue to the name of the Greek letter that defines the dihedral within the residue itself, ignoring incremental numbers if exists, e.g. $\chi 1$ dihedral angle of residue D80 is labelled "chi80".

C-type inactivation was initially investigated according to a pH-related pathway associated with a deprotonation/reprotonation process of E71 residue. The second part of the work did not involve any proton exchange and the states of the network was investigated in detail by means of metaD calculations.

5.2.1 pH-related inactivation

Simulations on proteins with deprotonated E71 were prepared by 10^4 steps of a minimization procedure applied to relaxed protonated structures. Four Cl^- ions were removed from the aqueous phase to restore charge neutrality without affecting the K^+ concentration. The oxygens involved in the E71–D80 H-bond were restrained with an harmonic potential with a spring constant of 2.5 kcal mol^{-1} $Å^{-2}$. Restraints were applied to prevent a new configuration from occurring during this preliminary stage.

The hydrogen bond analysis was performed using the algorithm implemented in VMD that finds interactions between a donor (X—H) and an acceptor (A) according to simple geometrical criteria: the angle X-H – A and the distance X - - - A. This algorithm has been used in order to produce statistics on the different residues bound to a certain residue over complete trajectories. Since we are interested in all the possible interactions that could stabilise a certain configuration, the applied criteria, distance 3.5 Å and angle 90°, also made it possible to locate weak, bifurcated hydrogen bonds.[12]

5.2.2 Free energy calculations

The free-energy calculations were prepared as described in sec. 4.7. Different sections of the FES underlying the dynamics of the network were computed by varying the state of L81 and the SF occupancy. Configurations for L81 were restrained with harmonic potentials ($K_{spring} = 5$ kcal/mol degree^2) centred in two positions: i) *L81 non-flipped*, chi81$_0 = 297.6°$; and ii) *L81 flipped*, chi81$_0 = 185°$. The SF occupancy was not maintained with additional restraints applied to the K^+ ions that could affect the dynamics of the SF. For this reason two meta-stable occupancies were chosen with life times comparable to the length of the sampling: 00101+0 and 10101+0, with a vacancy in S3. Vacancies have been seen in our simulations and discussed in previous works.[54,72] Spherical harmonic restraints were used in most of calculations with 00101+0 occupancy to prevent K^+ coming from the bulk from occupying S0 during the long sampling, similar to previous theoretical works.[4,5,69,92,109]

The two or three-dimensional FESs were computed with respect to the CVs chi80, d71, and d64 (see sec. 2.4.1) and a number of different states were identified. A convenient nomenclature for these states is introduced here. The space of the configurations is subdivided according to ranges of values of the three order parameters. Three regions are defined according to chi80: i) *D80nonflip*, chi80 between 0° and 140°; ii) *D80semiflip*, chi80 between −110° and 0°; iii) *D80flip*, chi80 between 140° and 250°. The definition of "flipped" conformation for D80 used in this work is different from that of the E71A D80 flipped structure described in previous works[35], which is associated with the flipping of the backbone region. We define "flipped" the conformations which involve the flipping of the side chain of D80 around $\chi 1$ dihedral angle. For each of the distances d71 and d64, "close" and "far" regions were defined: *E71close* was defined for d71 ≤ 4.5 Å and *E71far* for d71 > 4.5 Å; *R64close* for d64 ≤ 7.5 Å and *E71far* for d64 > 7.5 Å. The different ranges chosen for d71 and d64 depend on the different definitions of the CVs and for the purpose of describing the E71-D80 H-bond state with greater precision. For the investigations of the cooperativity between subunits the different configurations of the protein will be described by appending the labels of the subunits to the described state, e.g. D80flip-R64far-AB means that subunits A and B are in the state D80flip-R64far. Heterogeneous arrangements among the subunits were not used to initialise simulations in this study. We would mention that the couples A, B and C, D are opposing subunits in our labelling scheme.

5.3 Results

5.4 Deprotonation-reprotonation approach

The results of chapter 4 demonstrate that E71 and D80 can change their relative positions, in the event of E71–D80 H-bond breaking. Quantum mechanical/molecular mechanical (QM/MM) calculations suggested that the proton can exchange in the E71/D80 pair.[24] The H++ server (version 3.0, http://biophysics.cs.vt.edu/H++[6]) was used to perform pK_a calculations on the X-ray structure and on a snapshot from a MD simulation in which E71 and D80 were apart. The pK_a for E71 drops from > 12 to ~ 6.5 as a consequence of the breaking of the E71–D80 H-bond. The method applied is based on classical continuum electrostatics approximation and involve a number of assumptions and approximations, which involve large errors. However, these calculations provide a qualitative picture of changes in pK_a values for different states. Moreover, close examination of the water trajectories showed that water molecules from the bulk can diffuse into the protein and interact strongly with E71, mainly when E71–D80 H-bond is broken. Arginine has also been shown to promote proton exchange[63], and the shuttling of an arginine residue from a glutamate residue towards a Glu/Glu pair was suggested as the reason for driving the proton release in the light-driven proton pump bacteriorhodopsin[89,97] (Fig. 5.1). Similar dynamics were seen in our simulation for arginines R64 and R89 (Chap. 4). This raises the possibility that temporary deprotonation of E71 could be led by the combination of three factors: the dynamics of the arginines, the breaking of the H-bond and the diffusion of water from the bulk. This deprotonation would eventually facilitate conformational changes in the selectivity filter.

Deprotonation of E71 cannot be directly achieved by standard atomistic simulation approaches because the common force field implementations in classical force field MD does not allow proton transfer events, and because the quantum mechanics calculations cannot easily deal with long time-scales and wide rearrangements of the proteins. A new approach has been developed based on the difference in time-scale between the rare event of the proton exchange and the faster relaxation time of the protein. The methodology can be summarised as follows: i) a representative conformation for a state is obtained over a long classical MD simulation using RMSD analysis as a tool to validate the meta-stability; ii) the rare event, either the protonation or deprotonation of the acidic residue, is artificially induced in order to sample the new regions of the phase space which otherwise could not be achieved even if an additional biasing potential is applied; and iii) a new long simulation is performed to

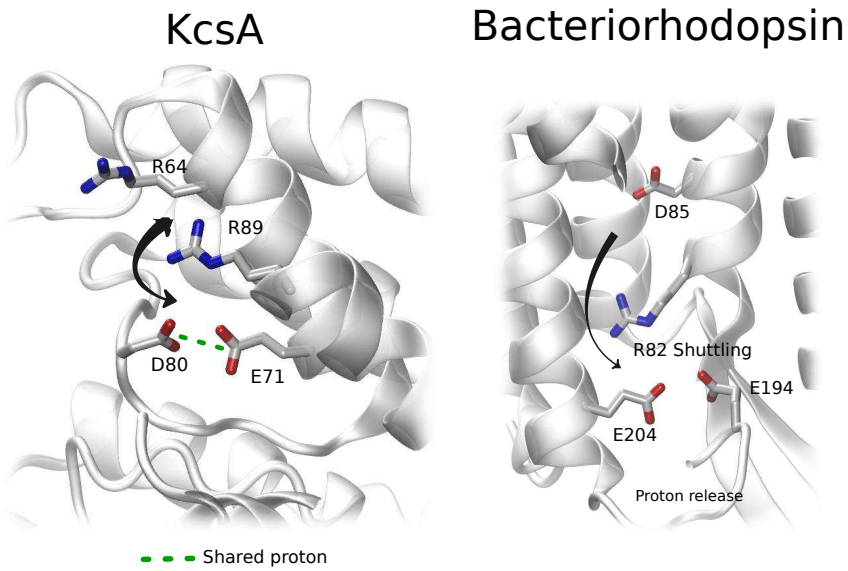

Figure 5.1: Comparison of dynamics of R89 in KcsA, and R82 in Bacteriorhodopsin (a light-driven proton pump, pdb code 1C3W[96]) where shuttling of R82 from a D85 towards an E204/E194 pair was suggested as the reason for driving the proton release.[89,97]

obtain new representative conformations over which step number (ii) is applied. By this method conformations are visited that are potentially available to the protein in the physiological environment but not accessible in the MD simulations because of the limitations of the force field.

Representative conformations for the conductive state of the KcsA WT were obtained from two different simulations ($\sim$ 20 and $\sim$ 38 ns) performed in the presence of the E71–D80 H-bonds. These simulations were performed after an accurate relaxation of the membrane, as described in Chap. 2. These conformations will be denoted C_p (Fig. 5.2). Occupancies of SF were 01010+1 and 10101+0 with a vacancy in S3 and the K^+ ions chelated with a square antiprism geometry in the same way as in the X-ray structure (Fig. 5.3a).

Two simulations were performed from the two different C_p configurations, in which E71 was considered in a deprotonated state from all four subunits, and which were initialised as described in Sec. 5.2.1. The simulations are labelled: Sim Ia started from the 01010+1 occupancy; and Sim Ib started from 10101+0 occupancy. The systems were then relaxed to alleviate the coulombic repulsion between E71 and D80 resulting from the deprotonation.

Both the simulations Sim Ia and Sim Ib showed very similar conformational changes. The trajectories and RMSD analysis show that protein underwent two

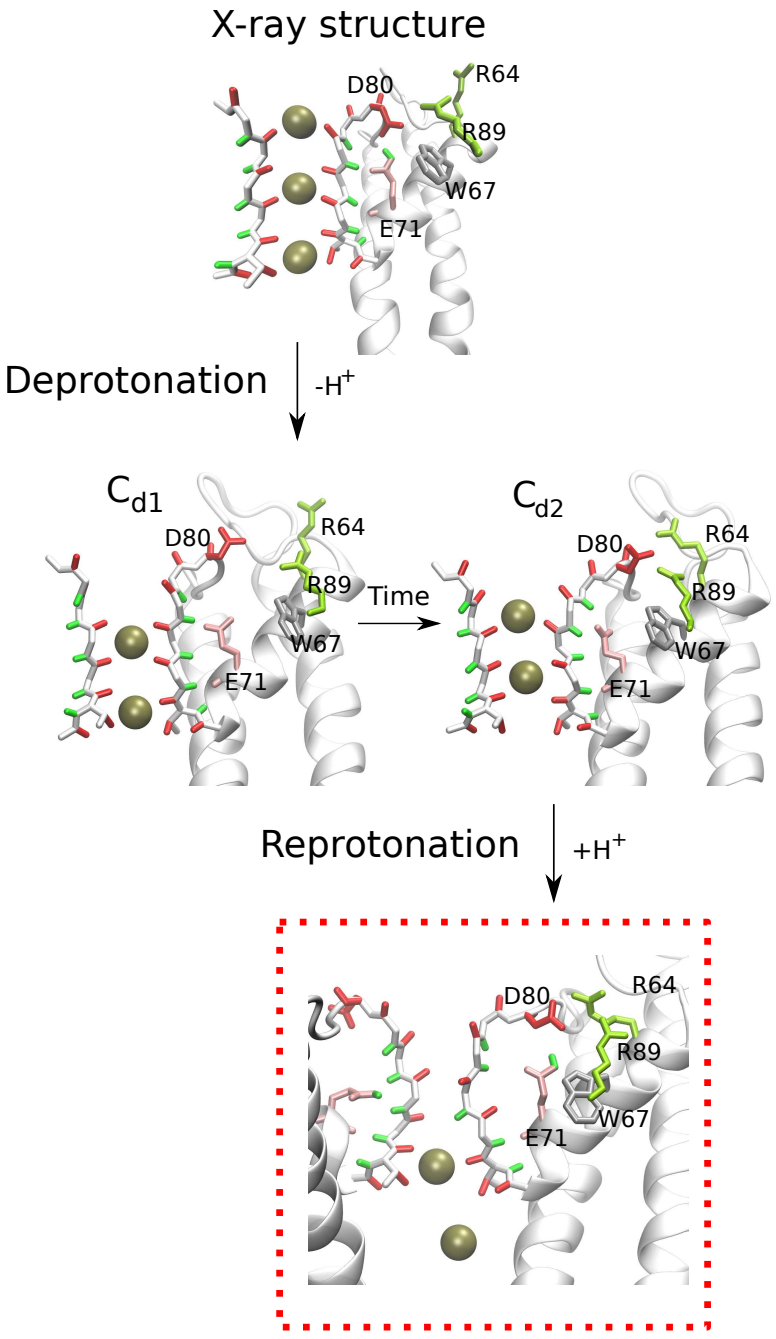

Figure 5.2: Snapshots representative for the transition from the "b" set of simulations. Starting from C_p, E71/D80 deprotonated, the conformation goes to C_{d1}. The filter undergoes a transition because of the strengthening of D80-R64 interactions leading to C_{d2}. The reprotonation of E71 induced several transitions that inactivated the channel (I_p).

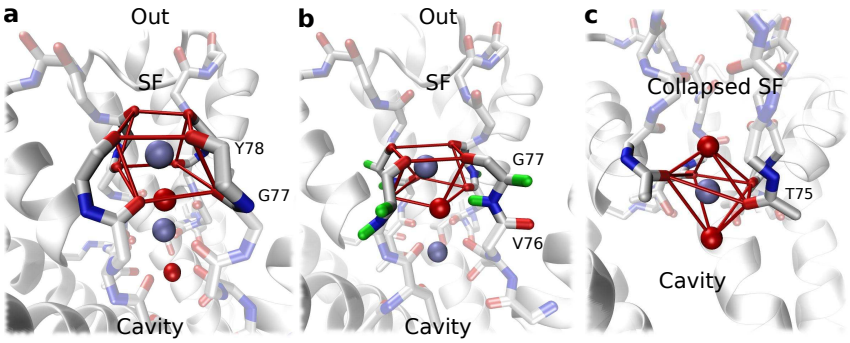

Figure 5.3: Geometry of the K^+ coordination in the different conformations of the selectivity filter: a) selectivity filter in the conductive conformation (square anti-prism); b) selectivity filter in the conductive conformation, where the G77-V76 peptide group assumed a flipped conformation (slightly distorted square anti-prism); c) selectivity filter in the inactive conformation (octahedral geometry).

main similar transitions. An initial relaxation led to the flip of the D80 side chain towards the extracellular region, similar to orientations seen in previous MD simulations[19,60,106], and a rotation of the E71 side chain of $\sim 120°$. Analysis on H-bonds revealed that the D80 flipped orientation was stabilised by weak, intermittent H-bonds with Y82, R89 and R64 (Fig. 5.4). The state was meta-stable on the scale of the tens of ns and will be denoted C_{d1} (Figs. 5.2 and 5.5).

Further conformational changes commenced after ~ 20 ns in both Sim Ia and Sim Ib (Fig. 5.5). This changes brought to a new meta-stable conformation: C_{d2}. In Sim Ib, stabilisation of $C_{d2}$was slower and we suggest that is because of the presence of a K^+ ion in S0 (the influence of the K^+ ions will be widely discussed later in this chapter). The origin of this second transition was recognised in the strengthening of the interactions between D80 and the neighbouring arginines, mainly R64 (Fig. 5.2). The transitions from C_{d1} to C_{d2} involved changes in the conformation of the SF structure, leading to *curved conformations* and to the widening of the outer entryway (S0), which was occupied by several water molecules (Fig. 5.6). In any event, the SF did not assume conformations that could be considered clearly inactive and the K^+ ions remained bound to the SF.

The conjecture behind the sets of simulations was that the E71 can undergo acid-base reactions with water. Such reactions should be reversible and so it is important to consider the results of reprotonation. From Sim Ia and Sim Ib, representative structures for C_{d1} (at 15 ns) and C_{d2} (final frames) were selected, and simulations in which E71 residues were neutralised by the addition of protons were conducted from each conformation. Two simulations were spawned from each of the two C_{d1} structures, while a single simulation was performed from each of the C_{d2}

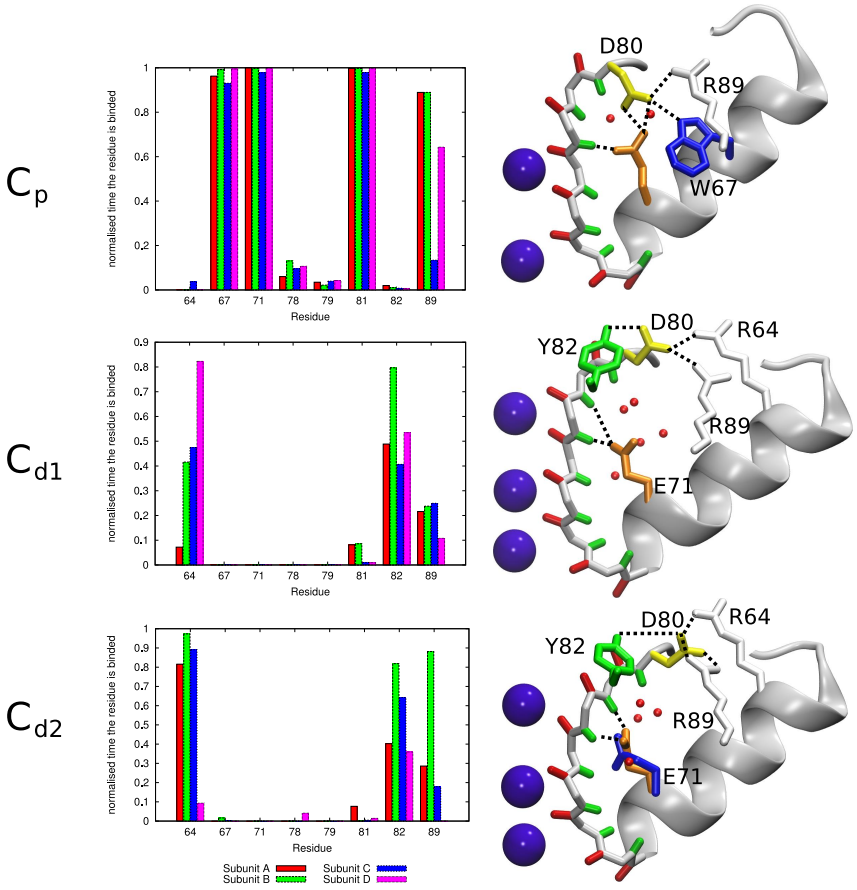

Figure 5.4: Hydrogen bond analysis on D80 in different conformations assumed by the protein during the pH-related inactivation mechanism: C_p, C_{d1} and C_{d2}. The plots report the fraction of the simulation time over which a hydrogen bond is found between the side chain of the residue D80 and the residue indicated in the x axis. Criteria for identifying hydrogen bonds are explained in the "Methods" section. The main differences among the different conformations are: i) in C_p D80 is H-bonded to E71, W67, R89 and L81 carbonyl group. ii) in C_{d1} D80 assumed a flipped conformation, it is H-bonded to Y82, R64, R89; the E71 side chain reorients by $\sim 120°$ (N-C_α-C_β-C_γ dihedral) with respect to C_p and a displacement of G77 can be seen; iii) In C_{d2} the TVGYG sequence assumed a curved conformation only in subunits B and C; D80 is H-bonded to Y82, R64, R89; E71 side chains assume two possible different conformations: (i) pointing towards D80 as in C_{d1}, or, more rarely, (ii) pointing toward the centre of the selectivity filter.

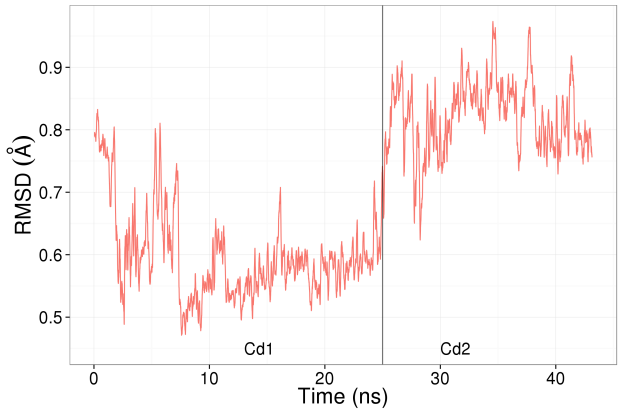

(a) Sim Ia

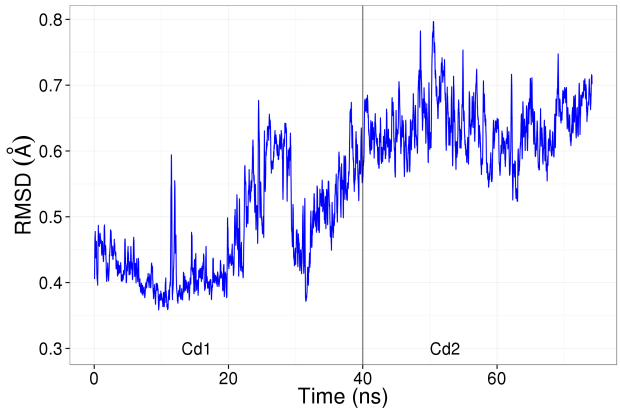

(b) Sim Ib

Figure 5.5: RMSD analysis for the SF (backbone atoms of residues 74 to 78) of KcsA simulated in the case of E71 deprotonated. The X-ray structure from which the system was built (pdb code 1K4CZhou et al. [157]) was used as reference. Both the simulations show comparable transitions in the structure of the SF compatible with the existence of two meta-stable states.

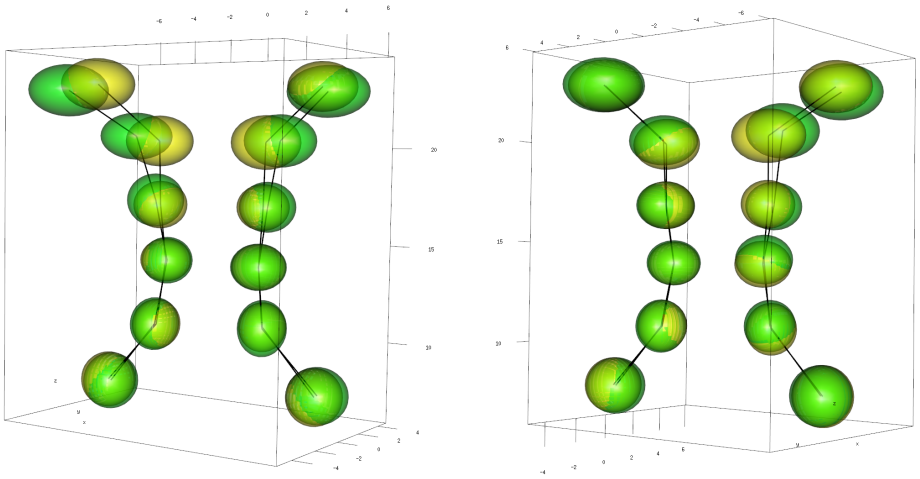

(a) Subunits A and B. **(b)** Subunits C and D.

Figure 5.6: Comparison of the SF conformation of C_{d1} (yellow) and C_{d2} (green). Each ellipse is draw according to the standard deviation of the trajectories of the atomic $C_\alpha$coordinates after optimal rigid body superposition performed using "measure fit" function implemented in VMD.[67]

from Sim Ia and Sim Ib, labelled respectively Sim_2 IIa and Sim_2 IIb.

Reprotonation of E71 led to major transformations in C_{d2} (Fig. 5.2). The TVGYG sequences adopted a *collapsed conformation* in all the subunits during Sim_2 IIb and in 3 out of 4 subunits during Sim_1 IIa. In both the cases the final conformation had a bottleneck in the S2, S3 sites, consistent with the constriction inactivation mechanism.[42,157] The resulting conformations (denoted I_p) were surprisingly similar to the X-ray structure reported for the X-ray structure of a putative close-inactive state, which was obtained in the presence of a low [K^+] (Fig. 5.7).[157] Moreover three of the four conformations found in our simulations (C_p, C_{d1}, and I_p) overlaid very closely with three of the conformation clusters identified in a recent crystal structure study, and I_p was very close to the proposed open-inactivated state in which the intracellular gate diameter was 32 Å (Fig. 5.8).[42] The K^+ remaining in the bottom part of the filter was chelated in an octahedral geometry by the T75 carbonyl oxygens in equatorial positions and by two water molecules in axial positions (Fig. 5.3c).

In contrast, protonation of E71 in C_{d1} led to different results. Of the four simulations performed, in two cases a structure which resembled the C_p was obtained in which most of the D80 side chains flipped back, re-establishing the E71–D80 bridges on several occasions. In one case the simulation led to a state with one distorted subunit but the ions were still located in the SF. In the last case an inactive state for the SF was obtained, once again with 3 subunits out of four in the collapsed

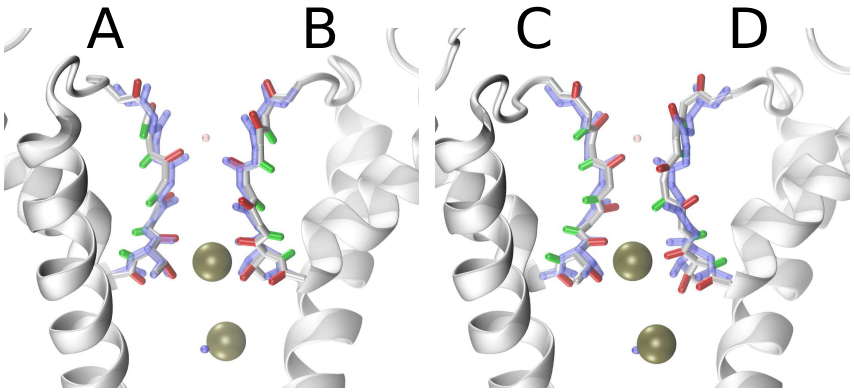

(a) Superimposition of a representative conformation with putative inactive structure (purple, pdb code 1K4D).

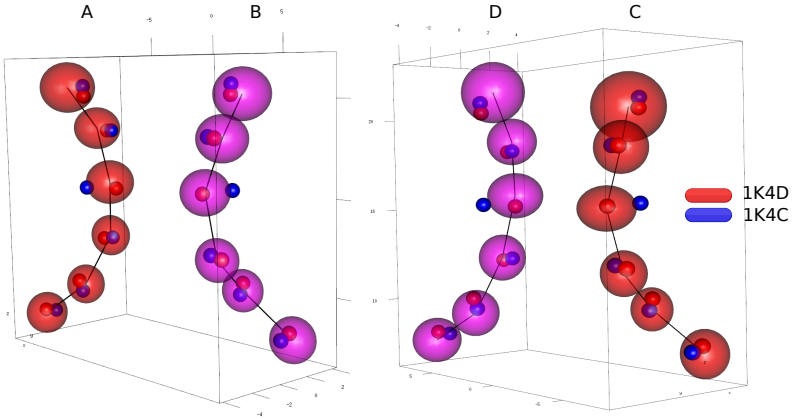

(b) Trajectory of the inactive state from Sim_2 IIb compared against the putative conductive and inactive X-ray structures (pdb codes 1K4C and 1K4C)

Figure 5.7: Comparison of the inactive configuration I_p obtained from the simulation Sim_2 IIb with the X-ray structure of putative conductive and inactive state proposed by Zhou et al.[157] (pdb code 1K4D[157]). Ellipses are drawn according to standard deviations of the trajectories of the atomic $C_\alpha$coordinates after optimal rigid body superposition performed using "measure fit" function implemented in VMD.[67]

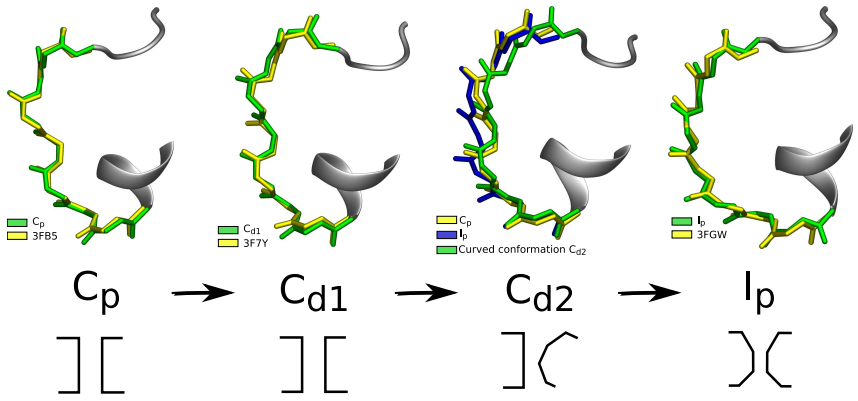

Figure 5.8: Conformation assumed by the TVGYG sequence during the inactivation process studied by selectivity filter superpositions: C_p superimposed with the "partially open"-conductive state with 14.5 Å opening at T112 ($C_\alpha - C_\alpha$ distance, pdb code 3FB5)[42]; C_{d1} superimposed with the conformation with 17 Å opening at T112 (pdb code 3F7Y), a proposed transition state towards C-type inactivation; C_{d2} compared with the conformation C_p and I_p; I_p superimposed with with open-inactivated state (32 Å opening at T112, pdb 3F5W). Conformations are named as described in the section "Methods". The resolutions at which the structures are solved, spanning from 3.00 to 3.40 Å, do not allow an accurate localisation of the carbonyl groups.

conformation.

The different behaviours demonstrated by C_{d1} and C_{d2} against reprotonation suggest a possible role of R64 in facilitating the process toward the inactive state because of the strong interactions with D80. The dynamics that led to the collapsed conformations were extremely complicated and appeared to be random. Clearly, a particular destabilisation was delivered by the interactions between E71 and D80 in the flipped conformation. The final conformations (I_p) supported the hypotheses of various studies that inactivation can arise from pore constriction.

5.5 C-type inactivation not related to pH

All the analysis performed up to this point showed that the state of D80 is a key factor in the regulation of the conductivity of the channel. Temporary and long-lived non-conductive states can be induced by conformational changes in side chains of D80 residues involving a high degree of cooperation with neighbouring residues. In the strongly-coupled network in which D80 acts as the main hub (sec. 4.9), a particular importance is assumed by H-bonds donors: E71, R64, W67, R89. They collaborate to define the state of D80, which finally results in either a stabilisation or a perturbation of the conductive state. The study of inactivation continued, focusing

on the dynamics and the energetics of the network in case a pH-related mechanism was not involved.

C-type inactivation occurs within time-scales that cannot be reached by standard MD because high barriers dominate the process.[29] An approach based on MetaD and unbiased calculations was used. In the previous chapter, the complexities arising from high dimensionality associated with the network reported in Fig. 4.15 were demonstrated. Metadynamics calculations that involve too many degrees of freedom are computationally very expensive and affected by greater errors.[88] Thus it was possible to achieve the object of the study exploring the conformations of the network by means of several low-dimensional calculations designed to deliver the overall picture. The relevant states obtained by this exploration were relaxed by means of unbiased simulations, which led to reach inactive states of the protein.

The relevant parameters for the calculations were chosen: i) $\Delta T = 2000$ K, ii) $w_0 = 0.005$ Kcal/mol (see Sec 2.2.4).

5.5.1 Investigation of relevant transitions of the network of residues

Experimental evidence demonstrated that the presence of E71 plays a key role in the inactivation and various authors have suggested a determinant role for the E71–D80 H-bond.[30,32,34–37] In Chap. 4, it was shown that the simple breaking of the E71–D80 H-bond is insufficient to undergo a complete inactivation (sec. 4.7). Within the complex dynamics of the network behind the SF, unbiased simulations in the deep-inactivating mutant Y82A (sec. 4.5.2) and investigation of pH-related inactivation suggested the possibility of a significant role in the destabilisation of the pore for the interactions between the R64 and D80 side chains, and for the rotations of the latter around its $\chi 1$ dihedral angle (Figs. 4.8 and 5.2). The combination of E71/D80 interactions with the variability of D80 was then explored, by means of the CVs d71 (the distance between E71 and D80 side chains) and chi80 ($\chi 1$ dihedral angle of D80, Fig. 5.9 and sec. 2.4.1). Relevant states were explored by means of different multi-dimensional sections of the overall FES, which were able to unravel the influence of R64 and the position of the K^+ ions bound to the SF.

In sec. 4.5.2, the existence of an interplay between L81 and R64 conformations was revealed in which the flipping of L81 permitted the creation of very strong interactions between the R64 and D80 side chains. Accordingly, the cases of L81 in the *non-flipped* and in the *flipped* conformations were studied. In the latter, the flipped case, the sections were computed considering an additional CV, i.e. the distance between the R64 and D80 side chains (*d64*, see sec. 2.4.1), which was able to capture the wide fluctuations of the R64 side chain towards D80. Similar to

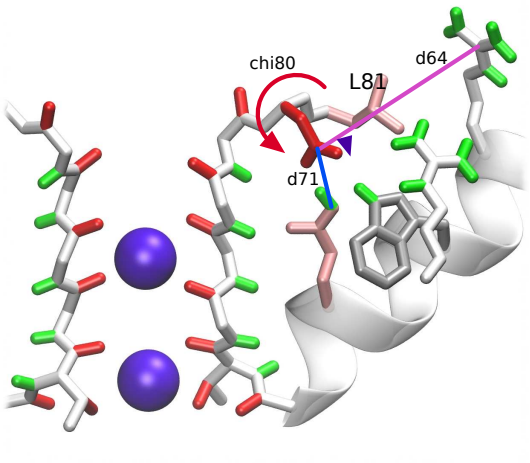

Figure 5.9: Collective variables (CVs) used to investigate the behaviour of the network of residue behind the SF.

sec. 4.6.1, the influence of the K^+ ions bound to the SF was investigated for the two meta-stable occupancies 00101+0 and 10101+0, with a vacancy in S3.

D80 transitions for L81 non-flipped

Side chains of R64 for L81 in the non-flipped conformation mostly fluctuate in a confined region relatively far from the D80 side chain. Thus, two-dimensional metaD calculations were performed with respect to chi80 and d71, and the influence of all of the remaining residues of the network, including R64, was considered to have been averaged out during the sampling.

SF occupancy 10101 The first section was considered for the SF occupancy 10101+0 (Fig. 5.11, K^+ in S0). The calculation revealed that the flipping of the D80 side chain can also be achieved without a concurrent deprotonation. According to the FES, three main states for the D80 side chain can be recognised: i) pointing towards the intracellular region and E71 (D80nonflip, chi80 between 0° and 140°), ii) pointing towards the extracellular bulk (D80flip, chi80 between 140° and 250°), iii) an intermediate position between the two (D80semiflip, chi80 between −110° and 0°). D80nonflip region contains two minima: "a" (D80nonflip-E71close), the absolute minimum of the FES and corresponding to the conformation found in the X-ray experiments; and "b", a weaker broad minimum for the broken E71–D80 H-bond (d71 between ∼ 5 and ∼ 8.5 Å). The barrier involved in the breaking (7 and 8 kcal/mol) is consistent with the one dimensional FES reported in Fig. 4.12 in Chapter 4, supporting a good convergence of the calculations. The minimum

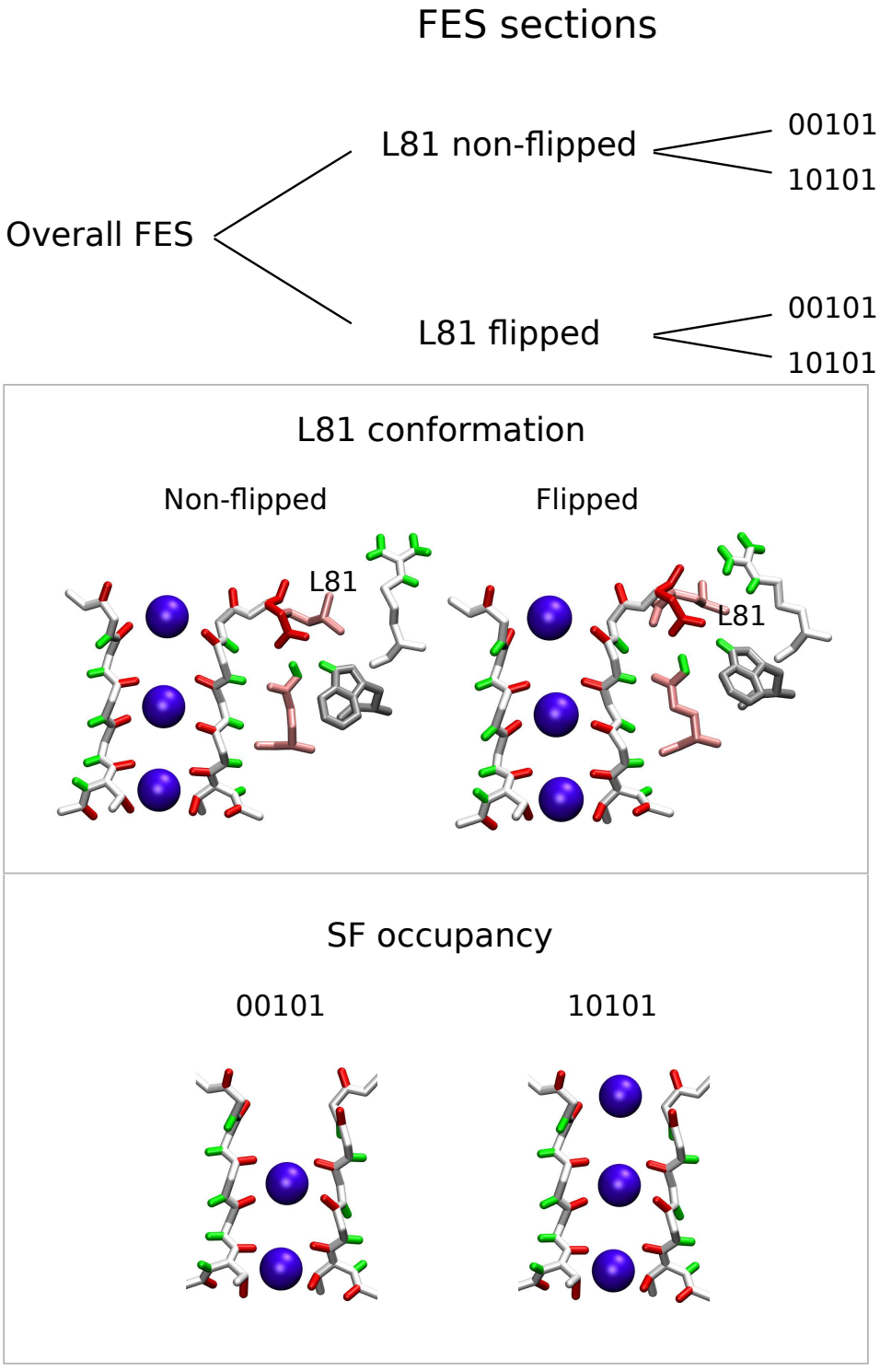

Figure 5.10: Scheme of the different multi-dimensional sections of the overall FES computed. Representative conformations are shown for the different states.

in D80flip region ("d") is a few kcal/mol deeper than the one in D80semiflip ("c"). For 10101+0 occupancy and with a limited influence of R64, the rotation around chi80 involves quite a large amount of energy ("a $\rightarrow$ b $\rightarrow$ d" or "a $\rightarrow$ b $\rightarrow$ c $\rightarrow$ d", $\sim 12-13$ kcal/mol), and the flipped and semiflipped conformations are not expected to have a long life time.

During the sampling, V76/G77 peptide groups were seen briefly flipping a few times from the subunit to which the biased D80 belonged, and also from the opposite subunit. The flipped states did not stabilise because no water molecule was in the site S3 .

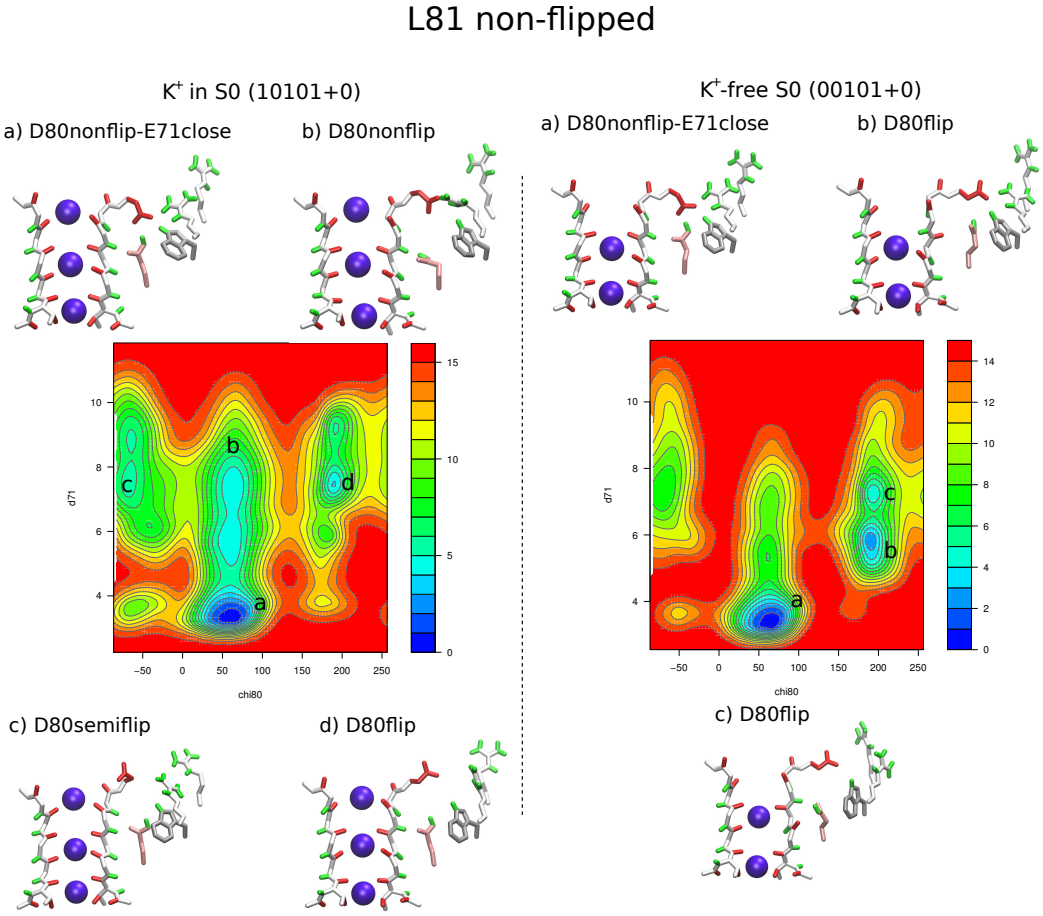

Figure 5.11: multi-dimensional sections of the FES as a function of the CVs chi80 and d71 computed for L81 in the non-flipped conformation (chi81 -62.4, the conformation suggested by X-ray experiments). Two sections are characterised by the occupancy of the SF: i) 10101+1 (K^+ in S0), and ii) 00101+0 (K^+-free S0). Energy in kcal/mol, distances in Å, lines in the contour plots are drawn every 1 kcal/mol.

A relaxation ($\sim$ 12 ns, no additional restraints) was performed from the

D80flip state "d", the second-deepest minimum of the surface. Although the conformation was meta-stable on the ns time-scale, the system evolved towards "a", via "c" and "b", consistent with the computed FES in which the E71–D80 H-bond is favoured.

SF occupancy 00101 The section computed for the SF occupancy 00101+0 is reported in Fig. 5.11 (K^+-free S0). The calculation revealed the strong influence of K^+ in the site S0 on the dynamics of the network. Although the shape of the FES is similar to the 10101+0 section, the D80flip state appears to be more stable. The enhanced stability mainly depends on the increment of the energy barriers in the pathways joining D80nonflip-E71close to D80flip ($13 - 14$ kcal/mol for the flipping of D80, $11 - 12$ kcal/mol for reverse transitions, "a $\leftrightarrows$ b" or "a $\leftrightarrows$ c"), derived from the near-suppression of the intermediate states: D80semiflip and D80nonflip with the broken E71–D80 H-bond. The absence of a K^+ in the site S0 promotes states with closer D80 and E71 side chains, both in D80nonflip and D80flip regions, because it is accompanied by a small widening of the external mouth of the SF. In D80flip, the interactions were facilitated by the rotation to $\sim -70°$ of $\chi 1$ dihedral angle of E71.

Interestingly, the transition of D80 caused distortions of the SF structure. Along with V76, G77 (G77-Y78 peptide group) also underwent similar flipping (Fig. 5.11, K^+-free S0, c and b). V76 and G77 were seen alternatively flipping, leading to the hypothesis that these transitions belong to adjustments of the SF induced by the conformation of D80, particularly by the D80 flipped state.

Given the high barriers, probability must be relatively low of the system performing the transition to D80flip along the minimum energy pathway of this section. However, as will be shown later, the system can go from "a" to "b" involving R64–D80 interactions. This means performing orthogonal movements with respect to the reported section. In a similar way, the life time of D80flip would be reduced by an incoming K^+ from the bulk to S0, which facilitates reverse transitions to D80nonflip states.

Two different relaxations were performed from the D80flip states "b" and "c", each $\sim$ 12.5 ns long. In both cases the D80flip state was found to be meta-stable for the length of the simulations and the side chain of the flipped D80 fluctuated between "b" and "c".

D80 transitions for L81 flipped: influence of R64

The analysis reported in Chap. 4 proved that L81 in the flipped conformation allows more stable interactions between the R64 and D80 side chains, which are able to deliver strong perturbations on the state of D80 and, consequently, on E71–D80 H-bond. Moreover, these perturbations propagate to the SF and to the K^+ ions bound to it. These behaviours were further investigated with specific focus on R64 motions by means of the CV d64 (see sec. 2.4.1). Therefore, the metaD calculations of the L81-flipped sections were performed with respect to chi80, d71 and d64.

SF occupancy 10101 It was not possible to compute the section for the SF occupancy 10101+0 successfully. Three different calculations were commenced and in each case the ion in S0 moved to the bulk a short time after the E71–D80 H-bond had broken. A definitive conclusion cannot be drawn because the origin of the transition was not deeply investigated. In any event, we hypothesise that some states of the network, visited during the metaD sampling were able to destabilise configurations with a K^+ in the site S0, consistent with the influence described in Chap. 4. These states are likely to have been promoted by the dynamics of R64.

SF occupancy 00101 The influence of R64 enhances the variability of the D80 side chain. The three-dimensional FES (chi80, d71 and d64) for the SF occupancy 00101+0 and L81 flipped is reported in Fig. 5.12, and for the sake of clarity it is accompanied by the two-dimensional projections over: i) *chi80-d71*, ii) *chi80-d64* and iii) *d71-d64* (see. Sec. 2.4.2). The influence of R64 is immediately noticeable from a direct comparison of the projection "chi80-d71" with the FES section computed for L81 non-flipped and the same SF occupancy 00101+0 (Fig 5.11), in which D80–R64 interactions are minimised. Intervention by R64 made the breaking of the E71–D80 H-bond and the flipping of the D80 side chain ("a $\rightarrow$ f") kinetically more accessible (lower barriers) and thermodynamically favoured. The absolute minimum of the section is D80flip-R64close ("f", d71 $\sim$ 7.2 Å, d64 $\sim$ 4.5 Å), which corresponds to D80 and R64 side chains tightly H-bound.

A lowest-energy pathway can be drawn joining D80nonflip-E71close ("a") which differs from the initial X-ray structure only for the flipped conformation of the L81 side chain, with the deepest minimum D80flip-R64close ("f"). In the first step ("a $\rightarrow$ b"), the R64 side chain moves toward D80 and destabilises E71–D80 H-bond. The guanidino group of R64 has the greatest destabilising effect when located close to D80 but not close enough to form a H-bond ("b", chi80 $\sim$ 65 degrees, d71 $\sim$ 3.5 Å, d64 $\sim$ 6.5 Å). The second step ("b $\rightarrow$ c") involves the breaking of E71–D80

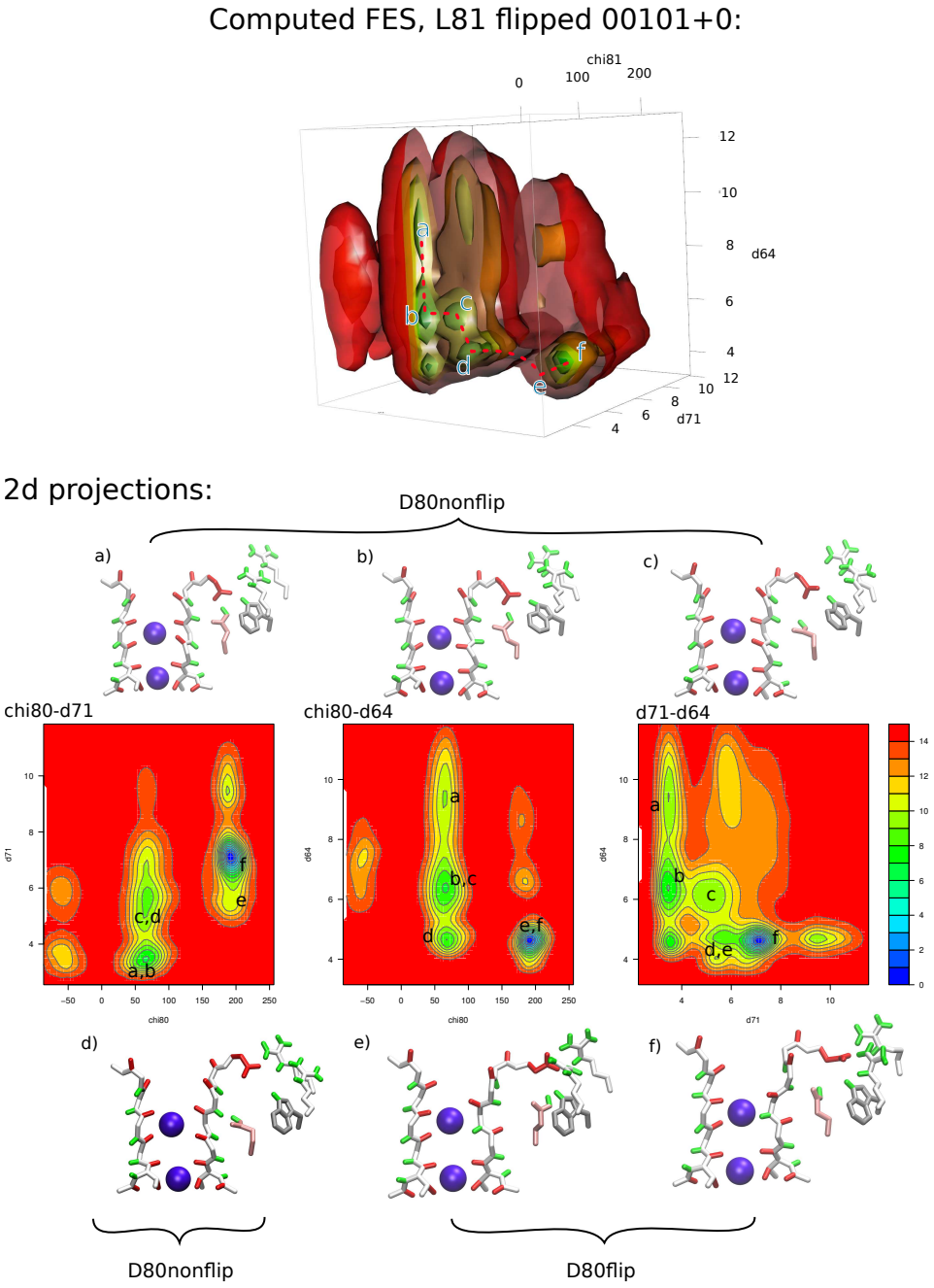

Figure 5.12: Multi-dimensional section of the FES as a function of the CVs chi80, d71 and d64 computed for L81 in the flipped conformation (chi81 $\sim 185°$) and SF occupancy 00101+0. The complete computed FES is reported as well as different projection over the planes: i) chi80-d71, ii) chi80-d64 and iii) d71-d64. A minimum energy pathway is drawn accompanied by representative conformations of the protein. Energy in kcal/mol, distances in Å, lines in the contour plots are drawn every 1 kcal/mol.

H-bond. A very peculiar transition state is obtained, in which D80 is approximately equidistant ($\sim$ 4.5 Å) from the H-bond donors belonging to E71, R64, R89, and is H-bound to W67 ("c", chi80 $\sim$ 65 degrees, d71 $\sim$ 5.5 Å, d64 $\sim$ 6 Å). H-bonds between R64 and D80 are then created while D80–W67 H-bond is broken ("c $\rightarrow$ d"). The one-dimensional FES for d71 in the case of L81 flipped and SF occupancy 00101+0 reported in Fig. 4.12 in Chap. 4 is effectively a projection of the path from "b" to "d". Consistent with that result, the existence of E71-D80 is favoured in the D80nonflip region, although the influence of R64 facilitates its breaking. The conformation "d" appears as a key transition state: the D80 side chain rotates $\sim$ 130° around chi80 until D80flip-R64close ("e", chi80 $\sim$ 195 degrees, d71 $\sim$ 6.5, d64 $\sim$ 4.5 Å) is reached in the most energetically expensive transition ("d $\rightarrow$ e"). After the flipping, the system fluctuated between two minima in the D80flip-R64close region, "e $\leftrightarrows$ f", with a predominance for the latter, which is the most stable configuration among those sampled. The states "e" and "f" are characterised by D80 H-bound with R64, R89, W67 and differ because of a rotation of E71 around its $\chi 1$ dihedral angle. The total energy for the transition "a $\rightarrow$ f" is $6-7$ kcal/mol, lower than the energies computed for similar transitions in the case of L81 non-flipped, i.e minimising the influence of R64 in the process. The highest barrier is the flipping of the D80 side chain that has a value of between 5 and 6 kcal/mol.

D80flip states were accompanied by strong distortions in the SF structure, stronger in the presence of R64–D80 H-bonds and compatible with the collapsed conformations suggested for the inactive structure by X-ray experiments.[42,157] A few representative distorted states, visited during the sampling are reported in Figs. 5.13a, 5.13b and 5.13c. These distortions destabilised the K^+ ions bound to the SF. The K^+ which was initially located in S2 fluctuated between sites S2 and S3, and displacements of the innermost K^+ to the cavity occurred a few times, accompanied by the entry of water molecules from the bulk between the ions. Thus, the computed FES can be better considered as the section for S0 and S1 not occupied by K^+ ions rather than the section for 00101+0 with a vacancy in S3.

Intriguingly, more prominent distortions were caused by D80semiflip states (chi80 $\sim$ 60°, Fig. 5.13d), when the side chain of D80 was H-bound to all the neighbouring residues E71, R64, R89, W67. The distortions allowed a large number of water molecules to enter into the SF from the region behind the SF, finally disrupting the single-file arrangement (Fig. 5.13e and 5.13f). Due to its high energy, this particular D80semiflip state was visited quite late during the sampling, Fig. 5.12 and several analyses suggested that a good convergence of the remaining regions of the FES was reached before the water molecules disrupted the single-file arrange-

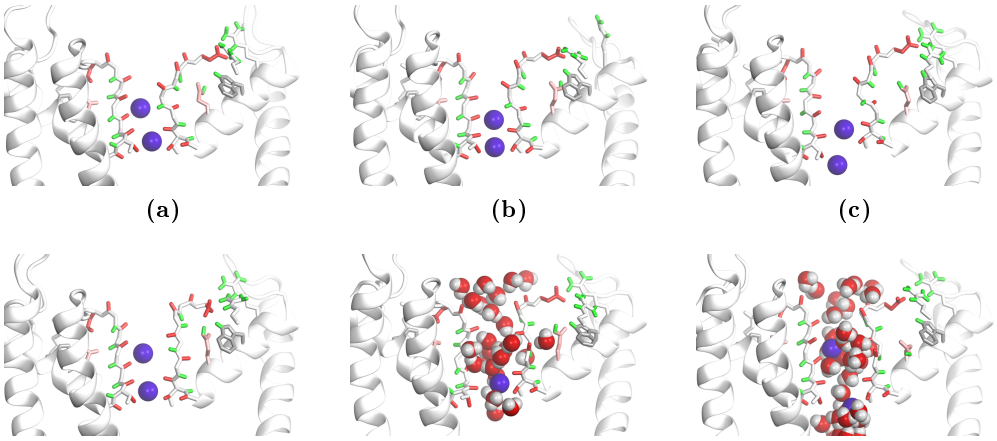

Figure 5.13: Snapshots obtained from the metaD calculation of the multi-dimensional sections of the FES as a function of the CVs chi80, d71 and d64 (L81-flipped and SF occupancy 00101+0).

ment. In any event, this state capable to produce a "disrupted" conformation of the filter belongs to the system phase space, and can be caused by the state of the D80 side chain the surrounding H-bond donors. The existence of these "disrupted" states might help to explain experimental observation of the "defunct" states of K^+ channels.[66]

E71CA-D80CA distance in the D80 side chain flipped conformation.

The stability of D80flip-R64close configuration "f", the deepest minimum of the FES, was investigated with an unbiased relaxation performed without any additional restraint.

A long simulation was performed ($\sim$ 114 ns) in order to collect good statistics. The flipped state of D80 was found to be meta-stable for all of the simulated time. D80flip-R64close was found to be the most visited state, but was not unique. The L81/R64 interplay discussed in Chap. 4 was confirmed. The equilibrium of L81 between flipped and non-flipped configurations affected the stability of the D80–R64 H-bonds, sometimes causing them to break. In any event, they demonstrated a better stability with respect to L81 reverse flipping in D80flip-R64close than in D80nonflip-R64close. In addition to the breaking of D80–R64 H-bonds, L81/R64 interplay enhanced the probability of the states which are similar to the minimum "e" in Fig. 5.12, and generated new states characterised by the creation of a H-bond between D80 in the flipped conformation, and E71 rotated with $\chi 1 \sim -70°$.

Similar to the MetaD calculation, some of the distorted conformations assumed by the subunit with the D80 in the flipped state were close to the putative inactive state (Fig. 5.14)[157], although none of them could be defined as "collapsed". Additionally, the conformation of the network of residues allowed water molecules to diffuse behind the SF (Fig. 5.14), similar to that which was observed by the X-ray experiments.

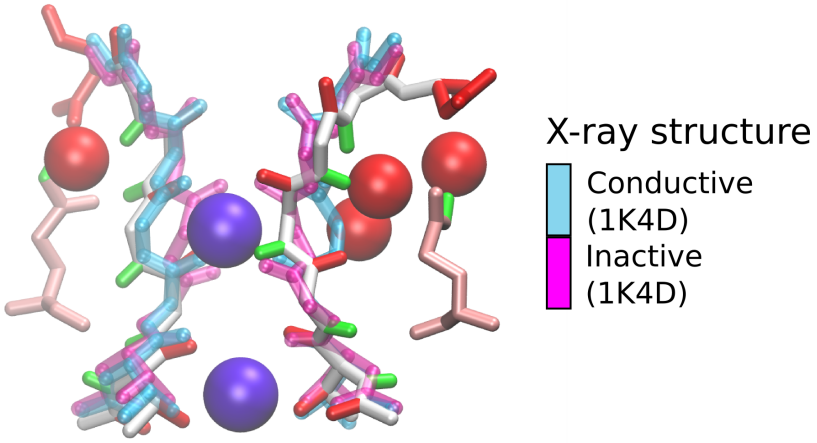

Figure 5.14: Superposition of a representative conformation observed during the simulation with two X-ray structures: the putative conductive structures (light blue, pdb code 1K4C[157]) and a structure obtained in the presence of a low [K^+], which has been proposed as being inactive (magenta, pdb code 1K4D[157]).

Recent studies proposed the lowering of the backbone distance $C_\alpha - C_\alpha$ between positions 71 and 80 (which will be called *E71CA-D80CA*, Fig. 5.15) directly linked to the inactivation process and to the inactivation probability among different mutants.[36,37] In any event, a mechanism that could lead to this reduction remains unclear for the WT. Analysis of the D80flip state showed the lowering of *E71CA-D80CA* can be caused by transitions of D80 side chain.

E71CA-D80CA was ~ 10 Å for the putative conductive state, D80nonflip, in the presence of the strong E71–D80 H-bond, both from simulations and X-ray experiments. Our simulations showed that the backbone distance increases as a consequence of the simple breaking of the E71–D80 H-bond. By contrast, the long simulation commenced from D80flip-R64close revealed values of E71CA-D80CA lower than 10 Å (Fig. 5.16). Fig. 5.16 shows that a linear dependence existed between E71CA-D80CA and the position of the D80 side chain (d71CA, Fig. 5.15 and Sec. 2.4.1 for the definition), with a Pearson's correlation coefficient= 0.93: the deeper the D80 side

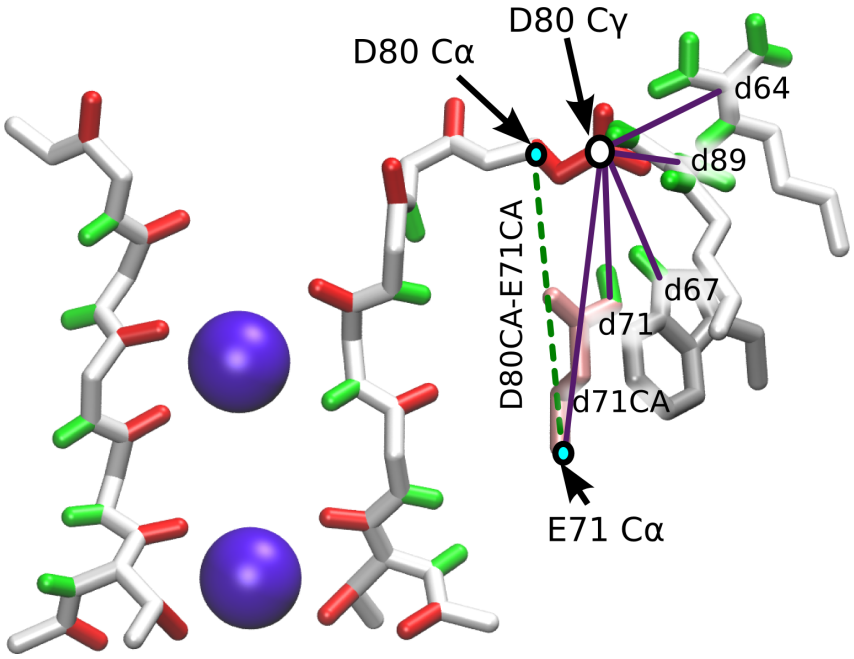

Figure 5.15: The definition of the order parameters used to perform statistical analyses on the simulation commenced from D80flip-R64close: i) E71CA-D80CA, backbone distance $C_\alpha - C_\alpha$ between positions 71 and 80, ii) d71CA, the position of D80 side chain with respect of the C_α atom of residue 71 used as a reference; the distances between the side chain of D80 (defined by the C_γ atom) and the side chains of the neighbouring H-bond donor residues iii) d71, the distance from E71 (defined by the H-bond donor oxygen belonging to E71 carboxyl group), iv) d64, distance from R64 defined by the C_ζ atoms, v) d89, distance from R89 defined by the C_ζ atoms, and vi) d67, distance from W67 defined by the $N_{\epsilon 1}$ atom.

chain was buried behind the SF, the lower E71CA-D80CA became. Two main states could be identified from distributions and scatter plots of d71CA and E71CA-D80CA: i) *D80flip-buried*, E71CA-D80CA < 10 Å, for values of d71CA < 10.8 Å (green regions in Fig. 5.16); and ii)*D80flip-nonburied*, E71CA-D80CA > 10 Å, in which the D80 side chain was more exposed to the extracellular bulk (d71CA > 10.8 Å).

The position of the D80 side chain and, consequently, the E71CA-D80CA distance, was dependent on the dynamics of E71, R64, R89 and W67, the H-bond donor residues of the first level of the network. Correlations between the position of the D80 side chain and its distance from the neighbouring H-bond donors were analysed by means of the order parameters d71CA, d71, d67, d89 and d64 (see Fig. 5.15, and Sec. 2.4.1 for definitions). Fig. 5.17d reports scatter plots, correlations matrix, and distributions. The high Pearson's correlation coefficients (between 0.63 and 0.91) suggest a very high degree of cooperativity in the network of residues. Magenta dashed horizontal lines separate the states D80flip-buried from D80flip-nonburied, whilst vertical dashed lines divide the states where H-bonds exist between side chains of D80 and the neighbouring donors (green regions), which are the most populated with d64, d89 and d67. Above the horizontal lines (D80flip-nonburied), side chains of H-bond donors E71, R89, W67 and R64 moved consistently with the negatively charged D80 side chain, even for relatively long distances (donor-acceptor distances up to ~ 12 Å in the case of arginines). A slight deviation for d64 was likely to have been caused by L81/R64 interplay. This proves the long actions of the electrostatic forces that dominate the dynamics of the network. The presence of intermittent H-bonds with R64, R89 and W64 promoted the burying of D80 side chain, since they mainly exist below the horizontal lines (D80flip-buried). In this region, the linear dependence of d71CA was weakly maintained only with d71, and it was related to rearrangements of E71 observed in the metaD calculations. These rearrangements mainly involved rotations among two main positions of $\chi 1$ dihedral angle, $\sim 180°$ and $\sim -70°$, while $\sim 70°$, the conformation of conductive structure, was rarely visited. In the collapsed X-ray structures, $\chi 1 \sim -70°$,[42,157] and in this conformation temporary H-bonds were formed between E71 and the flipped D80 side-chain. The presence of this H-bond corresponded to the maximum depth of D80 side chain in the region behind the SF (lowest values d71CA) and consequently to the shortest backbone distances $C_\alpha - C_\alpha$ between positions 71 and 80 (E71CA-D80CA). The creation of the H-bond appeared to have a strong destabilising effect on the SF structure, consistent with the hypothesis that a correlation exists between backbone distances E71 C_α and D80 C_α and inactivation.[36,37]

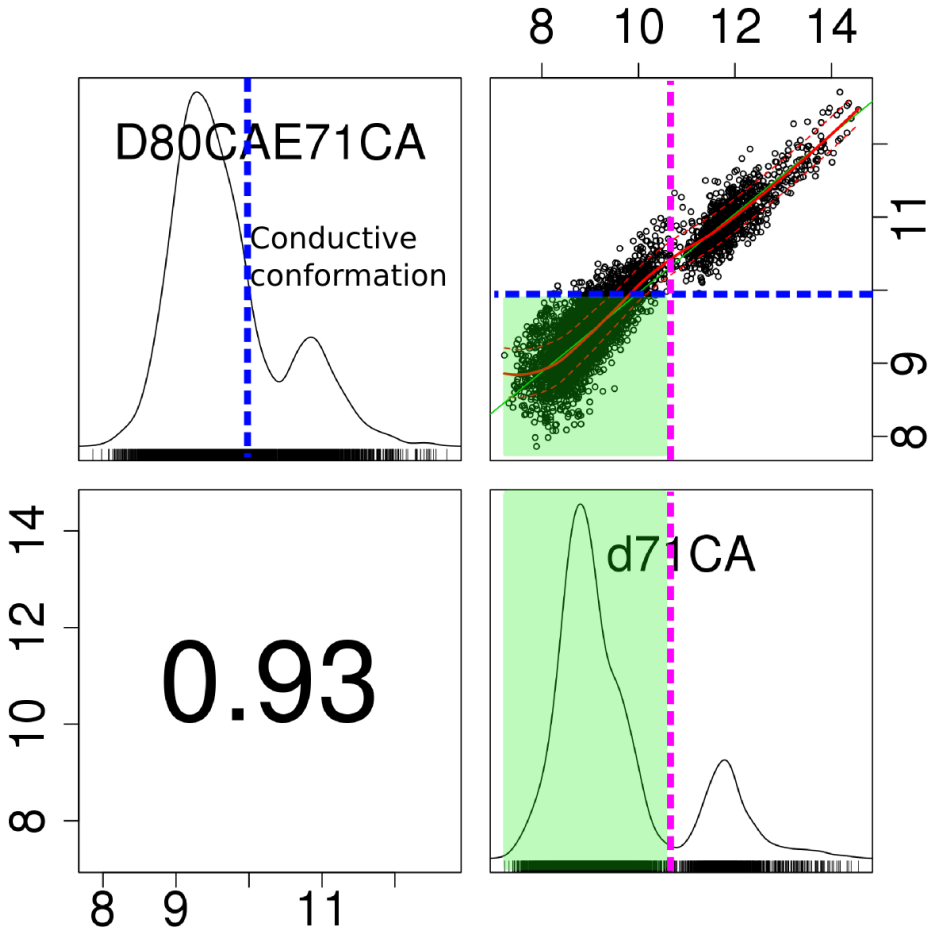

Figure 5.16: Upper left panel reports the scatter plot of the two order parameters E71CA-D80CA and d71CA from the simulation commenced from D80flip-R64close. A smoothing line (red, computed using "gam" function[52]) and a regression line (green) are added to aid the visualisation of the linear relationship between the two order parameters. The lower-left panel reports the correlation (Pearson) and the kernel density estimations of the order parameters are reported in the upper-left and lower-right panels (computed by density function as implemented in R[122]). Data are reported in Å. The magenta dotted line define the most populated region for d71CA which mostly correspond to values of E71CA-D80CA lower than in the putative conductive conformation (blue dotted line[157]). Previous works linked the lowering of E71CA-D80CA to the inactivation process and to the inactivation probability among different mutants of KcsA, but a possible mechanism for this lowering in the WT still remains obscure.[36,37] These result showed that a lowering E71CA-D80CA is achieved in the case of D80flip-R64close state.

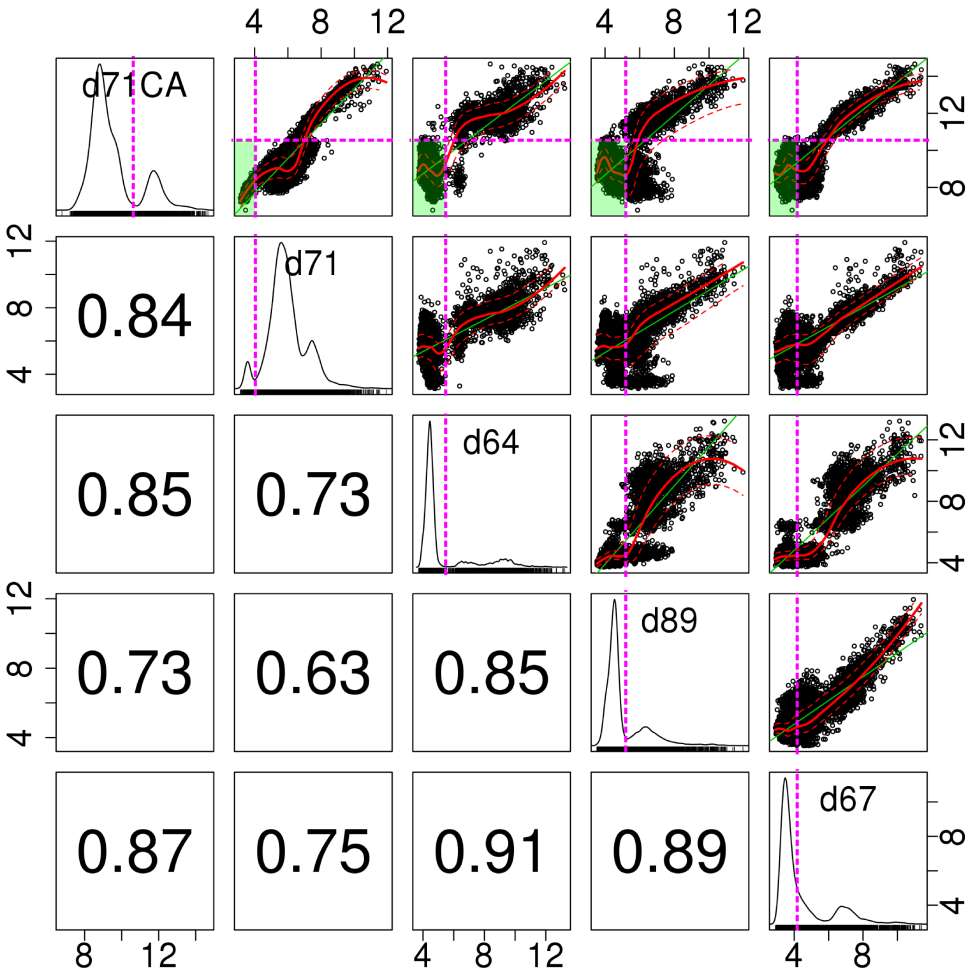

Figure 5.17: Scatter plot matrix from the simulation commenced from D80flip-R64close of the order parameters d71CA (which represents the position of the D80 side chain) and d64, d89, d64, d67 (the distances of D80 side chain from the neighbouring H-bond donors). Data are reported in Å. The figure reports also correlations (Pearson) in the lower triangle and kernel density estimations in the diagonal (computed by density function as implemented in R[122]). Smoothing lines (red, computed using "gam" function[52]) and regression lines (green) are added to aid the visualisation. The horizontal magenta dotted lines define the most populated regions for d71CA, while the vertical magenta dotted lines define the region in which an H-bond exists between D80 and the donor. The figure and the high correlations demonstrates that the lowering of d71CA, and thus of E71CA-D80CA, is a highly cooperative process, in which all the H-bond donors are involved.

5.6 D80 side chain flipped in two subunits

Conformational changes in D80 side chain of one subunit associated with rearrangements in the neighbouring donors E71, R64, R89, W67 were observed, accompanied by a strong destabilisation of the SF structure. Deeply non-conductive states ("disrupted") were reached during a metaD calculation as a consequence of the D80 side chain in the semiflipped conformation H-bound to all neighbouring donors E71, R64, R89, W67, in the case of SF occupancy 00101+0 and L81 flipped. However, different states that required less energy to be reached, such as D80flip, were able to deliver relevant distortions reminiscent of pore constriction mechanisms of inactivation without a completely contemporaneous closure of the filter. By contrast, a complete collapse was obtained whilst investigating the pH-related inactivation when analogous transitions occurred in more subunits. Moreover, a certain degree of cooperativity between subunits in the inactivation process was proposed by different studies.[42,66,90,114,116,125,157] This leads to the possible conclusion that different pathways for inactivation could arise from conformational changes in the networks behind TVGYG sequences of more than one subunit.

The investigation of the cooperativity between subunits is not not trivial. A single calculation able to deliver a comprehensive picture resulted excessively computational demanding due to the great number of degrees of freedom involved. A simplified approach was developed: *multi-D80flip* states for the protein were achieved promoting the transitions of D80 side chains individually on each subunit by means of metaD procedure using chi80 and d71 as CVs (see Sec. 2.4.1). Inactivation was looked for and eventually found by means of unbiased relaxations from these multi-D80flip configurations.

Both conformations, D80flip-R64close and D80flip-R64far, were investigated. The reason behind the investigation of the latter was mainly for the purpose of understanding possible pathways which might be responsible for inactivation in R64A, i.e. in which R64 does not form part of the process. Following the results on the influence of the K^+ ions bound to the SF, the investigation focused on the SF occupancy 00101+0, i.e. without a K^+ in S0 and with a vacancy in S3.

D80flip-R64far

Inactivation obtained during MetaD calculation Initially, MetaD calculations were performed to obtain D80flip-R64far-AB on a representative conformation of D80flip-R64far-A obtained from the relaxation described in Sec. 5.5.1 (2 ns, SF occupancy 00101+0). The biased residues belonged to the subunit opposite to the

one in the D80flip state.

The calculation ended in a collapsed structure which was considered to be inactive. The collapse of the SF happened after the flipping of D80 from the second subunit and was confirmed by two metaD calculations, which were respectively standard and a well-tempered. Fig. 5.18 reports the final state obtained from a $\sim 10\ ns$ of relaxation of the last frame from the metaD calculation. During the relaxation, the number of curved TVGYG sequences fluctuated between 2 and 3. The curved conformation obtained from simulation (coloured) superimposes very well with the putative inactive structure obtained by X-ray experiments in the presence of a low $[K^+]$ (pdb code 1K4D[157]).

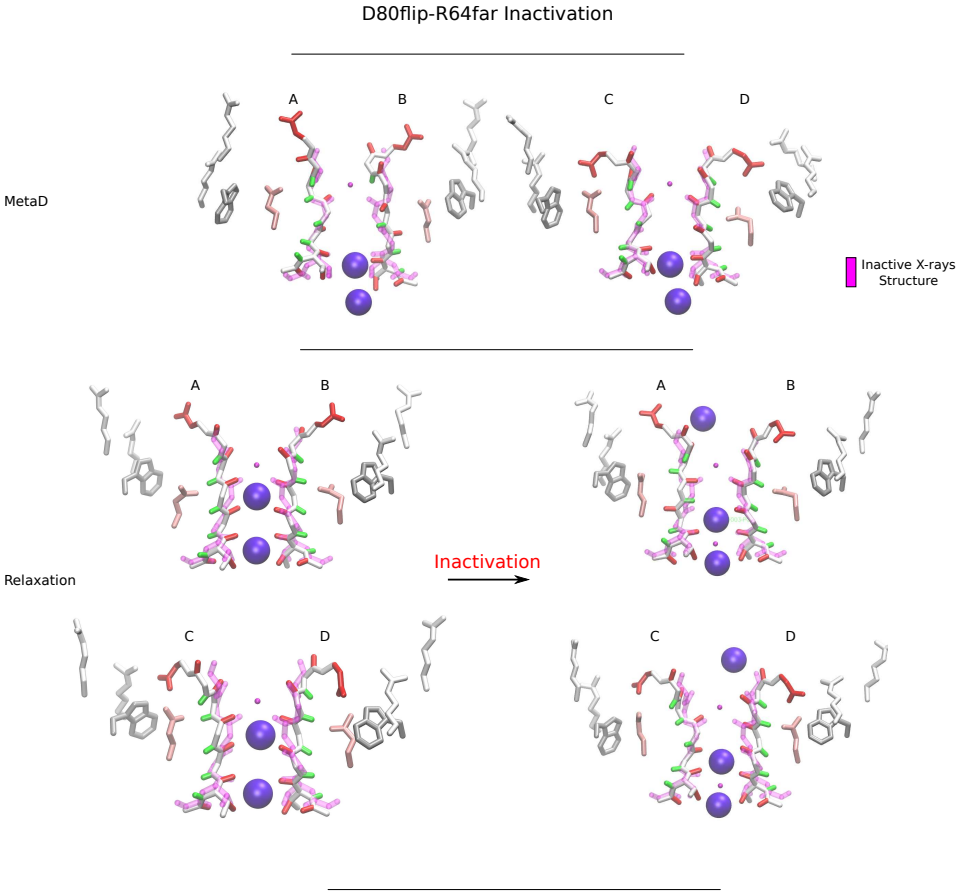

Figure 5.18: Inactive states reached from the states D80flip in simulations (both from metaD and unbiased calculations) commenced from D80flip-R64far-AB. The metaD calculation was followed by an unrestrained relaxation, from which the snapshot is reported. The conformations are superimposed with the putative structure of the inactive state of the SF (coloured in magenta, pdb code 1K4D[157])

Relaxation The result was confirmed by searching the collapsed inactive state by means of unbiased simulations.

Different multi-D80flip states in 00101+0 SF occupancy were obtained via well-tempered metaD calculations on chi80 and d71 for 10101+0 SF occupancy and L81 non-flipped, in order to avoid the collapse of the filter. These configuration were: i) D80flip-R64far-AB; ii) D80flip-R64far-AD; and iii) D80flip-R64far-ABD. The flipped state of D80 side chains previously demonstrated to be relatively unstable for this SF occupancy (Fig. 5.11). Accordingly, it was maintained with weak harmonic restraints ($K = 2.5$ kcal/mol degree^2) while transitions in different subunits were sampled. The FESs that were obtained are consistent with those for the first subunit, but with minor variations (Fig. 5.19). These differences are likely to be dependent on correlations between the different subunits mainly arising from the deformations on the SF structure imposed by D80flip states. However, it is difficult to draw a conclusive picture from these energy surfaces and the calculations were mainly performed to ease the occurring of rare events and overcome high barriers, reaching states which, though available to the system, were inaccessible because of computational limits.[86] Occupancy 00101+0 was obtained moving the K^+ in S0 to the bulk with an harmonic restraint ($K = 5$ kcal/mol Å^2).

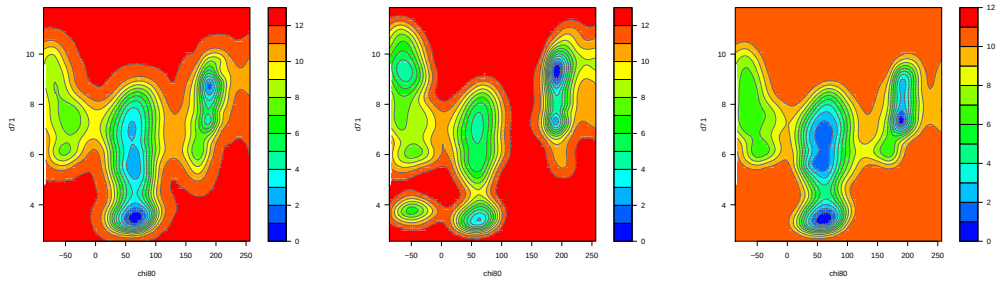

(a) D80flip-R64far-AB

(b) D80flip-R64far-AD

(c) D80flip-R64far-ABD

Figure 5.19: FESs as a function of chi80 and d71, for 10101+0 and L81 non-flipped, calculated for different multi-D80flip conformations. Transition of D80 were promoted individually for each subunit, maintaining the flipped state of D80 side chains of the remaining subunits with weak restrains ($K = 2.5$ Kcal/mol degree^2). Energy in kcal/mol, distances in Å, lines in the contour plots are drawn every 1 kcal/mol.

Six simulations were performed: two from each conformation. Only one of the relaxations, that was commenced from D80flip-R64far-AB, relaxed into putative inactive conformation within the first ns. Two subunits superimposed well with the

collapsed X-ray structure (Fig. 5.18). In addition to the reduced variability of D80 and the overall network, the inactivation process appeared random, variable and quite unfavoured without the intervention of R64 (one over six reached the inactive state). Inactivation probability in the metad calculations on D80flip-R64far and SF occupancy 00101+0, previously described, might have been increased by the life times of the D80flip states being extended by the bias potential. The fact that inactivation was obtained from D80flip-R64far-AB is hypothesised originating from the random nature of the process rather than from a real preferential pathway.

Intriguingly, a conformation with all the four subunits in the D80flip state was not reached via metaD because the filter collapsed during the calculation, with two opposite subunits in the curved conformation.

D80flip-R64close

Obtaining D80flip-R64close for more than one subunit was not an easy task. As previously described, Sec. 5.5.1, the flipping of the D80 side chain caused strong distortions in the conformation of the TVGYG sequence when R64 was in its proximity. Several tests performed when considering more than one subunit showed that SF underwent transitions irreversible within the length of the simulation and, therefore, would have required detailed consideration within the biased calculation. A simple CV, such as RMSD from the X-ray structures used for similar purposes in previous studies, was found to fail in distinguish most of the SF transitional states. Similar issues of computing free energies as a function of RMSD are known and discussed in literature, and more sophisticated CVs were recently developed to represent comparable complex systems.[27,144] Unfortunately, at the time of writing their implementation requires are computationally too expansive an consequently they have only been employed on systems smaller then the one considered in the present work. In the light of these considerations a simpler approach was applied.

The desired multi-D80flip-R64close states were obtained starting from the corresponding D80flip-R64far conformations. The side chain of R64 was moved closer to D80 by means of short MD simulations (250 ps), applying additional harmonic restraints on $\chi 1$ dihedral angles of residues R64 and L81 ($\text{chi64}_0 = -160$, $\text{chi81}_0 = 185$, $K = 20$) and on D80-R64 distance ($d64_0 = 4.7$, $K = 10$), followed by a relaxation. Given the complex variability of the system, numerous attempts to apply the approach failed, mainly because the reverse flipping of L81 did not allowed the stabilisation of the desired multi-D80flip-R64far state. The application of the approach to the state D80flip-R64far-ABD, after ~ 1.5 ns of relaxation, successfully resulted in the D80flip-R64close-BD, with the D80 side chain from subunit A that

flipped back and recreated the H-bond with E71 (after $\sim$ 1.3 ns), and SF occupancy 00010+1. A similar occupancy was seen during previous calculations that involved D80flip and was induced by the influence of R64 (Sec. 5.5.1 and 5.5.1). In any event, it never led to a state that could be considered to be completely inactive, even during long sampling ($>$ 100 ns).

Further relaxation of D80flip-R64close-BD inactivated the channel via pore constriction (within $\sim$ 5 ns), with the TVGYG sequences from three subunits having a curved conformation that closely resembled the X-ray structure of the collapsed state (Fig. 5.20). The superposition was particularly good for subunit A; subunit C and D differed mainly for V76 in a flipped conformation; conformation of subunit B was stabilised by an H-bond between V76 and G77 peptide groups from subunits B and D.

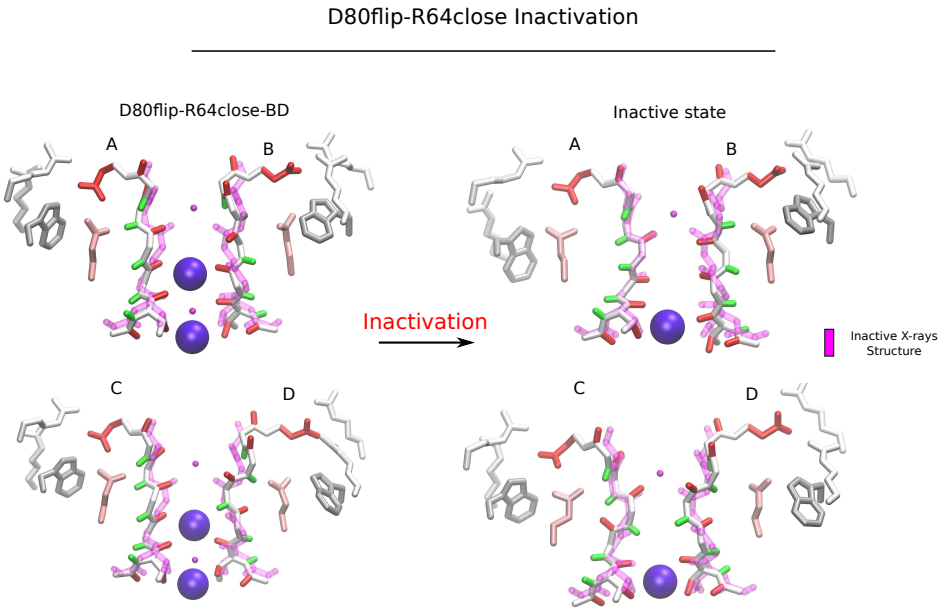

Figure 5.20: Inactive states reached from D80flip-R64close-BD, superimposed with the putative structure of the inactive state of the SF (coloured in magenta, pdb code 1K4D[157]).

5.7 FESs for Y82A and R64A

A mechanism for inactivation in KcsA has been proposed in this work. That mechanism involves the rich dynamics of the network of residues behind the SF, especially D80 and its neighbouring H-bond donors. The arginine R64 proved to have a strong influence in facilitating the transitions associated with inactivation. In Chap. 4,

residue Y82 was linked with the variability of R64, which was found to be enhanced by the mutation with an alinine (Y82A). The close relationship between R64 mobility and the ease with which the network, and in particular D80, is able to undergo transitions can explain the inactivation probability trend among the different proteins Y82A > WT > R64A.[35] This hypothesis was confirmed by comparing estimates of the FES with respect to chi80 and d71 computed for Y82A and R64A with those for WT.

Due to the comparative approach, no detailed calculations for all the K^+ configurations in the SF were performed. The initial relaxed configuration was obtained from simulations described in Chap. 4, with SF occupancy 01010+1 for R64A and 01011+0 for Y82A. No additional restraints were applied.

R64A

For R64A the K^+ ions converged once again to the 10101+0 configuration with an empty S3 site, via 01011+0. The shapes and barriers of the resulting FES (Fig. 5.21) very closely resembled those obtained for the WT in the case of L81 non-flipped and 10101+0 occupancy (Fig. 5.11). The main differences were in the D80flip region, in which the minima were deeper for R64A. In this mutant, the D80 side chain in the flipped conformation was stabilised by H-bonds with Y82 and R89 of the neighbouring subunit. In the WT, the presence of R64 opposite Y82 with respect to the D80 carboxyl group enhanced the variability of the latter, causing a slight destabilisation and a widening of the D80flip minima. The similarity between the two FES confirms the relevant role played by L81 in the inactivation process, in regulating R64 mobility, and indirectly affecting the stability of the SF. On the other hand, it strongly supports the hypothesis that the reduced inactivation probability originated from the absence of R64 that lead to a reduced variability of the network behind the pore.

Y82A

During calculations performed on Y82A, the SF region showed a strong variability until a collapsed state was reached with 00011+0 occupancy and two TVGYG assuming a curved conformation. In Fig. 5.22a the configuration obtained after a brief relaxation from the last frame of the metaD calculation is superimposed with the putative inactive X-ray structure.

Once again the dynamics of system was quite complex. Strong correlations between the different subunits arose. The breaking of E71–D80 H-bond in the sub-

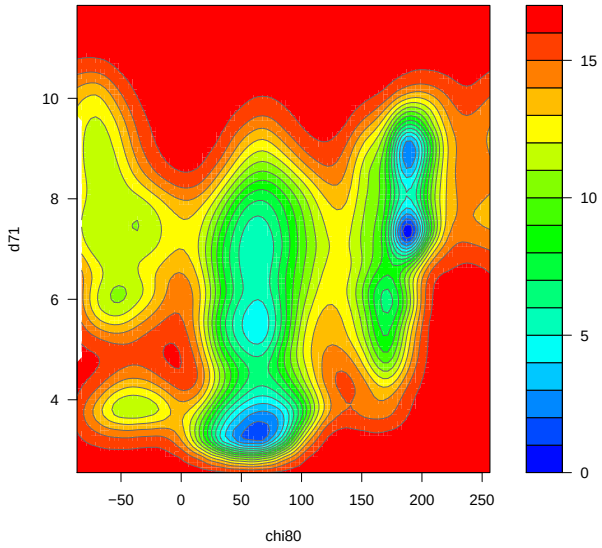

Figure 5.21: FES as a function of the CVs chi80, d71 for the mutant R64A.

unit A, promoted by the bias potential, was soon followed by a similar event in the nearby subunit (D). Similar correlations between subunits were seen also for the WT, but they were weaker the in Y82A. Despite the fact that the D80 residue of subunit D was not biased, a strong mobility around chi80 was observed, including the flipping. Intriguingly, E71 was also found quite soon to be rotating to ($\chi 1 = -70°$) and H-binding D80 in the flipped conformation, thereby greatly destabilising the SF. This was also seen in the final conformation (Fig. 5.22a).

The diabatic energy surface obtained from the calculation (Fig. 5.22b) cannot be considered as a good estimation of the FES because the filter performed irreversible transitions within the sampling. In any event, it gives an idea of the preferred configurations for chi80 and of the energies required to overcome the barriers. The biased D80 spent most of the time in the D80flip state. The energies involved in the transitions from the initial configuration (D80nonflip and E71–D80 H-bond formed) to reach D80flip were relatively low ($6 - 7$ kcal/mol), similar to WT in the case of L81 flipped and 00101+0 occupancy. A difference from the latter FES was that D80semiflip was visited more often. In any event, the calculation confirmed that the inactivation probability related to the dynamics of the network of residues behind the SF, and in particular D80, and the strong influences of R64 and E71 in the inactivation.

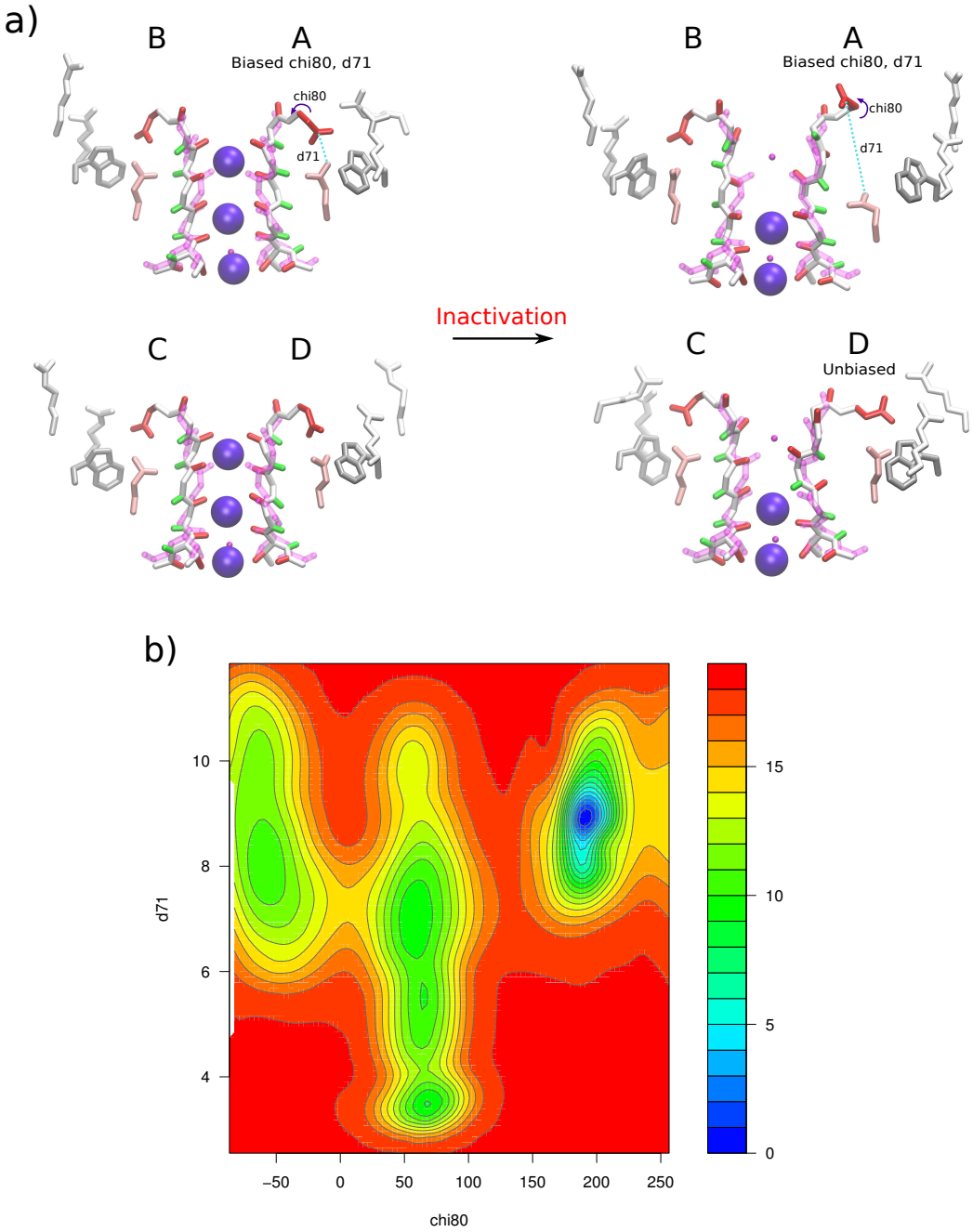

Figure 5.22: a) Inactivation of Y82A obtained via MetaD calculation; b) Diabatic energy surface for Y82A.

5.8 Conclusions

Conformational changes in the region of the selectivity filter are responsible for the gating process known as C-type inactivation in K^+ ion channel, which is crucial in the regulation of conductivity.[30,35,37,85,93,119,141,151,157] Current measurements suggest the existence of different inactive states, and two mechanisms for inactivation were proposed which involve either dilation or constriction of the pore.[41,66,147,155] Putative inactive structures were proposed for the K^+ ion channel KcsA, solved in the presence of a low [K^+] or associated to the concurrent opening of the inner gate, which is characterised by a collapsed state of the SF.[42,157] Mutagenesis studies proved the important roles of different residues surrounding the pore region in defining the probability of inactivation.[34–37] Previous works suggested that a network of hydrogen bonds between the E71, D80 and W67 side chains is involved in the stabilisation of the conductive conformation and E71–D80 bridge has a central role in the inactivation process.[34–37,42] Although either the disruption or the strengthening of the linkage were suggested as the reasons for the inactivation, pathways and the mechanisms for the influences of the remaining relevant residues remain elusive.[34–37,42,66] Extensive theoretical work, described in Chap. 4, demonstrated that the network of hydrogen bonds is in reality a small part of a highly coupled network of residues which are able to affect the state of SF and of the permeating ions. Central to this network is the residue D80, located at the outer entrance of the filter, as well as the hydrogen bond donors E71, R64, R89, W67, defined as the first level.

In the present chapter a mechanism for inactivation has been proposed which is based on the rich dynamics of the network of residues centred upon D80 (Fig. 5.23). Interactions with the neighbouring arginines, in particular with R64, promote the mobility of D80 side chain. A flipped state of D80 side chain is particularly favoured. However, because of the interactions with the neighbouring H-bond donors (E71, R64, R89, W67), this state delivers a destabilisation to the SF, which causes strong distortions to the structure of the TVGYG sequence and to the K^+ ions bound to it. The destabilisation is associated with a lowering of the backbone distance between positions 71 and 80 ($C_\alpha - C_\alpha$) which is maximal when flipped D80 is H-bound with E71 as well as all the remaining donors. When the flipping of D80 occurs in more than one subunit, the destabilisation becomes strong enough to cause the vacation the central region of the filter from the K^+ ions and the collapse of the filter structure, leading to the inactivation.

The results confirmed that the collapsed states proposed by different X-ray studies[42,157] can indeed represent inactive states and can be reached without the

concurrent opening of the intracellular gate or the presence of a low [K^+]. The determinant for the inactivation process is the network of residues behind the SF, and particularly the variability of the aspartic acid D80. The latter belongs to the sequence TXXTXGYGD, known as "signature sequence", which is highly conserved among K^+ ion channels. The fact that it is surrounded by different Hydrogen-bond donors in the different channels, suggesting that similar mechanisms for current regulation centred on the aspartic acid may have a wider importance among the K^+ ion channel superfamily.

Two different states for the D80 side chain were found to be capable of inducing relevant distortions on the structure of the SF: D80flip, $\chi 1$ dihedral angle between 140 and 250, and D80semiflip, $\chi 1$ between -110 and 0. Relevant changes in the state of the D80 side chains were determined by the creation of H-bonds with the neighbouring arginines, R64 and R89, which finally deliver strong destabilisation on the conductive conformation of the channel. Although not necessary to undergo inactivation, R64 was found to be particularly significant both kinetically and thermodynamically in promoting the process involved in the lowering of the barriers and in the stabilisation of the flipped states of D80. Moreover, a high degree of cooperation among all the H-bond donors E71, R64, R89, W67 was proved in the process. Electrostatic interactions appear to dominate the transitions and to act over a wide range. These results can explain experimental evidences on the role of the arginines in the inactivation of KcsA and their synergistic action.[35,105]

The mechanism is summarised in Fig. 5.23. Initial conformational changes involve the arginines which promote the breaking of the E71–D80 linkage and the flipping of the D80 side chain. These transitions are followed by an equilibrium associated with the rotation of E71 around $\chi 1$ dihedral angle. Within this equilibrium, the attractive forces between D80 flipped and E71, which are sometimes able to lead to transient H-bonds, collaborate with the H-bonds formed with R64, R89 and W67 in lowering the backbone distance between positions 71 and 80 ($C_\alpha - C_\alpha$). This causes strong distortions to the structure of the TVGYG sequences, which become dramatic when a similar process happens in more than one subunit, eventually leading to inward pushes on the K^+ ions bound to the filter and the collapse of its structure. Notably, backbone distance $C_\alpha - C_\alpha$ between positions 71 and 80 was directly linked to the inactivation process and the inactivation probability among different mutants in previous works[36,37] and cooperativity between subunits was proposed by experimental studies.[66,90,114,116,125] Collapsed states demonstrated different levels of inactivation containing either two or three out of four subunits in a curved conformation, which closely resembled X-ray structures of putative inactive

collapsed states obtained in the presence of a low [K^+] and of a concurrent opening of the inner gate.[42,157]

Pathways toward inactivation were found to be blocked by the presence of a K^+ in the site S0. This can explain the dependence of the inactivation probability of [K^+] in the outer bulk, which is reduced in the case of high concentrations.[66,157]

A similar inactivation pathway can occur via a pH-related mechanism, in which flipped conformations of the D80 side chain are stabilised by the deprotonation of the E71/D80 pair and the inactivation is promoted by the reprotonation. Although, contrary to other K^+ ion channels, it is believed that extracellular pH regulation on inactivation is very limited in KcsA,[29] we consider that this pathway is possible under physiological conditions given the acidic nature of E71, even if it is possible that it only rarely becomes available. One of the simulations that followed this pathway led to an inactive structure with all the four subunits in the curved conformation. The deeper state of inactivation than in other cases can be explained by the fact that transitions were induced in the networks behind the TVGYG sequences of all four subunits, thus supporting the hypothesis that cooperation between subunits can be relevant in determining the completeness of the inactivation.[66,90,114,116,125]

Calculations revealed the existence of a "disrupted" state of the SF. Strong H-bonds between the D80 side chain in a particular state, D80semiflip, and the neighbouring donors, E71, R64, R89, and W67, dilate the filter until water molecules diffuse inside from the region behind the TVGYG sequence, thereby disrupting the single-file arrangement. The calculations suggest that the transitions of the network involve higher energies along this pathway. Intriguingly, these states might explain the "defunct" states experimentally observed in different K^+ channels[66] or might represent one among the as-yet-unknown inactive states revealed by experimental evidences.[29]

The presented mechanisms can explain a number of different experimental results in which mutations of E71, R64, R89, and W67 were found to dramatically affect the inactivation probability of KcsA.[22,29,32,34,35,37,85,125] The key role of R64 was confirmed by free-energy calculations on the Y82A and on R64A. The latter low inactivation probability of R64A is derived from the suppression of the important kinetic influence of R64 on the transitions of the network. The enhanced inactivation probability of Y82A can be explained by the close interplay between R64 and L81. First proposed in Chap. 4 and deeply investigated in the present chapter, this interplay is crucial for defining the mobility of the R64 side chain and is closely related to the residue in position 82. In Y82A, the variability of R64 was enhanced and this

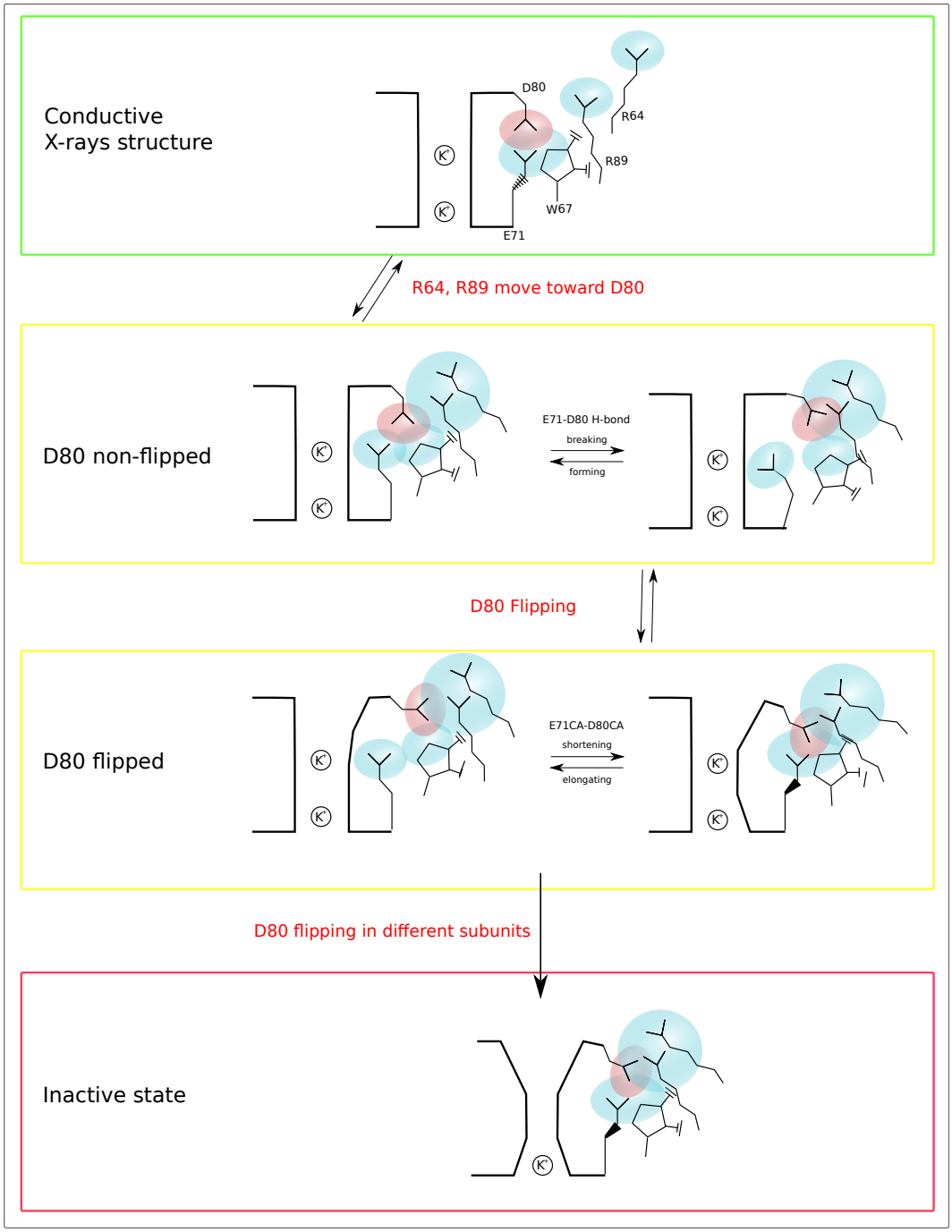

Figure 5.23: Scheme for inactivation in KcsA. Red and blue ellipses represent the influence of, respectively, negative and positive charges. E71 assumes three different conformations (refers to the main text) which are schematised as: i) $\chi 1 \sim 70°$ with a dashed-like triangle; ii) $\chi 1 \sim 180°$ with a solid line; and iii) $\chi 1 \sim -70°$ with a filled triangle.

allowed the inactive state to be reached more easily in the WT. Concerted motions between neighbouring subunits were observed which, it is suggested, also occur in a weaker state in the WT.

Future work is needed to address the detailed energetics associated with the SF transitions during the inactivation, and to further clarify the relationship between cooperativity among subunits and completeness of inactivation process.

———————————————

Chapter 6

Relationship between the protein dynamics and permeation and selectivity

Conduction in potassium ion channels has been widely studied. A wide variety of models have been suggested as being able to explain the permeation of ions from ionic current measurements, but none of them has been able to completely capture its features.[64] The relatively recent availability of structures of different channels[46,73,74,81,84,94,95,146,147] has allowed a detailed investigation to be made at microscopic level. The presence of a multi-site filter supports mechanisms for permeation where K^+ ions move in a single-file fashion, with at least two of them bound to the SF which stabilises the conductive conformation.[18,39,46,72,107,107,154] This was found to be consistent with the classic "knock-on" conduction mechanism, firstly proposed by Hodgkin and Keynes[65], in which the driving force behind conduction is an incoming ion that "knocks on" ions already bound within the SF.[18,72] In any event, the mechanistic details have remained elusive because they require a precise knowledge of the microscopic ions' positions and of the protein dynamics.

Theoretical methods have been employed to address detailed mechanisms and energetics, particularly MD simulations and free-energy calculations (see Maffeo et al.[101] and references therein). One of the most exaustive investigations was provided by Berneche and Roux[18]. Umbrella sampling was performed on K^+ ions permeating in KcsA. The authors concluded that ion conduction occurs according to the knock-on mechanism, and that conduction is limited by diffusion. In their hypothesis the ion-ion repulsion operates only at very short distances. Moreover, two different pathways for permeation were proposed: i) an "optimal pathway", char-

acterised by lower barriers and in which an intermediate state was observed with two K^+ ions in two neighbouring binding sites (S4 and S3); and ii) an alternative pathway reminiscent of the "vacancy diffusion" and of the "diffusive shaking stack" models.[104,133] Both mechanisms led to conformations in which the K^+ ions in the SF were separated by a single water molecule. These findings are consistent with the idea that more than one mechanism is involved in the permeation.[18,54,104] More recently, mechanisms based on the propagation of vacancies, derived from Hodgkin and Keynes[65], was proposed by Furini and Domene[54] based on umbrella sampling calculations performed on K^+ ions permeating in KcsA and KirBac channels, where a vacancy is an empty site which separates two K^+ ions in the SF. The creation of vacancies during permeation was also seen in long unbiased simulations performed by Jensen et al.[72], but the authors suggested a different interpretation, that vacancies diffuse in the direction of the permeation.[71,72]

Another fundamental feature of ion channels is selectivity among different ionic species. The ability of potassium ion channels to select K^+ over smaller ions, especially Na^+, is crucial for a physiological function. The mechanisms of selectivity have been the focus of decades of ion-channel research and it continues to attract a great deal of attention (see Andersen[7] and reference therein). Various hypothesis has been proposed for selectivity which originates from fundamentally different perspectives in the description of flexibility of the pore: a structure which is sufficiently rigid to eventually induce mechanisms governed by thermodynamic exclusion, or flexible enough to justify alternative explanations.

Earlier studies undertaken before the availability of crystal structures, proposed two different mechanisms for selectivity: i) a kinetic mechanism, determined by the rates at which ions enter the pore[21], and (ii) a thermodynamic mechanism, in which the channel demonstrates different affinities for the different ions.[108] The presence of the multi-site SF revealed by X-ray crystal structures[46,157] was considered to support the latter theory. Consequently, the so-called "snug fit" hypothesis became the standard textbook explanation: the oxygen atoms that constitute the sites of the SF do not coordinate the small Na^+ as well as the K^+ and therefore the ion dehydration energy is not compensated.[64]

In any event the debate is still continuing because many authors consider this explanation to be an oversimplification of the dynamical properties of the protein.[7,110,130] Significant contributions to the discussion were recently made by MD and free-energy calculations. Some of those studies suggested a small energetic cost associated with the entering of a Na^+ ion in the SF, which led the authors to suggest that the site S2, located at the centre of the pore, is responsible for a thermodynami-

cally driven selectivity.[18,48,130] Other studies suggested that the filter can coordinate the Na^+ ions[135] and the existence of sites for Na^+ in the SF have been proposed, called B sites, which are different from the sites for K^+. The location of the B sites was suggested as lying between the sites for K^+, with the Na^+ and the oxygen atom belonging to the SF in a planar arrangement.[78,110,135,141] Based on this hypothesis, the authors considered the binding of Na^+ inside the filter would not be thermodynamically unfavourable, so a kinetic-based selectivity was proposed occurring before the entrance of SF.[110]

Interestingly, although the B sites were detected via X-ray experiments for the smaller Li^+, they have never been confirmed in the conductive conformation for Na^+ ions which, by contrast, were found capable of reducing the open probability of the channel.[110,141,157] In addition to this "slow gating effect", which is mostly noticeable at high voltages, intracellular Na^+ was observed to be affecting the overall K^+ current with a fast block.[110,111,141] The two effects are believed to occur according to different mechanisms, and the entry of the Na^+ in the SF was suggested as being responsible for the slow effects on K^+ current.[110]

The difficulties of a definitive clarification of the mechanistic details related to the physiological behaviours of potassium ion channels originate from the *inherent complexities* associated with the system under investigation. In potassium ion channels, a wide variety of processes linked to permeation and gating are tightly correlated and lead to a complex behaviour pattern where inactivation and the conformational flexibility of the pore obscure the permeation and selectivity analysis, an issue which is expressly recognised by some of the authors of previously cited works (see Li, Andersen, and Roux[92]). This is a fundamental problem arising from the natural behaviour of the channels and from the complex dynamics that regulates the inactivation and gating modes in which a complicated equilibrium exists amongst the conductive and non-conductive states, and the states transitional between them. Conductive states are often intrinsically unstable, such as in KcsA.[28,29,35] Consequently their investigation is challenging. For instance, free energies of the permeating ions will mix unweighted components derived from conductive and non-conductive states and easily result in imbalance towards the non-conductive states. Free-energy calculations on ion channels usually rely on very short sampling to deliver an implicit method to address this problem is commonly implemented by performing very short umbrella simulations.[18,20,121,126,131] However, it has been shown in the literature[78,121], in Chap. 3 and it will be further shown in this chapter, that this approach does not guarantee, neither theoretically nor in practice, an accurate reconstruction of the free energies. This depends on the fact that the conforma-

tional variability of the pore is mainly determined by the evolution of the network of residues surrounding the SF which involves processes occurring over a wide range of time-scales and on their correlations with the motions of the ions.[28–30,34–37,42]

In some works a more focused approach is used in which conductivity of the SF was locally preserved in time and space by a direct restraint on the conformation of an area of the SF (V76),[77,78,141] believed to be linked with inactivation.[20] However, this solution directly limits the flexibility of the SF, which is widely indicated being a determinant factor in permeation and selectivity (see Andersen[7] and references therein), and therefore important properties might remain hidden. Moreover, its local nature tends to ignore detailed complexities related to the inactivation process and its origins, thereby overlooking additional relevant elements.

All the available data delivers a very complex picture of the close interconnections between selectivity, conductivity and gating in K^+ ion channels which can be hardly represented by simplified models and which require additional extensive investigations in order to be further clarified. In the present work, extensive analysis led to the recognition of the network of determinants for inactivation located behind the pore. The state of residue D80 was recognised as the key element in the process. This, in turn, primarily depends on the neighbouring H-bond donor residues. In particular, the transitions toward non-conductive and inactive conformations were found to be correlated with rearrangement in the conformations of the E71 and R64 side chains. These results allowed us to transparently uncouple the dynamics of the ions and the conductive/non-conductive equilibrium in order to deliver a clear confinement of the sampling within the conductive conformation. At the same time, the flexibility of the conductive SF, including of the region of V76, was preserved in our calculations. Free energies calculations of the permeation were performed by means of well-tempered metadynamics approach.[13,50]

Given the single-file fashion of the conduction, the entry of the incoming ion is the key step because it determines the mechanism of the process, including the creation of vacancies. Our investigations mainly focused on this fundamental step and showed that ion-ion repulsions act over longer distances and acquire greater importance than those previously suggested by similar works. These repulsions generate an electrochemical gradient across the SF which is suggested as being the main driving force in the permeation process. Additionally, the structure of the SF is suggested to be an additional element able to provide a preferential direction for ion diffusion. It will also be shown that inward transitions enhance the inactivation probability in KcsA WT, and this might explain the dependence of the inactivation on the voltage.[34]

Finally, selectivity over Na^+ ions was investigated in the case of outward permeation on the conductive conformation of KcsA. A mechanism for selectivity governed by thermodynamic exclusion is proposed which is able to harmonically combine the flexibility of the protein with the classic hypothesis of the molecular-sieve. In addition, the analysis confirmed the long range actions of electrostatic forces which will lead to an explanation for the fast and slow effects of intracellular Na^+ on the K^+ current.

6.1 Methods

The mechanism of permeation was investigated. A particular focus was directed towards the influence exerted by the incoming ion on the K^+ already bound to the SF and on the energetics involved in its entry. Permeation and selectivity were investigated in the outward direction of the K^+ current in KcsA which has been experimentally shown to be the preferred. Well-tempered MetaD calculations were employed as main approach of investigation. The ions in the present chapter will be labelled with the symbol of the element and an increasing number, commencing with the outermost in the SF, i.e. two K^+ ions in the SF and one in the cavity, will be labelled K1, K2 (in the SF) and K3 (in the cavity).

All the calculations performed in this chapter commenced with two K^+ ions placed in the SF (K1 and K2), consistent with the common hypothesis that two is the minimum number of K^+ ions needed to stabilise the conductive conformation over long time-scales.[18,45,46,72,107,107,154] Following the objective of the investigation and considering also the single-file fashion of the diffusion, a single CV was used to describe the motions of K1 and K2: the position of the their centre of mass along the channel axis (z_{K12}, Fig. 6.1). This choice is more appropriate considering the high correlations between K1 and K2 in the conductive state described in sec. 4.8. Two different definitions of the axis of the channel were used for this study. For most of the preliminary studies, some of which are presented in this chapter, the axis was considered to be approximately parallel to "z", consistent with a common definition which have been used for similar published works.[18,20,54,121] The axis origin was the centre of mass (COM) of backbone atoms of residues from 75 to 78 of the four subunits, similar to Berneche and Roux[18]. The final free-energy surfaces (FES) were computed using a dynamical definition of the axis: the vector passing through the COMs of atoms C, C_α and N of i) residues from 77 to 79 ($\mathrm{SF}^{up}_{\mathrm{COM}}$, corresponding with sites S0 and S1), and ii) residues 72 and 73 ($\mathrm{SF}^{low}_{\mathrm{COM}}$). The origin of the axis was set to $\left(\mathrm{SF}^{up}_{\mathrm{COM}} + \mathrm{SF}^{low}_{\mathrm{COM}}\right)/2$. Because of the relatively wide fluctuations occurring

during long simulations, this dynamical definition provided more precise FESs, with narrower minima.

Incoming ions of two species were investigated: K^+ (K3) and Na^+ (Na3). The incoming ion moves in three dimensions in the cavity. Considering the relatively good symmetry of the cavity on XY plane, it was represented by cylindrical coordinates with respect to the SF axis (Fig. 6.1): the height (z_{K3}or z_{Na3}), and the radial distance (xy_{K3}or xy_{Na3}).

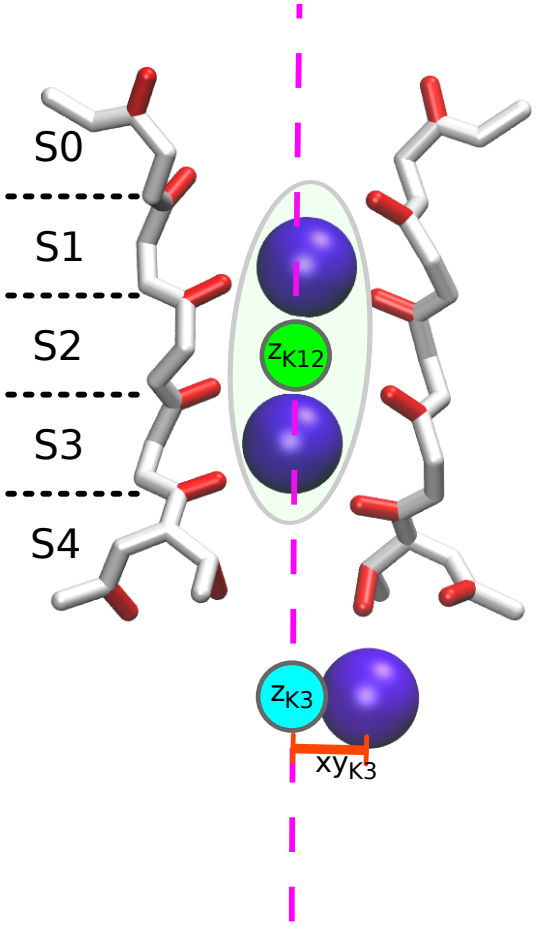

Figure 6.1: Collective variables for analysis on permeation.

The CVs z_{K12}, z_{K3} and z_{Na3} were computed as the projection onto a vector $\boldsymbol{v}$ (the channel axis) of a distance $\boldsymbol{d}$ (the distance between the considered elements and the origin of the axis):

$$\text{proj}_{\boldsymbol{v}}\,\boldsymbol{d} = \frac{\boldsymbol{v}\cdot\boldsymbol{d}}{|\boldsymbol{v}|^2}\boldsymbol{v}. \tag{6.1}$$

The distances xy_{K3} and xy_{Na3} were computed as the projection of the distance $\boldsymbol{d}$

onto the plane $\mathcal{W}$ orthogonal to the vector $\boldsymbol{v}$

$$\text{proj}_{\mathcal{W}}\,\boldsymbol{d} = \boldsymbol{d} - \frac{\boldsymbol{v}\cdot\boldsymbol{d}}{|\boldsymbol{v}|^2}\boldsymbol{v}. \tag{6.2}$$

The calculations were designed to obtain the best representation of the three ions using the minimum number of CVs, that is desirable in order to minimise errors in the metaD procedure.[88] The parameters $\Delta T = 2000$ K and $w_0 = 0.005$ Kcal/mol were used (see Sec 2.2.4).

Selectivity was investigated by substituting the K^+ located in the cavity with a Na^+ in the relaxed configuration that was used to initialise the calculation on permeation. The productive metaD calculation was anticipated by 10^3 steps of minimisation procedure and 260 ps of additional unbiased relaxation.

In this chapter, the occupancy of the SF and cavity are described by means of six upper-case letters: the first five refer to the element in the SF; the last (separated by a "+") refers to the element in the cavity. Water molecules are indicated by "W", K^+ ions by "K", vacancies (empty sites) by "0". For example, WKWKW+K means three K^+ ions arranged in S1/S3/cavity and water molecules in S0/S2/S4, whilst WKWK0+K refers to a similar arrangement of ions, water molecules in S0/S2 and a vacancy in S4. Two elements that approximately share the same site are indicated within parentheses and divided by "|", e.g. "(W|K)".

6.1.1 Umbrella Sampling

The choice of parameters for the US method followed the paper by Piccinini et al.[121], which was intended as a one-dimensional adaptation of those performed by Berneche and Roux[18]. The chosen CV was the z coordinate of ion K1, centred according the COM of the SF. The biased potential had an harmonic shape with a force constant 20 kcal/mol Å^2. Consistent to the work used as a reference, the biased potential was moved along z, with $\Delta z = 0.5$ Å; 14 umbrella simulations were performed of a length of 515 ps each, labelled $W1$ to $W14$: 275 ps were discarded as equilibration time. The coordinate z corresponding to a biased collective variable was stored at every time step. The PMF was obtained using WHAM method[83], with a histogram of 310 bins spanning from 0 to 8 Å, corresponding to moving K1 from the site S2 to S0.

6.2 Issues in the calculations of the free-energies

6.2.1 Free-energies computed on KcsA

Simple umbrella sampling which reproduced published calculations Piccinini et al. [121] using a well-established method such as umbrella sampling (US) failed to capture important features of the channel, such as the presence of the different binding sites. Moreover, similar results were published in various studies.[20,78,121] The origin of this failure did not simply depend on the selection of wrong parameters for US procedure, but on more intrinsic issues related to the application of free-energy methods on ion channels and biological systems in general.

Fig. 6.2 shows a summary of the computed FES. The distributions $\mathcal{P}_{\mathcal{W}_i}(z)$ clearly show there is adequate sampling over the CV, demonstrating that the issue originated from the evolution of the transversal degrees of freedom. Analysis of the trajectories revealed that during the sampling the SF assumed a clear non-conductive conformation which never observed in unbiased simulations. This conformation was initially promoted by the disruption of the E71–D80 H-bond and the formation of R64–D80 H-bond (Fig. 6.2b) and was finally stabilised by rotation of E71 around $\chi 1$ dihedral angle (Fig. 6.2c). Increasing the length of the sampling would not be useful because the stability of the non-conductive conformations reached in similar calculations was proved in several tests. The creation of these non-conductive states mainly depends on the strong coupling between the dynamics of the ions and of the pore region enhanced by the external potential used to vary the centre of subsequent US simulations. The issue arises from the intrinsic properties of the system, dependent on the instability of the conductive conformation proved by several lines of evidence on KcsA.[28,34]

It should be noted that, the problem is relatively independent from the method that is used. Similar results were obtained from a well-tempered metaD calculation designed to investigate the multi-ionic dynamics of the permeation. The calculation was performed over the CVs z_{K12}, $z_{\mathrm{K3}}$and xy_{K3}, with the channel axis defined as z, from a starting configuration with two K^+ ions bound to the SF (K1 and K2) and a K^+ ion in the cavity (K3). The details are described in sec. 6.1 ("Methods"). A non-conductive conformation of the SF was finally reached, although the smooth evolution of the metaD bias potential. As shown in Fig. 6.3a, the calculation failed to converge towards the underlying FES. As seen for the US calculation, the system evolved along the degrees of freedom orthogonal to the CVs during the sampling until a non-conductive conformation was arrived at. This evolution involved the creation of an R64–D80 H-bond and the subsequent rotation of the E71

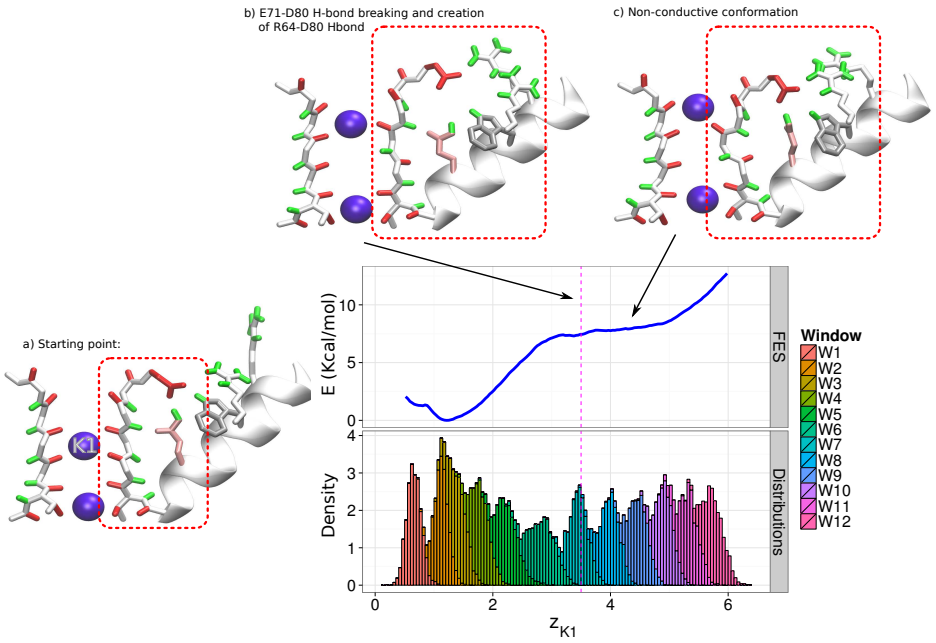

Figure 6.2: FES for K1 computed with US, which includes the distributions of the CV for each window.

side chain (Fig. 6.3b). The SF was unable to return towards the conductive state within the simulated time (58 ns). Instead, the non-conductive conformation was very stable, and this led to a greatest weight in the resultant energy surface. We suggest that, in contrast to the US calculation, the evolution to an inactive state was enhanced in this case by the inward K^+ transitions sampled by metaD which were able to promote an inactivation. This mechanism will be discussed further in this chapter and it will be suggested that it is linked to the voltage-dependent gating.[34]

In conclusion, a straightforward application of the methods commonly used to compute free-energies in biological systems failed to deliver an appropriate description of permeation in KcsA because of the complexity of the channel's behaviour, in which permeation is tightly linked to inactivation. A system-dependent approach must be developed.

6.2.2 Analysis of the issues

A generalisation of the issues encountered in the investigation of permeation helps to determine the appropriate strategy to approach the task. Biological systems are governed by complex free-energy landscapes with barriers of varying sizes, from the very low to the practically insuperable within the sampling. FES are computed to address specific processes that involve transitions which are generally small with

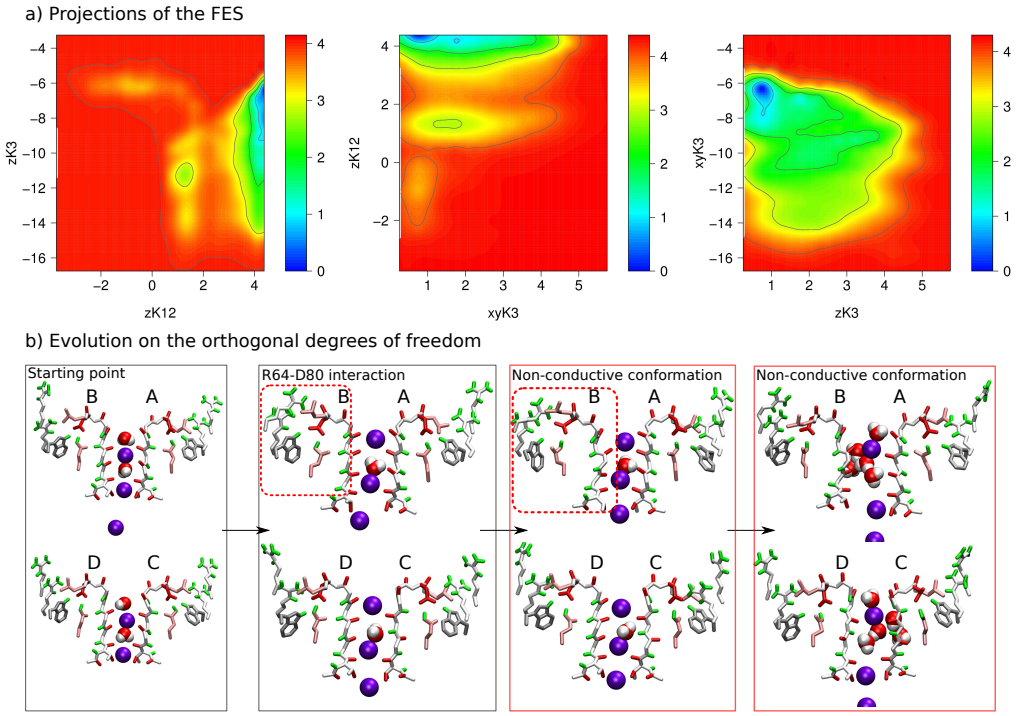

Figure 6.3: Multi-dimensional well-tempered metaD calculation performed over the CVs z_{K12}, $z_{\mathrm{K3}}$and xy_{K3}. No additional restrains applied.

respect to the complete dynamics of the system. Even relatively complex processes usually require the sampling of specific subspaces of the phase space. Moreover, a complete sampling would result in undesired FESs.

An example is suggested in Fig. 6.4, which considers the simple case of an umbrella sampling applied to explore a two-dimensional FES where only one degree of freedom is biased. Umbrella sampling is used because it allows a simple view but, as said, similar problems must be considered common to most of the methods used to compute free energies. As described in Chap. 3, umbrella sampling and the other biased methods involve a dimensional reduction which theoretically requires a complete ergodicity and mixing of the degrees of freedom orthogonal to the biased CVs. Even when exists in theory, ergodicity is not true in practice for biological systems, due the limited length of the sampling imposed by the computational resources. This lack of ergodicity does not necessary result in a loss of accuracy in the event that it does not produce non-stationary processes. Therefore it is often exploited in free-energy calculations, for instance when one among the many activities of a protein is investigated without sampling denaturation or unfolding. In the case of permeation in KcsA, an extended sampling of the protein phase space, even without includ-

ing the extreme cases such as unfolding, would result in an overall non-conductive FES, given the low probability of the conductive state. It means that this lack of ergodicity is usually exploited in free-energy calculations to confine the sampling to within an arbitrary region of interest which is eventually able to deliver as many features of the investigated process as possible. This implicit approach does not always work, especially when the barriers involved in the process are comparable with undesired events, such as in the case of permeation and inactivation in KcsA. When this happens important issues can easily arise which, in turn, can lead to undesired results. Three common cases are described in the Fig. 6.5, again referring to the simple example of a one-dimensional US over a two-dimensional system:

A: Issues in the initialisation of the subsequent umbrella sampling simulations;

B: Risk of being trapped outside the region of interest during the sampling;

C: Incoherent FES coming from improper sampling.

Case "A" is delivered by the diabatic displacements induced by external potentials associated with the different methods. In the example, the potential which was used to move the system between two subsequent windows. This step requires particular care for a good application of a biased method on biological systems because a displacement along the direction of the CVs is usually accompanied by unknown displacements along the remaining degrees of freedom, due to the high correlations which characterise these systems. When a previous extensive knowledge of the FES is missing, a common way of initialising new windows in US is to apply an external potential strong enough to guarantee the system will move the free-energy along an upwards gradient in the direction of the CV, and then relax. Very likely, this is the method that has been applied in most of the investigations on permeation and selectivity performed on ion channels.[20,36,78,121,141] However, this additional potential can perturb the system and push it towards unknown positions of the phase space when the barriers along the CVs and the orthogonal degrees of freedom have comparable heights. The displacements described can have dramatic effects, even if these are very small in the phase space due to the huge dimensionality of the investigated systems and the high correlations. Another common procedure used in the investigation of ion channels[39,54] is to perform the displacements by manual modification of the coordinates of the elements of the system. While, depending on the experience of the researcher, it can helps to avoid huge inconsistencies, it does not guarantee that the starting points of subsequent windows will belong to consistent pathways. This means that it is practically impossible to completely prevent the occurrence of issues similar to case "A". Thus, a similar approach does not have a general application.

Cases "B" and "C" derive from the natural complexity of the underlying FES, and their identification can be very difficult. The FESs appear consistent and the calculations are very likely reproducible (especially for case "C").

Several approaches can be applied to avoid the described issues. The simplest way to address issues similar to case "A" is to initialise the free-energy calculations according to extensive unbiased simulations. However, risks of experiencing issues similar to case "C" remain unchanged. Moreover, typically an extensive preliminary knowledge of the process and, especially, of the pathways which connect the different states is absent.[86,149] This is usually the case for research on ion channels, in which the recognition of detailed pathways is one of the ultimate objectives.[18,36,45,54,69,78,92,131,141] An alternative approach is the identification of the adiabatic pathways, followed by the reconstruction of the FES.[45,86,137,143,153] Well-temperad metaD (sec. 2.2.3) permit the reconstruction of quasi-adiabatic pathways and a straightforward derivation of the FES, which is theoretically true, without additional steps.[13] In metaD the construction of the biased potential is not truly adiabiatic, since the deposition of the Gaussians is not continuous and small perturbations occur when a new Gaussian is added. Preliminary tests demonstrated that the initial height of the Gaussians w_0 is the most important parameter for avoiding the occurrence of similar events, because higher w_0 caused problems similar to case "A". For this reason very small w_0 (0.005 kcal/mol) was selected. In any event, as previously shown, a straightforward application of metaD also failed because the method is very sensitive to being trapped in deep minima located outside the region of interest, similar to case "B".

In general, issues similar to cases "B" and "C" are observed in FES calculations aiming to complex systems by using any biased method and they related to the fact that the investigations often require to be focused on a small subspace of the whole phase space. The confinement represents a layer on the top of the free-energy calculations and it is strictly system-dependent.

In ion channels, similar procedures have been widely applied to study permeation and selectivity mechanisms by means of restraints on the dynamics of the ions[4,5,69,92,109,131], and sometimes to specifically investigate the behaviours of particular states of the proteins.[18,20] However similar transparent approaches have rarely been applied over the conductive states to improve the coherence of the samplings which, in consequence, were very often kept short. It was mainly due to a lack of understanding of the channel behaviour and the inactivation mechanisms. An attempt to confine the sampling to a conductive state was made in recent works via restraints on the V76 dynamics, which have been suggested being related to inacti-

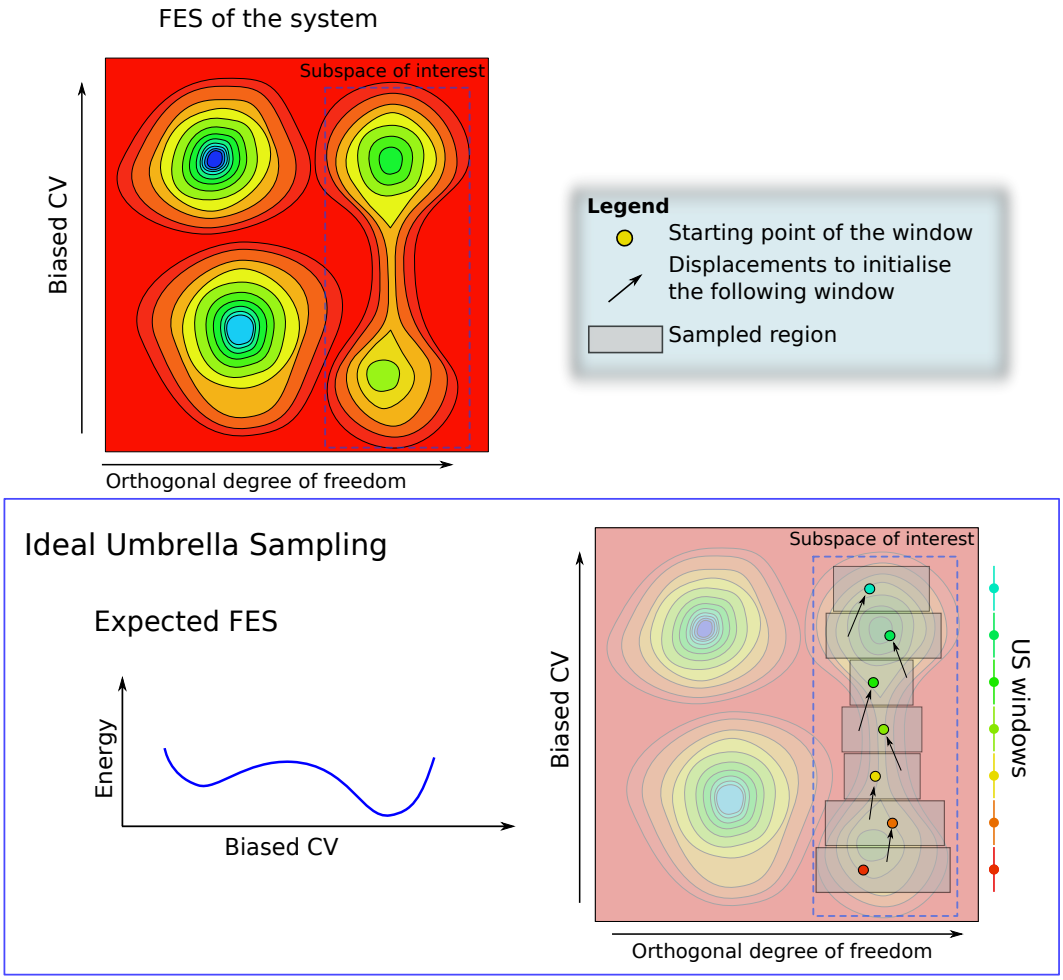

Figure 6.4: Ideal free-energy calculation with biased methods.

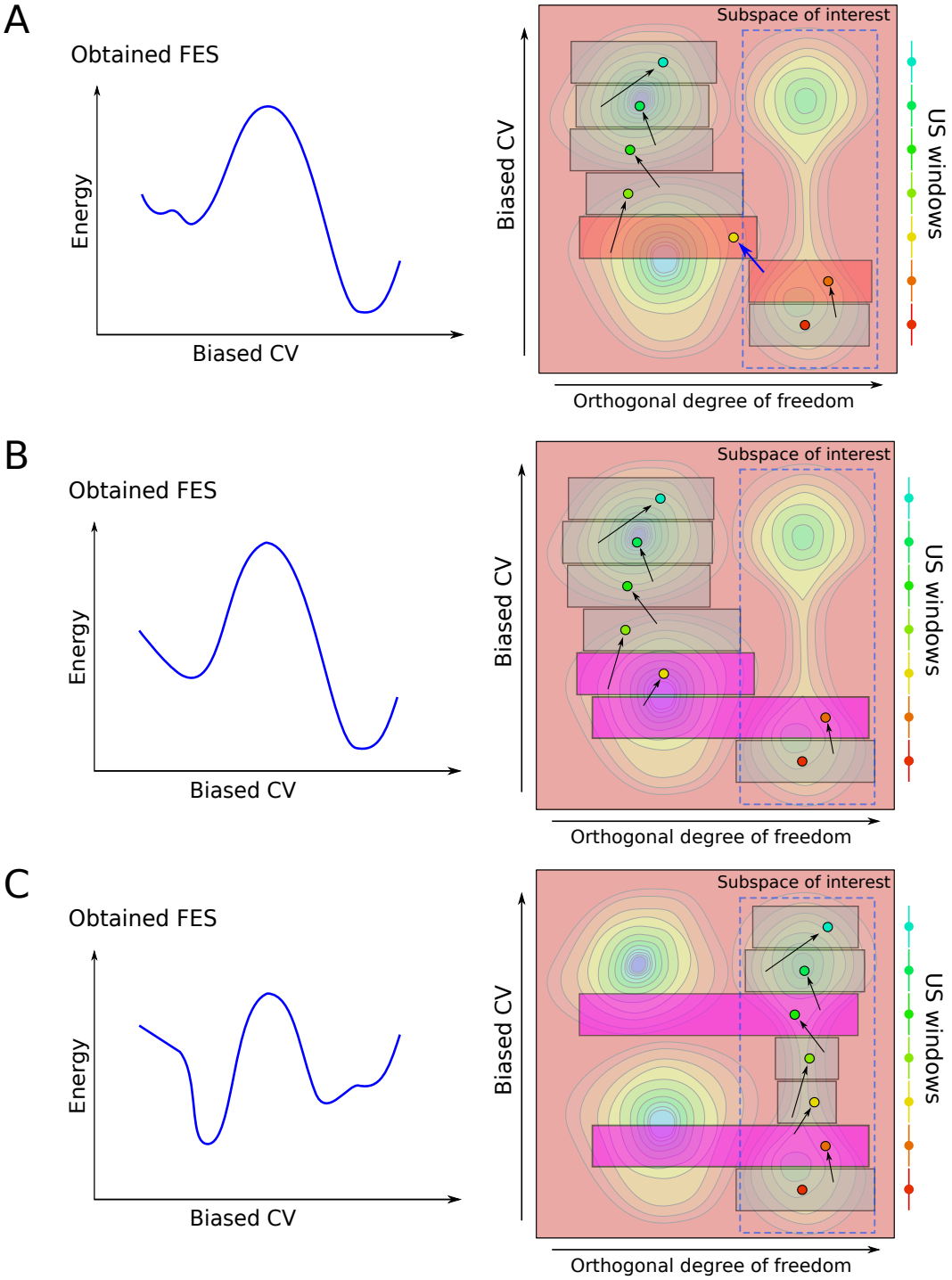

Figure 6.5: Common issues in free-energies calculations with biased methods.

vation.[77,78,141] In any event, these local restraints do not address the fundamental problem of conductive/non-conductive equilibrium in the SF, with the consequence that the related complex dynamics of the pore are mostly maintained. Moreover, they directly limit the flexibility of the SF in such a way that important properties of the SF might be hidden during the sampling.

In the present work, the analysis on permeation and selectivity was preceded by an extensive investigation of the molecular determinants of inactivation. The confinement of the sampling to a conductive conformation of the channel was transparently implemented by restraining the dynamics of the network behind the SF. Since the restrained residues do not belong to the SF, most of the pore flexibility and dynamics could be preserved, including the variability of V76 residues and their flipping.

6.3 Ion permeation in the conductive conformation

Given the huge dimensionality of the system, confinement to the region of interest implies an extensive knowledge about the determinant of the inactivation. The network of residues behind the SF plays the key role in the regulation of the conductivity. The state of residue D80 was identified as a leading factor. According to the results presented in the previous chapters and also to numerous additional tests, which are not reported because of limited space, two main elements were recognised as being determinant: i) R64 ii) and E71. As described in Chap. 4 and 5, they collaborate to control the state of the D80 side chain in the processes that lead to non-conductive states. Our calculations found that the distorted conformations of TVGYG sequences which distinguish the non-conductive states were promoted by the creation of strong D80–R64 interactions and by a rotation of E71 around its $\chi 1$ dihedral angle to $\sim -70°$. The residue R89 was not found to dramatically affect the SF conformation, not even during long sampling. This is consistent with the analysis performed in Chap. 4, where, without the concurrent intervention of R64, R89 influence was suggested as being exerted only in time-scales longer than the simulated times.

The dynamics of the ions in the SF is affected by the state of the network behind the SF, as demonstrated in previous chapters. Even when limiting its variability to suppress inactivation, many different states remain available. Consequently, many conductive conformations for the channel must exist and these are likely to be characterised by different conductivity. Our analysis suggests that the relevant conformational changes within the network occur on slower time-scales with respect

to the transition of K^+. In order to deliver a more coherent picture of permeation, our investigations focused on the state of the pore closer to the conductive state proposed by Zhou et al.[157] by means of X-ray experiments.

This conductive state was easily maintained by restraining two dihedral angles in each subunit (eight for the whole protein): $\chi 1$ dihedral angles of i) E71 ($\chi 1_0 = 64.45°$) and ii) L81 ($\chi 1_0 = 297.6°$ degrees). Restraint of L81 prevented the creation of the strong H-bonds between R64 and D80, as shown in section 4.5.2. Restraints were applied via harmonic potentials

$$\frac{1}{2}K(\chi 1 - \chi 1_0)^2 \qquad K = 10 \text{ kcal/mol degrees}^2 \tag{6.3}$$

and $\chi 1_0$ dihedral angles were chosen as averages from the unbiased simulations, computed on the conformation closer to the X-ray structure.

The state of the inner gate was closed in the investigated structure.[157] Accurate analysis on the open states performed on the X-ray structures of a constitutively open mutant channel (tKcsA-OM)[42] revealed that the cavity is wider when the inner gate is open, with side chains of residues I100 located further from the entrance of the SF than in the closed state. From our simulations on the active-closed state, I100 side chains in specific conformations were found to be affecting the dynamics of the incoming ion, thereby severely reducing the space available for its motions. In order to better mimic the wider cavity found in the open state of the channel, residues I100 were restrained in the conformation of the X-ray structure used to prepare the system by means of harmonic potential applied to dihedral angles $\chi 1$ and $\chi 1$ ($\chi 1_0 = -63°$, $\chi 2_0 = -165°$, $K = 5$ kcal/mol).

6.4 Mechanism of permeation

6.4.1 No incoming ion

Initially, the free-energy underlying the two ions bound to the SF (K1/K2) was investigated in the absence of an incoming ion. The FES can be considered as the "background" behaviour of the system, computed to qualify the influence delivered by the incoming ion, and thus of the knock-on. The FES was computed with respect to z_{K12}, K1 and K2 were respectively located in S2 and S4 in the relaxed starting configuration with no ion in the cavity. The sampling was improved by applying a spherical harmonic restraint from the COM of the SF (defined as atoms C, C_α, N of residues from 74 to 79) to prevent the remaining the K^+ ions from the outer bulk from entering the SF during the relatively long sampling. The restraint was implemented

via tclforces module of namd (including periodic boundaries conditions) according to

$$\mathcal{V}_S(r_{i,\mathrm{SF_{COM}}}) = \begin{cases} 0, & r_{i,\mathrm{SF_{COM}}} > r_{\mathrm{cutoff}} \\ \frac{1}{2}K(r_{i,\mathrm{SF_{COM}}} - r_{\mathrm{cutoff}})^2 & r_{i,\mathrm{SF_{COM}}} \leq r_{\mathrm{cutoff}} \end{cases} \tag{6.4}$$

with $r_{\mathrm{cutoff}} = 6$ Å and $K = 20$ kcal/mol Å^2. As mentioned, this is a common technique in the computation of free energies in ion channels.[4,5,69,92,109,131] The total length of the sampling was ~ 42 ns.

The FES that was obtained, shown in Fig. 6.6a, shows a single minimum for K1/K2 in the sites S2/S4. In this configuration V76 was mostly found in the flipped state. The result strongly supports the knock-on mechanism because it demonstrates that the permeation does not occur without the intervention of an incoming ion. In any event, it also suggests that electrostatic interactions act over long ranges, which differs from that which was suggested by Berneche and Roux[18]. Structural factors do not justify such a strong preference for the inner sites that it is suggested originate from the repulsive ion-ion interactions between the K^+ ions in SF and in the bulk. The presence of K^+ ions in proximity to the external mouth of the pore was proved considering their radial distribution function (RDF) from the site S0 computed on an unbiased simulation (Fig. 6.7). A broad region of relatively high K^+ concentrations was located immediately outside S0, with the highest peak in the RDF corresponding with the site S_{ext} described by previous works.[18,121,157]

The free energy acting on K1/K2 can therefore be simplified by the sum of two leading terms: i) the *electrochemical gradient* across the SF, and ii) the interactions *ions-SF*. The gradient in the free-energy across the SF is generated by the different ionic strength between the bulk in the proximity of the outer mouth, $[K^+] \geq 0.2$ M, and the cavity, $[K^+] = 0$ M. This difference generates a gradient in the chemical potentials that results in a clear inward push to K1 and K2. In any event, interactions ions-SF prevent the push from being turned into an inward diffusion, because the calculation demonstrated that the coordination of K^+ ions by the SF is thermodynamically favoured with respect to the K^+ in the aqueous cavity.

6.4.2 Permeation promoted by incoming K^+ ion

The effect on the ions in the SF K1/K2 of an ion incoming from the intracellular region was investigated by considering the case of a K^+ ion in the cavity (K3). The FES was computed with respect to z_{K12}, z_{K3} and xy_{K3}(Sec. 6.1). The sampling was enhanced by applying a half harmonic potential to z_{K12} centred on $z_{\mathrm{K12}} = 5.4$ Å, in order to prevent the diffusion of K1 to the bulk. For the sake of clarity the three-

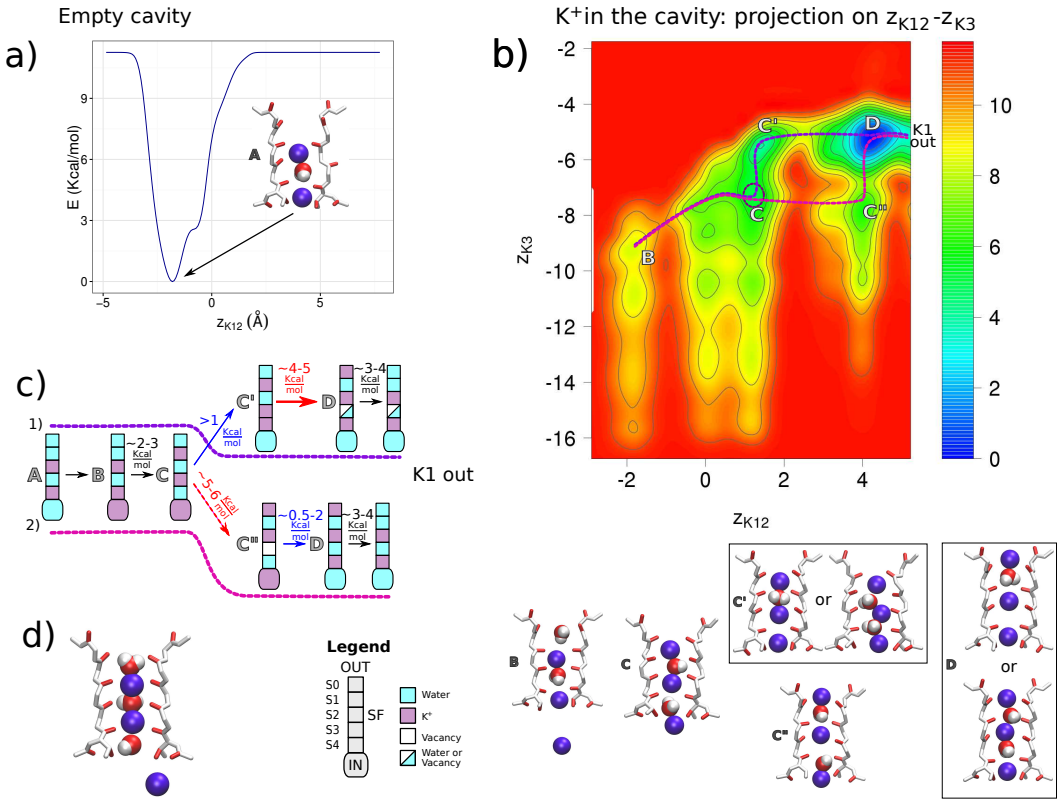

Figure 6.6: Summary of the free energy calculation on the permeation mechanism for the ion channel KcsA.

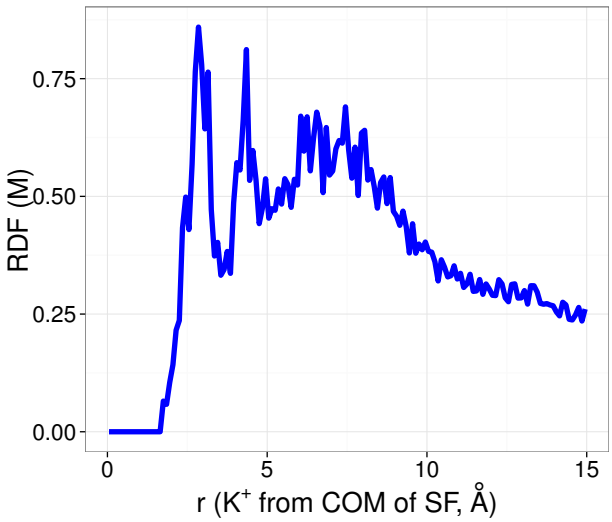

Figure 6.7: Radial distribution function (RDF) from S0 for the K^+ ions excluded K1, K2 and K3. The RDF was computed from an unbiased simulation and the position of S0 is defined by the centre of mass of oxygen atoms of Y78, G79 carbonyl groups. The $g(r)$ is normalised on the concentration of the K^+ ions at the top boundary of the box, averaged over the trajectory, considered to be the concentration in the bulk. This value converged to ~ 0.2 M.

dimensional FES was projected onto one and two-dimensional surfaces, integrating out the remaining CVs, as described in the Chap. 2. No additional restraints were applied to the ions in the bulk. The total length of the sampling was ~ 190 ns.

The projection of the FES onto z_{K12}-z_{K3}(Fig. 6.6b) demonstrated that permeation is possible in the presence of K3, which completely modified the free-energy profile underlying the motions of K1/K2. At least two permeation pathways could be recognised, which resulted in K1 leaving the SF. These results confirm "knock-on" as the main conduction mechanism: the permeation in the potassium ion channel is promoted by an incoming ion.

Energetics and detailed mechanisms

As previously mentioned, two permeation pathways were identified for the permeation in KcsA. They are described here in the outward direction, the preferred current direction in KcsA.[31,34]

According to the labels used in Fig. 6.6b, both start with the transition B $\rightarrow$ C, corresponding to K1/K2 from S2/S4 to S1/S3. Unlike the calculation performed in the absence of K3, the conformation S2/S4 (B, $z_{K12} <\sim -1$ Å) became the least probable state for K1/K2.

Pathway 1 can be considered to be consistent with the most common idea of the "knock on" mechanism, in which the entry of K3 in S4 is the determining event that "knocks on" K1/K2.[18,39,72] We will define this pathway as *classic knock-on*. By focusing on a truly conductive state of the channel, the entrance of K3 in the SF was discovered to be practically barrier-less for the classic knock-on (less than 0.5 kcal/mol along z_{K3}, C $\rightarrow$ C$'$). This is lower than those obtained by similar published calculations, where the lowest barrier reported has been between 2 and 3 kcal/mol.[18] Furthermore, a thermodynamic benefit for the incoming K^+ ion in being coordinated by the inner mouth of the pore was demonstrated for the first time.

Of considerable significance, the state C$'$ (K1/K2/K3 in S1/S3/S4) was found in two different forms: i) with a water molecule separating K2 and K3, WKWK(W|K)+K; and ii) without any water molecule between the two ions, WKWKK+K, which eventually evolved into the *creation of a vacancy*. Pathway 1 is then an average between these two different detailed mechanisms and explains the occurrence of vacancies reported in published works[71,72] and is also seen on our unbiased simulations. The possibility of vacancies occurring adds an additional level of complexity to the conduction process. The origin of a the very low barrier for "C" $\rightarrow$ "C$'$" is suggested as being the weighted average between the two detailed mechanisms. The barrier for the transition toward WKWKK+K is expected to be close to 0, because the determinant transition in the process is the diffusion of the water molecule in S4 into the cavity, i.e. translational motions orthogonal to the investigated CVs. On the other hand, the barrier for the transition toward WKWK(W|K)+K is expected to be sightly larger than the final averaged value. For this reason, although it appears as a transitional state in the FES, conformation "C" was found to have a life-time of the scale of few ns from unbiased simulations, because both of the processes associated with "C" $\rightarrow$ "C$'$" involve diffusional transitions that occur on the ns time-scales (water diffusing from S4 to the cavity or K3 pushing on the water in S4). The two detailed mechanisms of pathway 1 cannot be distinguished from the calculations presented here because additional CVs would be necessary to take into account the motions of the water molecules. However, the calculation demonstrates that the entry of the incoming ion is practically barrier-less when averaged over all the incoming ions that promote a classic knock-on.

The remaining transition of pathway 1, C$'$ $\rightarrow$ D, involved the pair K1/K2 which move until the ions reach the configuration S0/S2/S4, the absolute minimum for the surface. The computed barriers are slightly ($1-2$ kcal/mol) higher than those reported in published works.[18,141] This is because we considered and averaged

out the dynamics of the central region of the SF and V76, including its flipping. These transitions did not immediately result in a dramatic block of the permeation, supporting our hypothesis that additional rearrangements in the network behind the SF must accompany V76 flipping in order to hinder the permeation. The vacancy between K2 and K3 are created in classic knock-on within the transition C′ → D.

Pathway 2 differs from pathway 1 because the pair K1/K2 moved from S1/S3 to S0/S2 before K3 entered the SF (C → C″). It bears some resemblance to a pathway suggested by Berneche and Roux [18], which was proposed characteristic of a "vacancy diffusion" mechanism [104,133], In this mechanism permeation arises from the random walk of the ions in the pore, which generates a vacancy that favours the entry of the incoming ion. Although during the process a vacancy is temporarily created in S3 which precedes the entry of K3 (KWK0W+K), our results demonstrated that a random walk of the K^+ ions in the pore is precluded without the presence of the incoming ion (sec. 6.4.1), and the transition C → C″ is mainly promoted by the presence of K3 close to the filter entrance (z_{K3}between ∼ −8 and −6.8 Å). Thus we propose that pathway 2 would be better defined by a *purely electrostatic knock-on* mechanism in which the determinant step is the translation of K1/K2 from S1/S3 to S0/S2 which is promoted by the long range ion-ion repulsions with the incoming ion still in the cavity. Some affinities can be found between this mechanism and the "loosely coupled knock-on" mechanism proposed by Corry and Thomas [39] for voltage-gated sodium ion channels.

Additionally, the purely electrostatic knock-on involves similar energies to the classic knock-on, with the highest barriers being between 4 and 5 kcal/mol for the latter, and between 5 and 6 kcal/mol for the former. The barrier for the entry of the incoming ion in the filter reported in the Fig. 6.6b (C″ → D, between 1 and 2 kcal/mol), must be considered a slight overestimate for the process because it arises from the projection onto the z_{K12}- xy_{K3} plane and it is also averaged with respect of the configuration KWKWW+K. Even if it was not sampled in the metaD calculation, creation of the vacancies during the purely electrostatic knock-on was observed to be occurring in an unbiased simulation, with K3 swapping its position with the water molecule in S4 (KWK0W+K → KWK0K+W). We therefore suggest it is an available mechanism but with only a low probability of its occurrence.

Importantly, the permeation mechanism KWKWW+K → WWKWW+K was sampled. In any event, the energies required suggest a much lower probability than for the previously mentioned pathways.

A representative snapshot of the states corresponds to the minima for z_{K12} ∼ 0 Å is shown in Fig. 6.6d, where K2 is in S3 and K1 is located between the sites

S1 and S2, approximately arranged in a planar manner with respect to the oxygen atoms of G77. These states were not very stable, but they are relevant since they often preceded the flipping of V76.

The entry of the incoming ion in the SF was found to be barrier-less when averaged over all the sampled pathways. The FES for K3 was obtained as the projection of the computed FES onto an ideal plane which crosses the channel axis, averaged over all the possible planes, summarising xy_{K3} with respect to 0 (z_{K3}-$xy_{\mathrm{K3}sym}$, Fig. 6.8a). The figure reveals that the protein structure *drives* the incoming ion toward the SF entrance, in particular with the carbonyl groups of residues T74 and A73 and the side chains of T75 which point towards the cavity. Hydroxyl groups of T75 side chains are responsible for the dehydration of the K^+. Figs. 6.8a and 6.8c (the projection of the computed FES onto z_{K3}) show that this process is accompanied by a strong thermodynamic benefit (~ 5 kcal/mol), thus demonstrating two leading factors of the permeation: i) a free-energy gradient for the incoming ion toward the SF mouth; and ii) the strong difference in the free energy between the cavity and S4.

Interestingly, the calculation revealed that the ions K1/K2 move in the SF only when aligned with the incoming ion K3 along the channel axis, as shown by the FES projected onto the plane z_{K12}-$xy_{\mathrm{K3}sym}$ (Fig. 6.8b). When a conductive state is considered, a further relevant result is the existence of a gradient in the free-energy (from "B" to "D") capable of locally driving the permeation.

6.4.3 Driving forces

The detailed driving forces of the permeation are analysed by considering the influence of the incoming ion (K3) on the two ions bound in the SF (K1/K2). Fig. 6.9 shows the FES as function of z_{K12} for three relevant cases: i) when there is not any ion in the cavity (*no incoming ion*, purple line); ii) when an incoming K^+ ion freely moves within the cavity (*K^+ in the cavity*, blue line); and iii) when permeation is accompanied by the entry of the incoming K^+ ion in the SF (*Knock-on process*, red line). The case of a Na^+ in the cavity is also reported (green line), but will be more widely discussed later in this chapter. The FESs for cases (ii) and (iii) were computed from the FES described in the previous section, integrating z_{K3} over the regions of interest and xy_{K3} being averaged out. These regions were defined as: (ii) K^+ in the cavity for $z_{\mathrm{K3}} < -6.8$ Å, and (iii) Knock-on process for $z_{\mathrm{K3}} > -8$ Å. Dashed lines in the figure were obtained by simple linear regression and are shown to simply visualise the free energy gradients.

As previously discussed, the incoming K^+ ion affects the dynamics of K1/K2

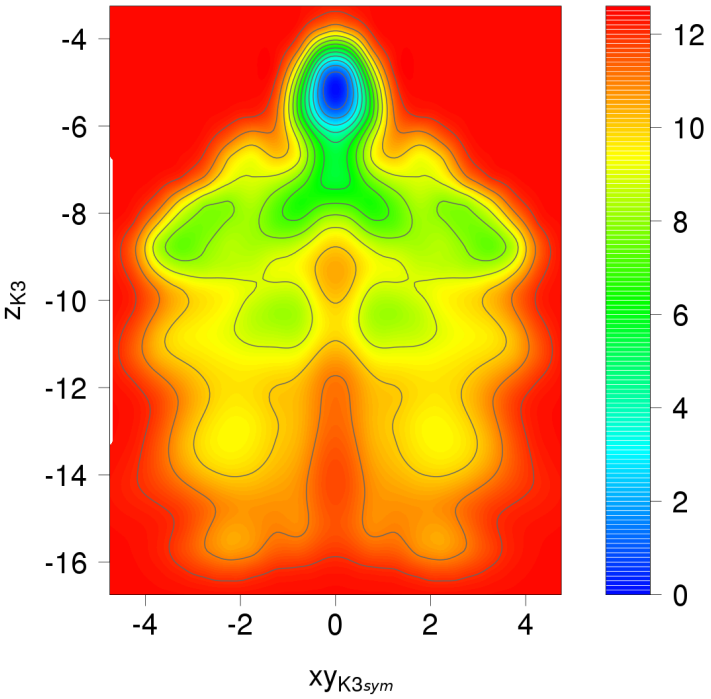

(a)

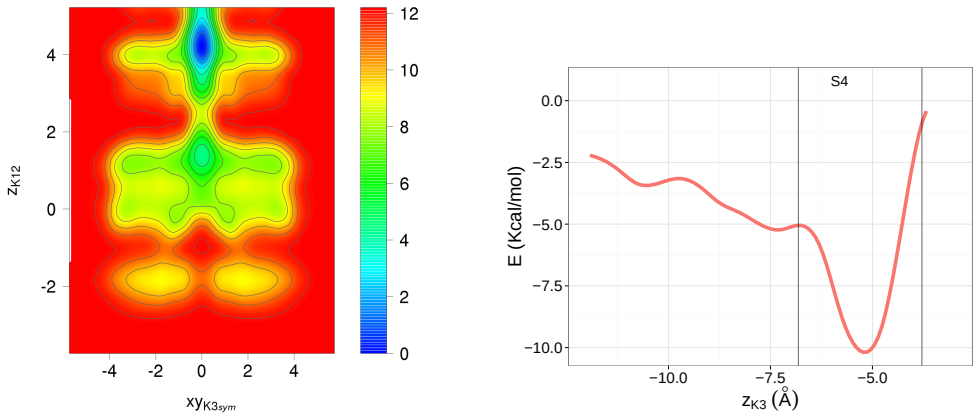

(b) (c)

Figure 6.8: Different projections of the FES which governs K3: a) and b) FES on ideal planes crossing the channel axis (averaged over all the possible planes), obtained as an average over all the possible planes symmetrising xy_{K3} (Å) with respect of 0; the remaining CVs are, respectively, z_{K3} (Å) and z_{K12}(Å). c) FES projected onto z_{K3}(Å). Energies are reported in Kcal/mol.

as soon as it gets into the cavity. Conformation S2/S4 was the most stable in the case of no incoming ion (Fig. 6.9, purple), and a strong inward gradient dominated the free-energy. The diffusion process of K^+ ions in the pore does not occur without the intervention of incoming ions. The mere presence of K3 in the cavity is able to promote a process consistent with an activated diffusion, with transitions taking place between three main positions: S2/S4, S1/S3, S0/S3 (Fig. 6.9, blue). Among the three, S2/S4 had the highest probability, even for values of z_{K3} lower than -10 Å, that is K3 relatively distant from the SF entrance (as shown by Fig. 6.6b), and, interestingly, S0/S2 was more stable than S2/S4. This analysis confirmed the long ranges of electrostatic interactions in the conductive state of KcsA. We explain this by considering that under the simulated conditions the ion in the cavity was able to compensate for the influences of the K^+ ions in the bulk on K1/K2 suppressing the electrochemical gradient across the SF. This hypothesis will be further confirmed when selectivity over Na^+ will be discussed. This gradient must be considered to be a determinant factor in permeation, which can be inverted in different cases depending on the ionic strength of the bulk and on the number of ions in the cavity.

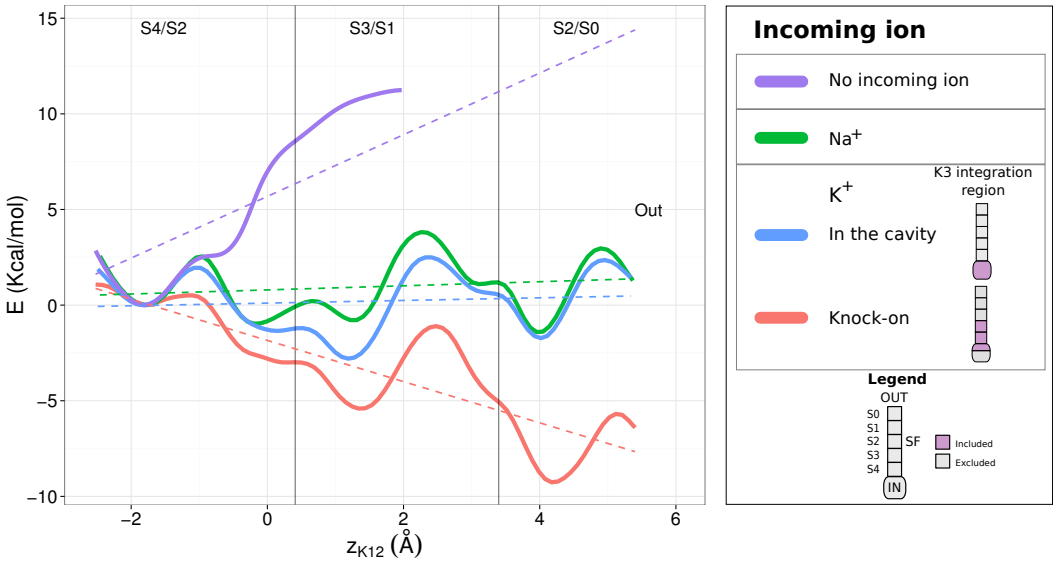

Figure 6.9: Driving force of the permeation, FES for the two ions bound to the SF.

Interestingly, the activated diffusion, a random walk of K1/K2 among the three different states, is prevented in practice by K3 entering in the SF. This is both kinetically and thermodynamically favoured and gives a directionality to the overall process, resulting in a clear free-energy gradient (Fig. 6.9, red). According to our results, the "knock-on" acquires a wider meaning and greater importance in

guaranteeing the efficiency of the ion flux because the incoming ion plays a dual role: i) promoting the transitions of K^+ ions in the SF; and ii) generating an overall free-energy gradient toward the permeation. According to standard thermodynamics, the overall energetic contribution of knock-on can be defined

$$E \geq \int dz_{\mathrm{K12}} \left(G(z_{\mathrm{K12}})_{\mathrm{K}^+} - G(z_{\mathrm{K12}})_0 \right), \tag{6.5}$$

where $G(z_{\mathrm{K12}})_0$ is the free energy when there is no incoming ion and $G(z_{\mathrm{K12}})_{\mathrm{K}^+}$ when the incoming ion is a K^+. This contribution is very relevant and can be regarded as being the difference between the purple and red line in Fig. 6.9. Fig. 6.10 summarises the results of the calculations and fits them into the general case of outward conduction in KcsA, the preferred direction.[31,34]

It is important to note that the picture is not complete because the migration of the vacancy in pathway 1 has not been studied in detail. In any event, all our biased and unbiased simulations suggest that a propagation occurs in the direction of the permeation, as suggested in previous works.[71,72]

6.4.4 Confirmation on unbiased simulations

The validity of the results was compared with unbiased, unrestrained simulations. Permeation was promoted by the presence of two K^+ ions in the cavity which created strong electrostatics repulsion. This repulsions had the effect of inverting the electrochemical gradient across the filter. This was done so as to have a better resolution of the trajectories because shorter simulations allowed us to store positions and velocities every time step (1 fs). The simulations confirmed the two pathways of permeation. The time series from two representative cases are reported in Fig. 6.11. The figures further confirm the hypothesis that the transitions are activated processes. In particular, the additional K^+ (K4) created a 4-ions concerted process in the "classic knock-on".

6.5 Selectivity: a thermodynamic mechanism

Selectivity was investigated on the conductive state of the KcsA for the case of a Na^+ diffusing from the intracellular region. The well-tempered metaD calculation was prepared as described in sec. 6.1 and started from a configuration with a Na^+ in the cavity (Na3) and two K^+ ions (K1 and K2) in the SF.

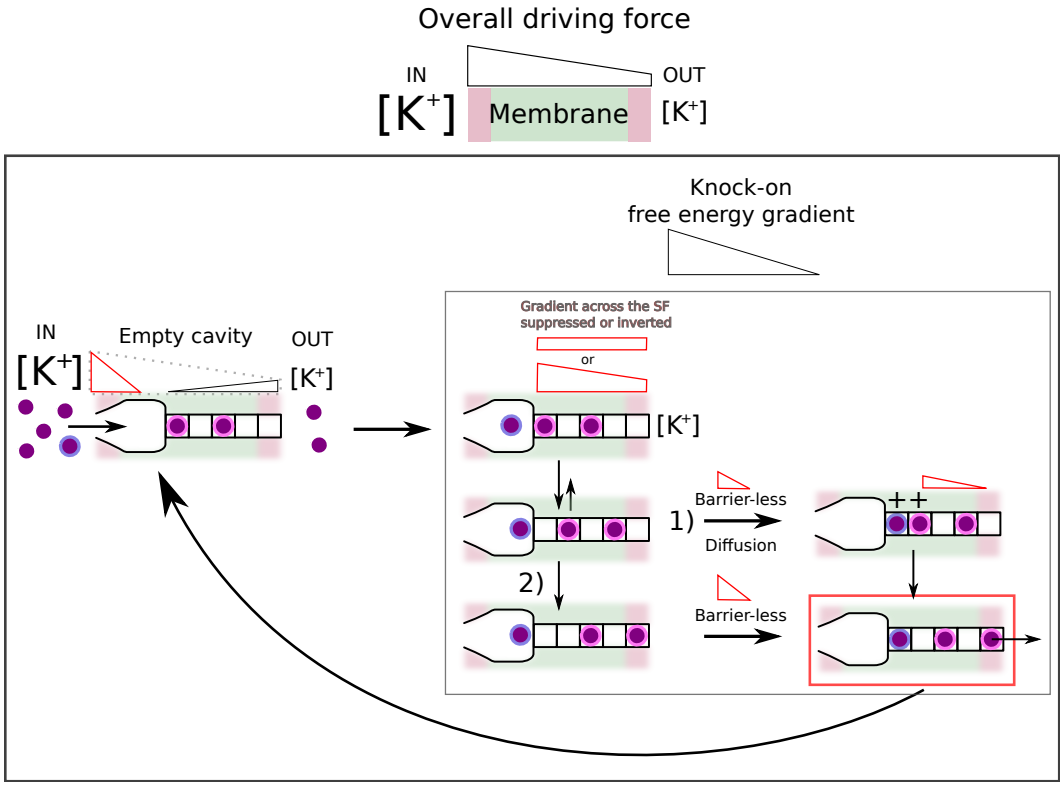

Figure 6.10: Summary of the results on permeation fits into the general case of outward conduction in KcsA, the preferred direction.[31,34] The overall driving force of K^+ current is the electrochemical gradient across the membrane generated by the different K^+ concentrations between the two sides, higher inside than outside.[64] The gradient across the SF determines the preferred state for the K^+ ions bound to the channel; the gradient between the intracellular side and the cavity leads the ionic diffusion towards the cavity. Once the incoming K^+ has diffused into the cavity, negative charges drive it close to the mouth of the SF. In cases where the electrochemical gradient across the SF is suppressed (or inverted) the permeation occurs. It occurs according to two main pathways and in both cases the entry of the incoming ion is practically barrier-less and promoted by the strong affinity between K^+-SF.

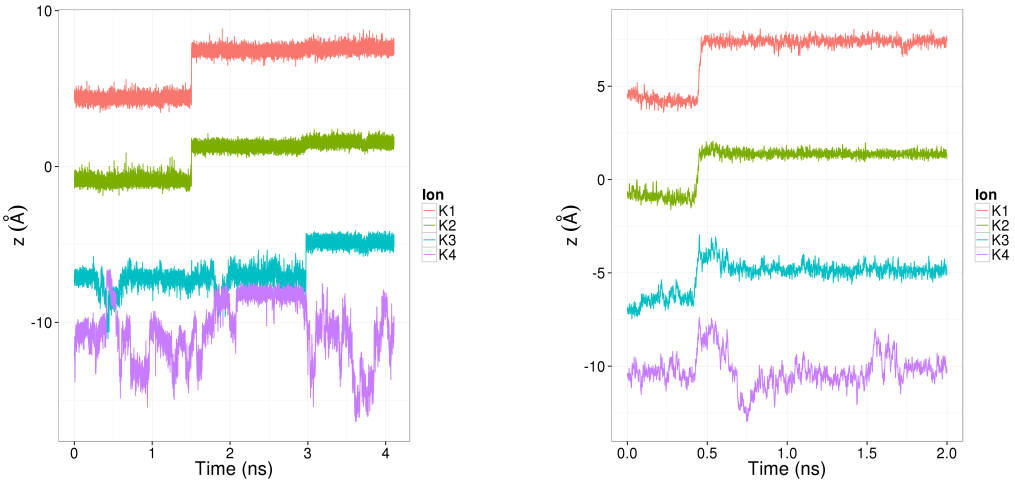

(a) **(b)**

Figure 6.11: Time series for the two mechanisms of permeation. Trajectories of each relevant ions (the K^+ ions in the cavity and the K^+ ions bound to the SF) were stored every time step (1 fs) speeding up the process by initially placing two K^+ ions in the cavity. On the left the "purely electrostatic knock-on" is shown: i) the two K^+ ions in filter move outwards coherently, ii) the incoming ion enter in the filter after some time. On the right the "classic knock-on" is shown: the incoming K^+ performs the initial transition into the filter, soon followed by the outward transition of the two K^+ ions still in the filter. In the latter case it is possible to see that the correlated multi-ions transition involved also the second K^+ in the cavity.

6.5.1 Energetics

The FES was computed with respect to the CVs z_{K12}, z_{Na3} and xy_{Na3}, defined as described in the section 6.1. The length of the sampling was $\sim$ 200 ns and an identical set-up was used as for the calculations described in the previous sections.

The calculation revealed a selectivity mechanism driven by thermodynamic exclusion which occurs before the entrance of the SF (Fig. 6.12). For any state of the pair of K^+ in the SF (K1/K2), the preferred location for Na^+ was fully hydrated in the cavity ($z_{\mathrm{Na3}} <\sim 6.8$). This is clearer from the comparison with the case in which a K^+ (K3) is the incoming ion. Fig. 6.13 reports the FESs projected onto z_{K3} or z_{Na3}, the positions of the incoming ions along the channel axis. A gradient drives the K^+ toward the SF and strong stabilisation accompanies the dehydration and the coordination by the SF in S4, while for Na^+ S4 (z_{Na3} between -6 and -6.8) is not even a binding site. A weak minimum exists for Na3 bound to the external entrance of the SF, coordinated by the hydroxyl groups of the T75 side chains of two neighbouring subunits and either two or three water molecules (Fig. 6.14a), or, more rarely, by the hydroxyl groups from all four subunits without any water molecule in S4 (Fig. 6.14b). The different states corresponding to this minimum will be referred to as B_{in}, consistent with previous literature in which the putative sites for Na^+ were labelled by the letter "B".[78] The states B_{in} occurs only when K1/K2 are located in the sites S1/S3, because when the two ions are located in the sites S0/S2 they cause a small spread between the hydroxyl groups of the T75 side chains sufficient to destabilise the coordination of Na^+. On the other hand, the fully hydrated Na3 in the cavity was $\sim$ 2.5 kcal/mol more stable than B_{in}, with a high probability of residing in close proximity to the SF entrance (z_{Na3} between -6.8 and -8), which suggests the existence of an inner binding sites. For convenience this sites will be labelled C_{in}, and Fig. 6.12b shows them as being located in the region of the carbonyl groups of residues T74.

As previously described, Fig. 6.9 shows a comparison of the free-energies $G(z_{\mathrm{K12}})$ along the channel axis for the pair K1/K2 in the different cases, including the case of the incoming Na^+ ion (green line). The latter FES is very similar to FES computed for K^+ residing in the cavity (blue line). This further confirms the long range actions of the ion-ion electrostatic repulsions because the presence of any ion in the cavity, whether Na^+ or K^+, facilitates the transitions of K1/K2, and in the simulated conditions it was able to suppress of the gradient across the SF (from purple to green and blue lines). We define this as a "partial knock-on" effect. Partial because, as previously discussed, knock-on is finalised by the incoming (K^+) ion entering the filter that produces a free-energy gradient toward permeation (red

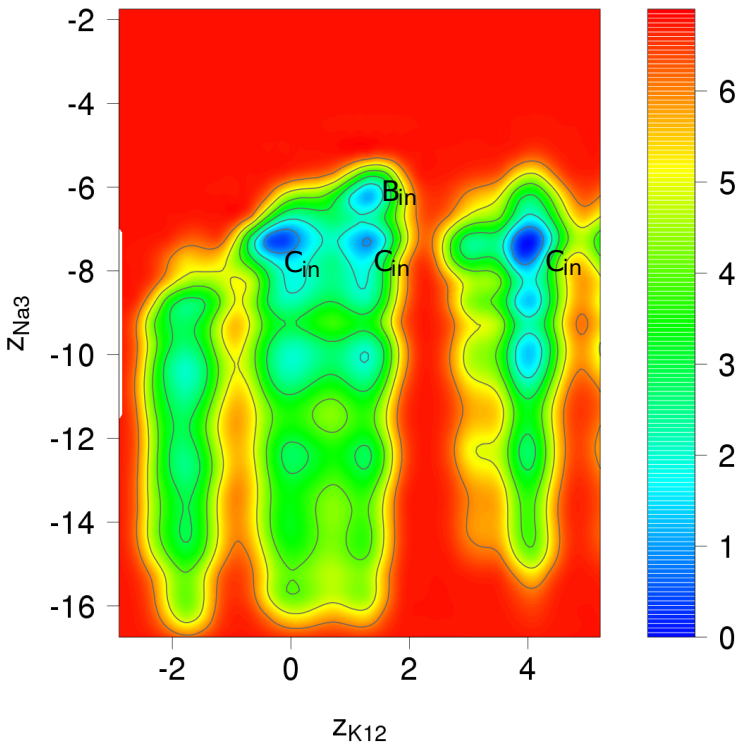

(a)

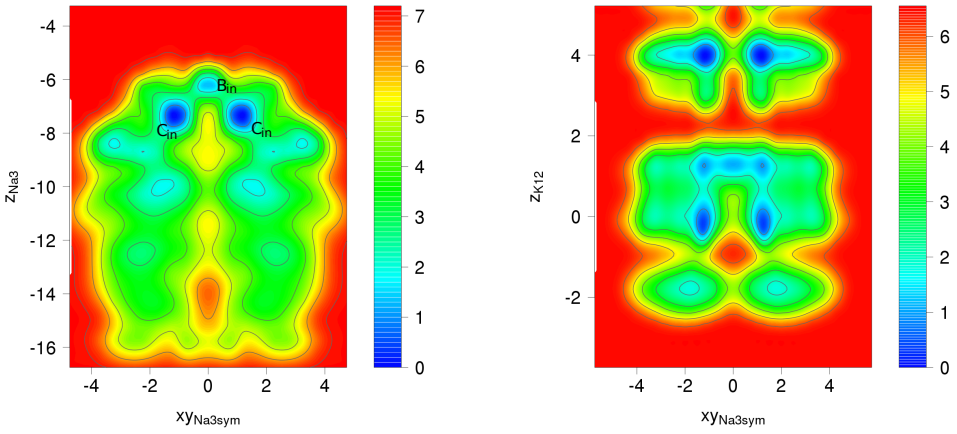

(b) (c)

Figure 6.12: Different projections of the multi-dimensional FES computed with a Na^+ ion in the cavity, computed with respect of z_{K12}, z_{Na3} and xy_{Na3}. The latter is symmetrised xy_{K3} with respect of 0 to represent on ideal planes crossing the channel axis. Binding sites C_{in} and B_{in} are shown.

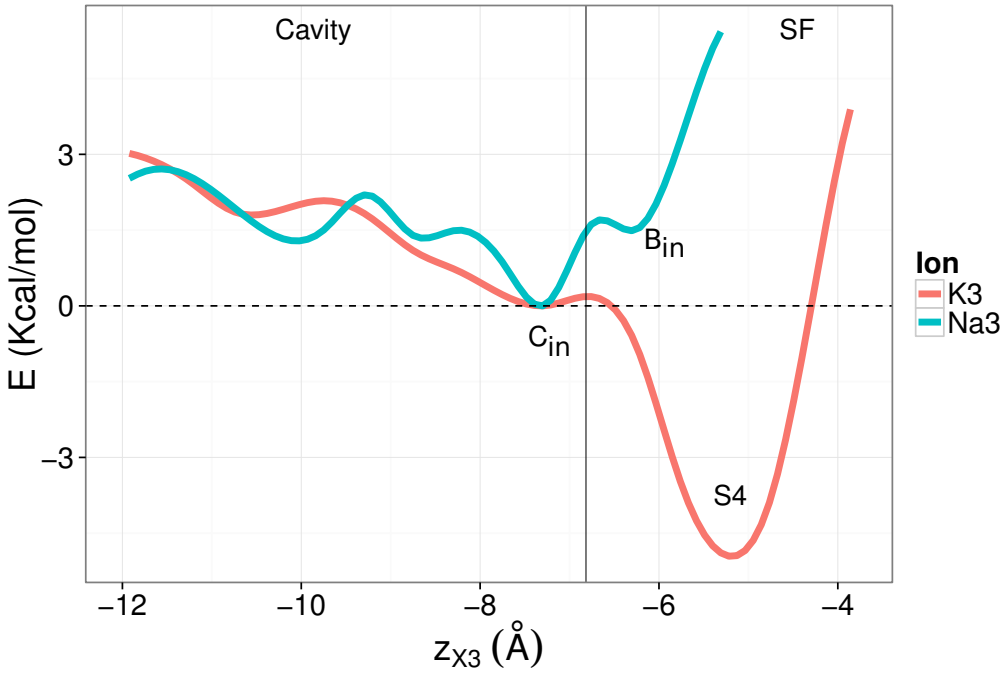

Figure 6.13: Free energies for the incoming ion, either K^+ of Na^+ projected into the channel axis, i.e. respectively onto z_{K3} and z_{Na3}.

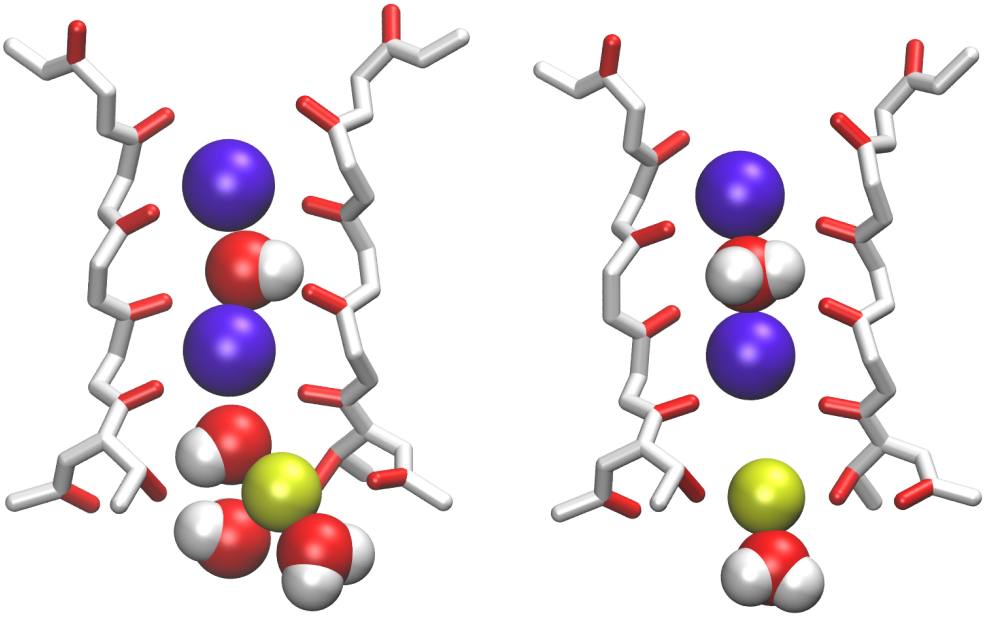

(a) **(b)**

Figure 6.14: Coordination of Na^+ atom in the entrance of the SF (B_{in}).

line). This finalisation does not occur in the case of the incoming Na^+ which, it is therefore suggested, is unable to promote conduction.

This inability to promote conduction is proposed as a possible explanation for the fast block induced by intracellular Na^+. In the case of relevant intracellular concentrations, Na^+ ions rapidly diffuse to the cavity, probably faster than K^+[61,113] eventually binding to C_{in}. The fast block of the K^+ current is suggested as being caused by the combination of the inability of Na^+ ions to give rise to an efficient conduction combined with the lowering of the electrochemical gradient between the intracellular side and the cavity, which must be considered capable of reducing the diffusion of K^+ near to the pore entrance.

Fig. 6.12a shows also that less energy is required for the outer K^+ ion (K1) to leave the SF than for the Na^+ ion to enter the SF in the conductive conformation. This is proposed as a possible cause for the slow gating effect of intracellular Na^+. This effect is more prominent at high voltages, when the gradients reported in Fig. 6.12a are expected to change, eventually promoting K1 to exit without the concurrent entry of an additional ion. Even if neither the energy required to completely empty the SF nor the transition toward inactive conformations were computed, the presence of a single K^+ ion in the SF was suggested as being insufficient to stabilise the conductive conformation over long time-scales.[45]

6.5.2 Mechanism of selectivity

All the results lead to a thermodynamically driven mechanism for selectivity which occurs prior to the SF and which can be interpreted as an extension of the classic "snug fit" hypothesis. Even taking into account the flexibility of the channel over extended sampling, the Na^+ are excluded from the SF. This is consistent with the RMSD analysis from long unbiased simulations (Fig. 4.7) which demonstrated fluctuations of T75, the SF entrance being the smallest within the whole protein in the conductive state, with A73 and T72. Although the structure of the pore's entrance is not completely rigid, as proved by the lack of B_{in} when K1/K2 were in S0/S2, its fluctuations are limited in the conductive conformation and a proper coordination of Na^+ is not favoured. The states B_{in} for Na^+ in Fig. 6.14b and C'' for K^+ in Fig. 6.6 appear to be very similar and accordingly to our results both are able to promote transitions of K1/K2. However, they strongly differ in the energetic: Na^+ is more favourable found in the aqueous cavity and it was rarely seen coordinated by the atoms of the SF entrance; K^+ is more stable in coordinated in the SF than in the cavity. Contrary to what has been suggested in previous studies[110], our results showed that the position of the pair K1/K2 does not modify the probability of Na^+

entering. It is important to note that we performed an extensive sampling over the states in which the D80 side chains cannot be driven by E71 and R64 so as to disrupt the conductivity of the channel. The Na^+ ion might find an easier way into the SF in some inactive conformation.[85,136]

6.6 Inward transitions and voltage-dependent inactivation

In KcsA the conduction has an outward preferred direction.[31,34] A dependence between this direction and the residues surrounding the pore has been found by experiment. Moreover, the dependence of the inactivation on voltage and on the inversion of the current was proved to exist. In any event, current measurements performed after pH jumps revealed different completeness and kinetics of inactivation according to the direction of the K^+ flux.[34] We propose that inactivation occurs with different mechanisms according to the flux direction. In this section we discuss the voltage-dependent inactivation promoted by inward transitions which is different from the mechanism proposed in chapter 5, although it bear a resemblance to it. The same network of residues is in fact involved in the process, and an interplay between V76 backbone and the E71 side chain is proposed playing the key role.

During the multi-ion metaD sampling described in secs. 6.2, an inactive conformation was reached. Although the extent of the distortions in the final state might be enhanced by the bias potential, inward transitions of the K^+ ions in the SF were recognised as enhancing the inactivation probability with a mechanism different from those described in the Chap. 5. These events were investigated using metaD as a tool to promote rare events: the inward transitions.[86]

A well-temperad metaD was performed with an identical set-up and starting point as the calculation which finished in the inactive state, restraining only the conformation of L81. This was intended to limit the influence of R64 in the process and thereby make it more easy to investigate the influence of E71 conformation. MetaD bias potential induced transitions in both directions. Although inward transitions of K1 and K2 occurred, as shown by the trajectories in Fig. 6.15, they were accompanied by lateral "pushes" on the central region of the SF, in particular on V76. This push originates the flipping of V76 in more than one subunit which, directly interacting with E71 side chains, caused the rotation around their $\chi 1$ dihedral angles to to $\sim -70°$ degrees. These transitions of E71 were finally responsible for the non-conductive states and any further movement of K^+ ions promoted by the metaD bias potential resulted in deeper inactive states.

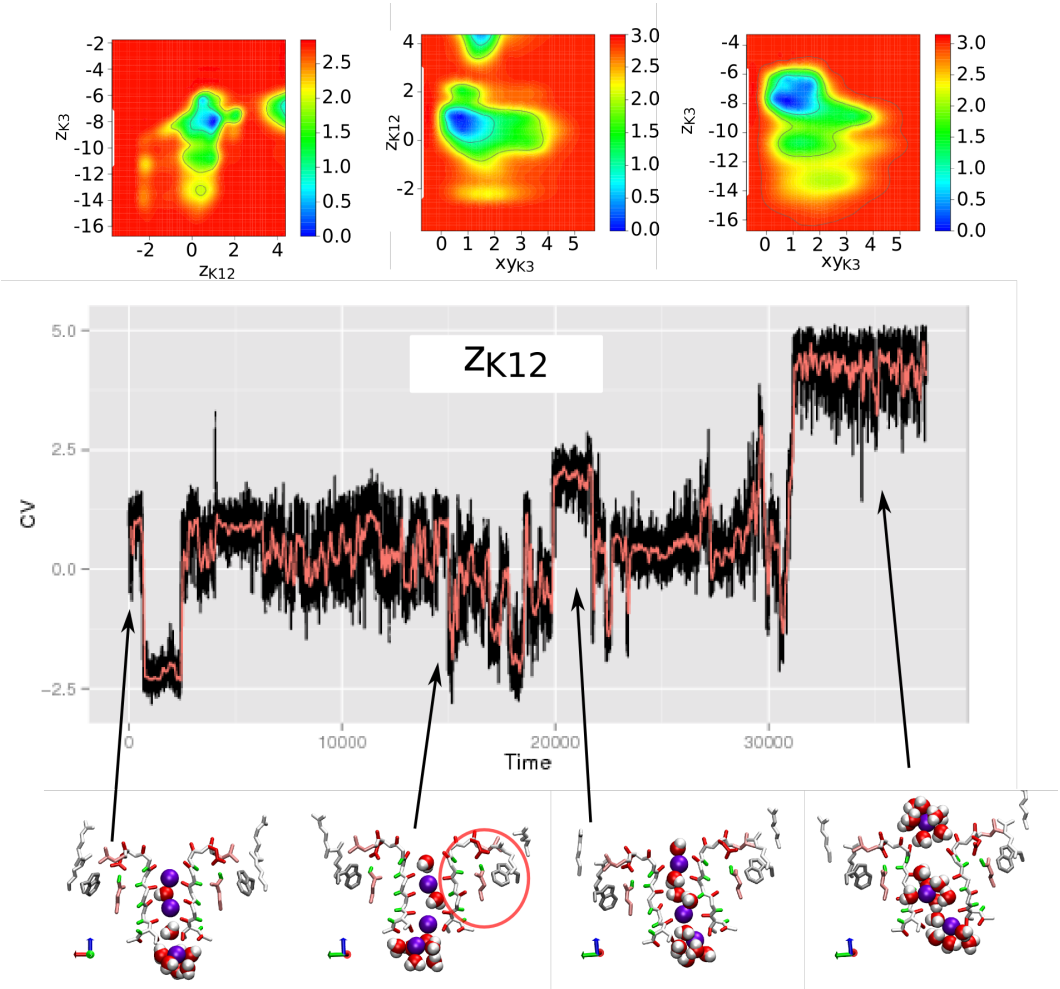

Figure 6.15: Detailed trajectories of the metaD calculation that underwent inactivation (L81 restrained to avoid the influence of the R64-D80 interactions on the dynamics of the SF). Three CVs were used: i) z_{K12}, ii) z_{K3} and iii) xy_{K3}(Fig. 6.1). The figures shows that inward transitions of the permeating K^+ ions (K1 and K2), sampled thanks to the MetaD bias potential, enhanced the probability of distortions in the SF structure. These distortions, initially stabilised by rearrangements of the neighbouring residues, in particular E71, finally led to the complete loss of the conductive conformation. Due to the major structural rearrangements of the SF, the obtained energy surfaces (upper panels, energy in Kcal/mol) do not represent the free energy.

A second calculation was performed from a different initial conformation of the K^+ ions (K1/K2/K3 in S0/S2/S4) and was halted before a complete disruption of the SF occurred. The calculation confirmed that permeation is not completely reversible in KcsA. Inward permeation easily generates non-conductive states similar to the one reported in Fig. 6.16 in which V76 flipped state is stabilised by the rotated E71, and can lead to a complete disruption of the SF conductive conformation. Similar results further stress the importance of focusing on conductive states of the protein when permeation and selectivity are investigated.

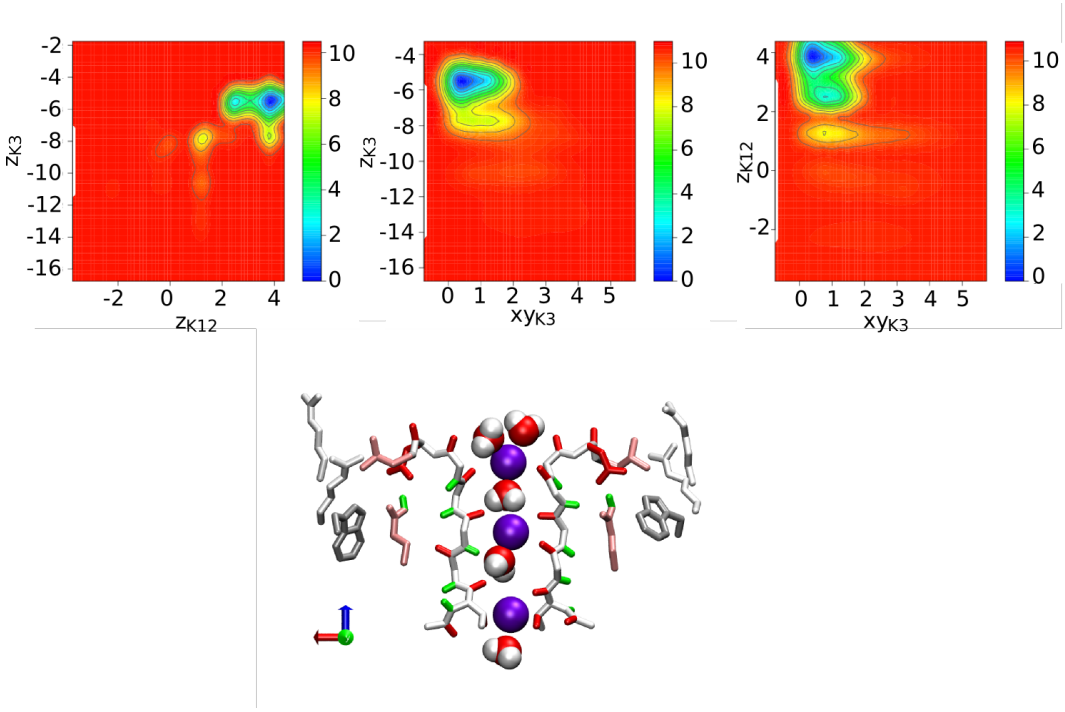

Figure 6.16: Structure of the filter with a low conductivity in which the V76 flipped state is stabilised by the rotation of E71 ($\chi 1 \sim -70°$), obtained during a MetaD calculation started from ion occupancy 10101+0 (L81 restrained to avoid the influence of the R64-D80 interactions on the dynamics of the SF). The occurrence of similar states was found enhanced by inward transitions of the K^+ ions in the filter. The energy surfaces demonstrate that similar configurations strongly affect the permeation, generating high barriers. The units of measurements of the energy surfaces are Kcal/mol.

6.7 Discussion

The investigation of permeation and selectivity on a truly conductive state of the SF allowed us to define the main driving forces of the processes. Differently from simi-

lar previous works,[18] electrostatic forces have been revealed as having a crucial role. Moreover the permeation has been shown to occur only via the knock-on mechanism, even if one of the two revealed pathways might appear at a first sight, and has been interpreted in the past, as associated to a "vacancy-diffusion" mechanism.[18] The dehydration of the incoming K^+ ion has been found barrier-less and accompanied by a strong thermodynamic benefit due to the ion-SF interactions. This is proposed as the main driving force which promotes the permeation, because it generates a favourable free-energy gradient. On the other hand, Na^+ was found preferably located in the cavity, fully hydrated, so that the selectivity can be explained.

In the previous chapters we recognised a network of residues responsible for the regulation of the state of the SF in KcsA. In this chapter we further demonstrate its importance in the conductivity. The occurrence of non-conductive states, including inactive, were transparently suppressed by controlling the conformation of the network. Interestingly, only two degrees of freedom per subunit appeared as the most determinant: $\chi 1$ dihedral angles of residues E71 and L81. This result confirms the hypothesis proposed in the previous chapters that the pore is mainly regulated by the state of D80, the main hub of the network, which is determined by a set of H-bond donor residues, among which E71 and R64 play a relevant role. Restraint on L81 conformation acts on the dynamics of the latter because they are closely interconnected, as shown in sec. 4.5.2. The results are consistent with the results of considerable experimental evidences in which mutations on E71 and R64 have been proved to be strongly affecting inactivation probability.[29,32,34–37,125] Furthermore, we suggest that voltage-dependent inactivation occurs with a different mechanism. It is suggested this mechanism is based on the coupling between inward transitions of K^+ ions an configurational changes in the network of residues behind the filter, that are spread via rearrangements in V76 and E71.

Extensive preliminary analysis revealed the influence on the dynamics of the incoming ion of the fluctuations of residues L100 in the closed state of the channel, which on average slow down the permeation and enhance the free-energy minima in the cavity, directly interacting with the K^+ and affecting its hydration shell. This suggests that the closed state of the protein might not be the optimal conformation on which to investigate permeation, unless precautions are taken to mimic the cavity in the case of the opened inner gate. In this work we did this by restraining the dynamics of L100.

Free-energy calculations on permeation and selectivity are particularly sensitive to the conductive/non-conductive equilibrium of the channel because permeation, selectivity and inactivation are closely related.[20,35,36,92] The uncoupling of the

dynamics of the ions and the conductive/non-conductive equilibrium allowed us to confine the investigation of permeation and selectivity to within the region of the phase space closer to the putative conductive structure proposed by Zhou et al.[157]. This led to a coherent multi-ion FES for the the permeation within the conductive state.

It is suggested that permeation occurs according to two main pathways, similar at what has been done in previous works[18] but with several relevant differences. Ion-ion repulsions have been proved to act over longer distances than previously suggested in similar works,[18] confirming the classic hypothesis that electrostatic interactions play a fundamental role in the process. Motions of K^+ ions bound in the SF occurred only in the presence of an incoming ion, and in the absence of a K^+ in the cavity they were pushed toward the innermost sites (S2/S4) by the repulsive interactions with the K^+ in the outer bulk. Consequently, it is proposed that both pathways occur according to the "knock-on" mechanism: "classic knock-on", in which the transitions of the K^+ bound to the pore are promoted by the entry of the incoming ion; and "purely electrostatic knock-on", in which the initial outer displacements of the K^+ in the SF promoted by the long range ion-ion repulsions with the incoming ion close to the pore mouth are followed by its entry into the SF. Both mechanisms were seen accompanied by the possible occurrence of vacancies.

Within this framework, the overall conduction is mainly limited by the diffusion of the K^+ ions to the cavity and secondly by a low barrier (between 4 and 5 kcal/mol) associated with the flexibility of the central region of the filter. This is different from previous works based on MD and free-energy calculations, where the transitions within the pore were suggested to be limited by a simple diffusion.[18,48] Permeation is thermodynamically favourable as soon as the electrochemical gradient across the SF has been compensated by the incoming K^+ ion(s). Protein structure drives it towards the pore mouth exposing negative charges to the cavity, particularly the carbonyl groups of residues T74 and A73 and side chains of T75. The dehydration of the incoming K^+ that occurs at the pore entrance is almost barrierless and is accompanied by a strong thermodynamic benefit given by coordination in S4. This preference for the incoming K^+ to be bound to the SF rather than to stay in the cavity is suggested as being the local driving force of permeation, which results in an overall gradient of free-energy favourable to the permeation.

Additionally, the selectivity over intracellular Na^+ was investigated. A mechanism driven by thermodynamic exclusion is proposed as occurring prior to entry into the SF. The most stable states for the Na^+ were found fully hydrated in the cavity (C_{in}), while a high barrier prevents entry into the SF. This barrier is sug-

gested as being caused by the low flexibility of the SF entrance and its inability to adequately coordinate the Na^+. These results are consistent with the classic "snug fit" hypothesis.

Explanations for the fast and slow blocking effects on K^+ current are also suggested. The former is proposed as originating from the negative influence of the Na^+ weakly bound in the cavity on the diffusion of the K^+ towards the mouth of the SF; the latter is suggested as originating from the lower energy required for the outermost K^+ ion to leave the pore than the higher energy required for the Na^+ to enter. In the case of high voltages this will eventually lead to a single K^+ in the SF which is unable to stabilise the conductive conformation over long time-scales.[45]

Additional work is needed to more deeply understand the influence of the network of residues behind the SF on conductivity and to investigate additional conductive states. These investigations might lead to the discovery of the origin of the different modes of the current. Moreover, additional work is also necessary to further clarify the relationship between inward transition and inactivation.

Chapter 7

Conclusions

Single-channel measurements of current in K^+ ion channels demonstrate an extreme variability in the patterns of the current which arises from complicated interdependencies between ions-protein interactions and fine structural rearrangements.[29,66,92] These patterns reflect inherent complexities associated with the microscopic dynamics of the channels which are crucial for physiological functions. These cannot be easily addressed by available experimental techniques[132] and can hardly be accurately represented by the simplified theoretical models that have been used over past decades. By contrast, molecular dynamics represents an important tool in the understanding of these systems because it is able to deliver a realistic description of the microscopic details as well as provide important macroscopic properties of experimental interest.[2,101,126] In this work, molecular dynamics combined with approaches for determining free energies (particularly well-tempered metadynamics) has been used to investigate the properties of K^+ ion channels and the key factors in their regulation. The bacterial channel KcsA, which shares important similarities to eukaryotic K^+ channels,[46] has been used as a model in the understanding of the relationship between structure and function. A thorough dynamical description has provided the existence of the strong coupling between permeation and the pore region and has demonstrated that the selectivity filter, the functional region which is fundamental in conduction, is not an independent structure and must be considered within the more general dynamics of the protein in order to draw a realistic picture of macroscopic currents.

In the first part of the work, Chapter 3, the strong influence of the motions of the protein on the permeating ions has been shown by the existence of $1/f$ component in their dynamics. Moreover, the presence of this $1/f$ scaling affects calculations of free energies and it has been shown that longer sampling is necessary to reach

convergence. However, this comes with a loss of accuracy, meaning that free-energy calculations on K^+ channels must be considered capable of deliver reliable qualitative pictures, whilst quantitative analyses would be associated with an uncertainty which it is difficult to determine. It has also been shown that a complete description of ions in the selectivity filter should be based on under-damped particle motion, thereby taking into account the a role for inertia.

The principal molecular determinants for structural rearrangements which involve the permeation path have been revealed (Chapter 4). They form a highly-correlated network of residues behind the filter which has its main hub in the aspartic acid D80 which is located at the external entrance. Conformational changes in this network are spread to the filter and the permeating ions via D80, which acts as a "handle" in determining the state of the pore. The core of the network (first level) consists of the aspartic acid and the surrounding H-bond donors, E71, W67, R64 and R89, which collaborate in determining its state. Among these, E71 and R64 have been found to have the strongest influence. An important role is played by conformational changes of the residues L81, located next to the main hub D80, which are closely interconnected with the dynamics of R64. These results can explain a number of experimental evidences and assume a more general importance considering that the aspartic acid D80 belongs to the signature sequence TXXTXGYGD, which is highly conserved among K^+ ion channels, commonly surrounded by different H-bond donors.[26,31,37,85] In the same chapter, V76 flipped states, referred to in the published literature as being responsible for non-conductive states,[20,30] have been proved to be transient and not able to hinder K^+ permeation unless associated with additional conformational rearrangements.

Among the structural rearrangements of the filter region in K^+ channels, C-type inactivation is one of the most important because of its crucial role in current modulation.[30,37,66,85,119,141,157] Different hypotheses have been advanced to explain this process and structures obtained via X-ray experiments have been suggested as being the C-type inactive state, characterised by a constriction in the central region of the filter and hence often referred as "collapsed".[42,157] Nevertheless, mechanisms of inactivation and its nature remain mostly obscure.[29,66]

In Chapter 5 inactivation has been described, its causes investigated and a mechanism of the C-type inactivation has been proposed. The inactive states obtained from our calculations closely resemble the collapsed structures obtained via X-ray experiments. The mechanism is based on highly cooperative conformational changes in the network of residues behind the filter and also involves cooperation also among the different domains. Variability of the main hub D80 has been demonstrated

as having a central role in the process, and in particular the "flipping" of its side chains. This flipping was seen also in unbiased simulation of the deep-inactivating Y82A mutant, and has been found to be dependent on the positions of the ions in the filter and of the nearby H-bond donors. Among these, arginine R64 has been confirmed as having a strong influence. This influence can explain different experimental evidence and was confirmed by free-energy calculations on the mutants R64A and Y82A, reported in the literature as having respectively a reduced and an increased inactivation probability with respect to inactivation compared to the WT.[35]

Rotation of E71 side chain has been also found to be associated with the inactivation process. These results were confirmed by a well-tempered metadynamics calculations performed on the deep-inactivating Y82A which ended with the filter in an inactive state. Within this calculation, the sampling over the rotation of the D80 side chain and the breaking of E71–D80 H-bond was increased by a time-dependent bias potential.[13]

The performed calculations provide a dynamical picture which is able to reveal the key features of the control of current at the filter in K^+ channel KcsA. These results can help to design novel experiments to better target C-type inactivation. In particular mutagenesis experiments on D80 and L81 would be useful to confirm the inactivation mechanism, while simultaneous mutations of different residues could confirm the existence and the extent of the network of residues responsible for the conformational changes in the permeation path as being described in the present work.

However, the picture is not complete because a high number of residues interacting in the network and an huge number of possible rearrangements in the network leave a room for other mechanisms to be found, although they are expected to share strong similarities with the one described above. Examples of such mechanisms have been seen in the present work: i) a mechanism of inactivation promoted by inward permeation of K^+ which is suggested as being related to the voltage-dependent gating; and ii) a pH-related mechanism linked to the acid/base reactions of E71.

The thorough investigation of dynamical behaviours of the pore region allowed us to study permeation and selectivity unambiguously, separating all the relevant fast motions from the slower ones associated with inactivation and conformational flexibility of the pore, which are widely known to obscure similar analysis.[20,35,78,92,141] In Chapter 6 the results from these studies are presented. A detailed picture of multi-ions conduction was built on a truly conductive state of the channel, the equilibrium conductive/non-conductive states being transparently suppressed.

Multi-dimensional free-energy calculations unveiled the driving forces and energetics associated with the permeation and selectivity in the case of the outward direction of the current.

Conduction is proposed mainly limited by the diffusion of the K^+ ions into the cavity. Once the incoming K^+ diffuses into the cavity, protein structure drives it towards the pore mouth exposing negative charges of residues T74, A73 and T75 to the cavity. Its dehydration has been found to be practically barrier-less and accompanied by a strong thermodynamic benefit. Motions of the K^+ ions within the pore are governed by the superposition of the electrochemical gradient across the filter and the ion-protein interactions. This superposition results in the absence of permeation without the intervention of an incoming ion, supporting a "knock-on" conduction mechanism. When the incoming K^+ ion balances the electrochemical gradient across the filter, it induces concerted multi-ionic transitions which, due to the dehydration benefit, are characterised by an overall free-energy gradient which promotes the permeation. A small barrier (4 and 5 kcal/mol) has been found to be associated with the flexibility of the central region of the pore, which include the so-called V76 flipping.

It has been demonstrated that permeation occurs along to two main pathways. The first one resembles mechanisms suggested in previous works[18,72] and is therefore referred as "classic knock-on": the transition of the K^+ bound to the pore is promoted by the entry of the incoming ion. The second pathway is promoted by the ion-ion repulsions between the incoming K^+ and those bound to the filter. The electrostatic repulsion has been proved in this work to act over longer distances than previously suggested by similar works.[18] This pathway is defined as "purely electrostatic knock-on". Both mechanisms were seen to be accompanied by the creation of vacancies, although the probabilities of these events have not been investigated in detail.

Additionally selectivity over intracellular Na^+ has been investigated and a mechanism based on thermodynamic exclusion has been proposed. The Na^+ ion has been found to be preferentially located in the cavity, fully hydrated, in specific binding sites that have been called C_{in}. The inner mouth of the filter showed a small affinity for the Na^+ ions, although a weak coordination has been seen under certain conditions. This weak binding site has been labelled B_{in}. The exiting of outermost K^+ ion from the filter into the bulk requires less energy than the entry of Na^+ ion into the filter, which has not been seen during the long enhanced sampling. Na^+ ions can generate a "partial knock-on", balancing the filter electrochemical gradient. However, a proper conduction is not promoted because they do not enter into the

filter.

Starting from this results explanation of the fast block and slow block on K^+ current caused by intracellular Na^+ have been moreover suggested. A Na^+ ion in C_{in} would affect diffusion of K^+ ions towards the filter reducing the gradient between the cavity and intracellular side and obstructing its entrance, without being able to induce a conduction. In the case of high voltages, the outer K^+ ion is more likely to leave the filter than the Na^+ to enter, leading to the slow block of the current, because a single K^+ would not be capable of stabilising the conductive state of the pore over long time-scales.[45]

Bibliography

[1] D. Adler and D. Murdoch. *rgl: 3D visualization device system (OpenGL)*, 2012. R package version 0.92.892.

[2] M. P. Allen and D. J. Tildesley. *Computer Simulation of Liquids*. Oxford science publications. Oxford University Press, USA, June 1989.

[3] T. W. Allen, T. BaÅ§tuÄ§, S. Kuyucak, and S.-H. Chung. Gramicidin a channel as a test ground for molecular dynamics force fields. *Biophysical Journal*, 84(4):2159 – 2168, 2003.

[4] T. W. Allen, O. S. Andersen, and B. Roux. Energetics of ion conduction through the gramicidin channel. *Proceedings of the National Academy of Sciences of the United States of America*, 101(1):117 –122, Jan. 2004.

[5] T. W. Allen, O. S. Andersen, and B. Roux. Molecular dynamics–potential of mean force calculations as a tool for understanding ion permeation and selectivity in narrow channels. *Ion Hydration Special Issue*, 124(3):251–267, Dec. 2006.

[6] R. Anandakrishnan, B. Aguilar, and A. V. Onufriev. H++ 3.0: automating pK prediction and the preparation of biomolecular structures for atomistic molecular modeling and simulations. *Nucleic Acids Research*, 40(W1):W537–W541, July 2012.

[7] O. S. Andersen. Perspectives on: Ion selectivity. *The Journal of General Physiology*, 137(5):393–395, Jan. 2011.

[8] J. Aqvist and V. Luzhkov. Ion permeation mechanism of the potassium channel. *Nature*, 404(6780):881–884, Apr. 2000.

[9] Y. Arinaminpathy, E. Khurana, D. M. Engelman, and M. B. Gerstein. Computational analysis of membrane proteins: the largest class of drug targets. *Drug Discovery Today*, 14(23-24):1130–1135, Dec. 2009.

[10] S. K. Bagal, A. D. Brown, P. J. Cox, K. Omoto, R. M. Owen, D. C. Pryde, B. Sidders, S. E. Skerratt, E. B. Stevens, R. I. Storer, and N. A. Swain. Ion channels as therapeutic targets: A drug discovery perspective. *Journal of Medicinal Chemistry*, 56(3):593–624, Feb. 2013.

[11] P. Bak, C. Tang, and K. Wiesenfeld. Self-organized criticality: An explanation of the $1/f$ noise. *Physical Review Letters*, 59:381–384, Jul 1987.

[12] E. N. Baker and R. E. Hubbard. Hydrogen bonding in globular proteins. *Progress in Biophysics and Molecular Biology*, 44:97–179, Jan. 1984.

[13] A. Barducci, G. Bussi, and M. Parrinello. Well-tempered metadynamics: A smoothly converging and tunable free-energy method. *Physical Review Letters*, 100(2):020603, Jan. 2008.

[14] M. Bastian, S. Heymann, and M. Jacomy. Gephi: An open source software for exploring and manipulating networks. *International AAAI Conference on Weblogs and Social Media*, 2009.

[15] J. S. Bendat and A. G. Piersol. *Random Data: Analysis and Measurement Procedures.* John Wiley & Sons, Sept. 2011.

[16] J. M. Berg, J. L. Tymoczko, and L. Stryer. *Biochemistry.* W. H. Freeman, Dec. 2008.

[17] S. Bernèche and B. Roux. Molecular dynamics of the KcsA K^+ channel in a bilayer membrane. *Biophysical Journal*, 78(6):2900–2917, June 2000.

[18] S. Berneche and B. Roux. Energetics of ion conduction through the K^+ channel. *Nature*, 414(6859):73–77, Nov. 2001.

[19] S. Bernèche and B. Roux. The ionization state and the conformation of glu-71 in the KcsA K^+ channel. *Biophysical Journal*, 82(2):772–780, Feb. 2002.

[20] S. Bernèche and B. Roux. A gate in the selectivity filter of potassium channels. *Structure*, 13:591–600, Apr. 2005.

[21] F. Bezanilla. Negative conductance caused by entry of sodium and cesium ions into the potassium channels of squid axons. *The Journal of General Physiology*, 60(5):588–608, Nov. 1972.

[22] M. P. Bhate and A. E. McDermott. Protonation state of E71 in KcsA and its role for channel collapse and inactivation. *Proceedings of the National Academy of Sciences*, 109(38):15265–15270, Sept. 2012.

[23] R. Blunck, H. McGuire, H. C. Hyde, and F. Bezanilla. Fluorescence detection of the movement of single KcsA subunits reveals cooperativity. *Proceedings of the National Academy of Sciences*, 105(51):20263–20268, Dec. 2008.

[24] D. Bucher, L. Guidoni, and U. Rothlisberger. The protonation state of the Glu-71/Asp-80 residues in the KcsA potassium channel: A first-principles QM/MM molecular dynamics study. *Biophysical Journal*, 93(7):2315–2324, Oct. 2007.

[25] M. Buck, S. Bouguet-Bonnet, R. W. Pastor, and A. D. MacKerell. Importance of the CMAP correction to the CHARMM22 protein force field: Dynamics of hen lysozyme. *Biophysical Journal*, 90(4):L36–L38, Feb. 2006.

[26] W. A. Catterall. Ion channel voltage sensors: structure, function, and pathophysiology. *Neuron*, 67(6):915–928, Sept. 2010.

[27] M. Ceriotti, G. A. Tribello, and M. Parrinello. Simplifying the representation of complex free-energy landscapes using sketch-map. *Proceedings of the National Academy of Sciences*, 108(32):13023–13028, Sept. 2011.

[28] S. Chakrapani, J. F. Cordero-Morales, and E. Perozo. A quantitative description of KcsA gating i: Macroscopic currents. *The Journal of General Physiology*, 130(5):465 –478, Nov. 2007.

[29] S. Chakrapani, J. F. Cordero-Morales, and E. Perozo. A quantitative description of KcsA gating II: single-channel currents. *The Journal of General Physiology*, 130(5):479 –496, Nov. 2007.

[30] S. Chakrapani, J. F. Cordero-Morales, V. Jogini, A. C. Pan, D. M. Cortes, B. Roux, and E. Perozo. On the structural basis of modal gating behavior in K^+ channels. *Nature Structural & Molecular Biology*, 18:67–74, Dec. 2010.

[31] M. L. Chapman, H. S. Krovetz, and A. M. J. VanDongen. GYGD pore motifs in neighbouring potassium channel subunits interact to determine ion selectivity. *The Journal of Physiology*, 530(1):21–33, 2001.

[32] W. W. L. Cheng, J. G. McCoy, A. N. Thompson, C. G. Nichols, and C. M. Nimigean. Mechanism for selectivity-inactivation coupling in KcsA potassium channels. *Proceedings of the National Academy of Sciences*, 108(13):5272 – 5277, Mar. 2011.

[33] T. Claydon, S. Makary, K. Dibb, and M. Boyett. K^+ activation of Kir3.1/Kir3.4 and kv1.4 K^+ channels is regulated by extracellular charges. *Biophysical Journal*, 87(4):2407–2418, Oct. 2004.

[34] J. F. Cordero-Morales, L. G. Cuello, and E. Perozo. Voltage-dependent gating at the KcsA selectivity filter. *Nature Structural & Molecular Biology*, 13(4): 319–322, Mar. 2006.

[35] J. F. Cordero-Morales, L. G. Cuello, Y. Zhao, V. Jogini, D. M. Cortes, B. Roux, and E. Perozo. Molecular determinants of gating at the potassium-channel selectivity filter. *Nature Structural & Molecular Biology*, 13:311–318, Mar. 2006.

[36] J. F. Cordero-Morales, V. Jogini, A. Lewis, V. Vasquez, D. M. Cortes, B. Roux, and E. Perozo. Molecular driving forces determining potassium channel slow inactivation. *Nature Structural & Molecular Biology*, 14(11):1062–1069, Oct. 2007.

[37] J. F. Cordero-Morales, V. Jogini, S. Chakrapani, and E. Perozo. A multipoint hydrogen-bond network underlying KcsA c-type inactivation. *Biophysical Journal*, 100(10):2387–2393, May 2011.

[38] J. F. Cordero-Morales, V. Jogini, S. Chakrapani, and E. Perozo. A multipoint hydrogen-bond network underlying KcsA c-type inactivation. *Biophysical Journal*, 100(10):2387–2393, May 2011.

[39] B. Corry and M. Thomas. Mechanism of ion permeation and selectivity in a voltage gated sodium channel. *Journal of the American Chemical Society*, 134 (3):1840–1846, Dec. 2011.

[40] S. M. Cosseddu, I. A. Khovanov, M. P. Allen, P. M. Rodger, D. G. Luchinsky, and P. McClintock. Dynamics of ions in the selectivity filter of the KcsA channel: Towards a coupled brownian particle description. *The European Physical Journal Special Topics*, 222(10):2595–2605, Oct. 2013.

[41] L. G. Cuello, V. Jogini, D. M. Cortes, A. C. Pan, D. G. Gagnon, O. Dalmas, J. F. Cordero-Morales, S. Chakrapani, B. Roux, and E. Perozo. Structural basis for the coupling between activation and inactivation gates in K^+ channels. *Nature*, 466(7303):272–275, July 2010.

[42] L. G. Cuello, V. Jogini, D. M. Cortes, and E. Perozo. Structural mechanism of c-type inactivation in K^+ channels. *Nature*, 466(7303):203–208, July 2010.

[43] P. D. Dixit and D. Asthagiri. Thermodynamics of ion selectivity in the KcsA K^+ channel. *The Journal of General Physiology*, 137(5):427–433, May 2011.

[44] C. Domene and S. Furini. Dynamics, energetics, and selectivity of the low-K^+ KcsA channel structure. *Journal of Molecular Biology*, 389(3):637–645, June 2009.

[45] C. Domene, M. L. Klein, D. Branduardi, F. L. Gervasio, and M. Parrinello. Conformational changes and gating at the selectivity filter of potassium channels. *Journal of the American Chemical Society*, 130(29):9474–9480, July 2008.

[46] D. A. Doyle, J. M. Cabral, R. A. Pfuetzner, A. Kuo, J. M. Gulbis, S. L. Cohen, B. T. Chait, and R. MacKinnon. The structure of the potassium channel: Molecular basis of K^+ conduction and selectivity. *Science*, 280(5360):69 –77, Apr. 1998.

[47] P. Dutta and P. M. Horn. Low-frequency fluctuations in solids: $1/f$ noise. *Reviews of Modern Physics*, 53:497–516, Jul 1981. doi: 10.1103/RevModPhys.53.497.

[48] B. Egwolf and B. Roux. Ion selectivity of the KcsA channel: A perspective from multi-ion free energy landscapes. *Journal of Molecular Biology*, 401(5): 831–842, Sept. 2010.

[49] U. Essmann, L. Perera, M. L. Berkowitz, T. Darden, H. Lee, and L. G. Pedersen. A smooth particle mesh ewald method. *The Journal of Chemical Physics*, 103(19):8577, 1995.

[50] G. Fiorin, M. L. Klein, and J. Hénin. Using collective variables to drive molecular dynamics simulations. *Molecular Physics*, 111(22-23):3345–3362, 2013.

[51] P. W. Fowler, E. Abad, O. Beckstein, and M. S. P. Sansom. Energetics of multi-ion conduction pathways in potassium ion channels. *Journal of Chemical Theory and Computation*, 9(11):5176–5189, 2013.

[52] J. Fox and S. Weisberg. *An R Companion to Applied Regression.* Sage, Thousand Oaks CA, second edition, 2011.

[53] D. Frenkel and B. Smit. *Understanding Molecular Simulation, Second Edition: From Algorithms to Applications (Computational Science Series, Vol 1).* Academic Press, 2 edition, Nov. 2001.

[54] S. Furini and C. Domene. Atypical mechanism of conduction in potassium channels. *Proceedings of the National Academy of Sciences*, 106(38):16074–16077, Sept. 2009.

[55] R. Furrer, D. Nychka, and S. Sain. *fields: Tools for spatial data*, 2013. R package version 6.7.6.

[56] H. Goldstein, C. P. Poole, and J. Safko. *Classical Mechanics*, volume 2011. Addison-Wesley, 3rd edition edition, 2002.

[57] B. J. Grant, A. P. C. Rodrigues, K. M. ElSawy, J. A. McCammon, and L. S. D. Caves. Bio3d: an r package for the comparative analysis of protein structures. *Bioinformatics*, 22(21):2695–2696, Jan. 2006.

[58] A. Grossfield. WHAM: the weighted histogram analysis method. URL membrane.urmc.rochester.edu/content/wham. version 2.0.6.

[59] H. Grubmüller, H. Heller, A. Windemuth, and K. Schulten. Generalized verlet algorithm for efficient molecular dynamics simulations with long-range interactions. *Molecular Simulation*, 6(1-3):121–142, 1991.

[60] L. Guidoni, V. Torre, and P. Carloni. Potassium and sodium binding to the outer mouth of the K^+ channel. *Biochemistry*, 38(27):8599–8604, July 1999.

[61] H. S. Harned. Ninth spiers memorial lecture. some recent experimental studies of diffusion in liquid systems. *Discussions of the Faraday Society*, 24(0):7–16, 1957.

[62] L. Heginbotham. Single streptomyces lividans K^+ channels: Functional asymmetries and sidedness of proton activation. *The Journal of General Physiology*, 114(4):551–560, Sept. 1999.

[63] G. D. Henry and B. D. Sykes. Determination of the rotational dynamics and pH dependence of the hydrogen exchange rates of the arginine guanidino group using NMR spectroscopy. *Journal of Biomolecular NMR*, 6:59–66, July 1995.

[64] B. Hille. *Ion Channels of Excitable Membranes*. Sinauer Associates, 2001.

[65] A. L. Hodgkin and R. D. Keynes. The potassium permeability of a giant nerve fibre. *The Journal of Physiology*, 128(1):61–88, Apr. 1955.

[66] T. Hoshi and C. M. Armstrong. C-type inactivation of voltage-gated K^+ channels: Pore constriction or dilation? *The Journal of General Physiology*, 141 (2):151–160, Jan. 2013.

[67] W. Humphrey. VMD: visual molecular dynamics. *Journal of Molecular Graphics*, 14:33–38, Feb. 1996.

[68] S. Imai, M. Osawa, K. Takeuchi, and I. Shimada. Structural basis underlying the dual gate properties of KcsA. *Proceedings of the National Academy of Sciences*, 107(14):6216 –6221, Apr. 2010.

[69] H. I. Ingólfsson, Y. Li, V. V. Vostrikov, H. Gu, J. F. Hinton, R. E. Koeppe, B. Roux, and O. S. Andersen. Gramicidin a backbone and side chain dynamics evaluated by molecular dynamics simulations and nuclear magnetic resonance experiments. i: Molecular dynamics simulations. *The Journal of Physical Chemistry B*, 115(22):7417–7426, June 2011.

[70] C. D. James Kew, editor. *Ion Channels From Structure to Function*. Oxford University Press, USA, Nov. 2009.

[71] M. O. Jensen, D. W. Borhani, K. Lindorff-Larsen, R. O. Dror, and D. E. Shaw. Reply to domene and furini: Distinguishing knock-on and vacancy diffusion mechanisms. *Proceedings of the National Academy of Sciences*, 107 (33):E129–E129, Aug. 2010.

[72] M. O. Jensen, D. W. Borhani, K. Lindorff-Larsen, P. Maragakis, V. Jogini, M. P. Eastwood, R. O. Dror, and D. E. Shaw. Principles of conduction and hydrophobic gating in K^+ channels. *Proceedings of the National Academy of Sciences*, 107(13):5833–5838, Mar. 2010.

[73] Y. Jiang, A. Lee, J. Chen, M. Cadene, B. T. Chait, and R. MacKinnon. Crystal structure and mechanism of a calcium-gated potassium channel. *Nature*, 417 (6888):515–522, May 2002.

[74] Y. Jiang, A. Lee, J. Chen, V. Ruta, M. Cadene, B. T. Chait, and R. MacKinnon. X-ray structure of a voltage-dependent K^+ channel. *Nature*, 423(6935): 33–41, May 2003.

[75] G. J. Kaczorowski, O. B. McManus, B. T. Priest, and M. L. Garcia. Ion channels as drug targets: The next GPCRs. *The Journal of General Physiology*, 131(5):399–405, Jan. 2008.

[76] S. J. Kehl, C. Eduljee, D. C. H. Kwan, S. Zhang, and D. Fedida. Molecular determinants of the inhibition of human kv1.5 potassium currents by external protons and zn^{2+}. *The Journal of Physiology*, 541(1):9–24, May 2002.

[77] F. Khalili-Araghi, E. Tajkhorshid, and K. Schulten. Dynamics of K^+ ion conduction through kv1.2. *Biophysical Journal*, 91(6):L72–L74, Sept. 2006.

[78] I. Kim and T. W. Allen. On the selective ion binding hypothesis for potassium channels. *Proceedings of the National Academy of Sciences*, 108(44):17963–17968, Oct. 2011.

[79] J. B. Klauda, R. M. Venable, J. A. Freites, J. W. O'Connor, D. J. Tobias, C. Mondragon-Ramirez, I. Vorobyov, A. D. MacKerell, and R. W. Pastor. Update of the CHARMM all-atom additive force field for lipids: Validation on six lipid types. *The Journal of Physical Chemistry B*, 114(23):7830–7843, June 2010.

[80] G. R. Kneller, K. Hinsen, G. Sutmann, and V. Calandrini. Scaling laws and memory effects in the dynamics of liquids and proteins. *Physics of Particles and Nuclei Letters*, 5(3):189–195, June 2008.

[81] A. Kreusch, P. J. Pfaffinger, C. F. Stevens, and S. Choe. Crystal structure of the tetramerization domain of the shaker potassium channel. *Nature*, 392 (6679):945–948, Apr. 1998.

[82] S. Kumar, J. M. Rosenberg, D. Bouzida, R. H. Swendsen, and P. A. Kollman. THE weighted histogram analysis method for free-energy calculations on biomolecules. i. the method. *Journal of Computational Chemistry*, 13(8): 1011–1021, Oct. 1992.

[83] S. Kumar, J. M. Rosenberg, D. Bouzida, R. H. Swendsen, and P. A. Kollman. Multidimensional free-energy calculations using the weighted histogram analysis method. *Journal of Computational Chemistry*, 16(11):1339–1350, Nov. 1995.

[84] A. Kuo, J. M. Gulbis, J. F. Antcliff, T. Rahman, E. D. Lowe, J. Zimmer, J. Cuthbertson, F. M. Ashcroft, T. Ezaki, and D. A. Doyle. Crystal structure of the potassium channel KirBac1.1 in the closed state. *Science*, 300(5627): 1922–1926, June 2003.

[85] H. T. Kurata and D. Fedida. A structural interpretation of voltage-gated potassium channel inactivation. *Progress in Biophysics and Molecular Biology*, 92(2):185–208, Oct. 2006.

[86] A. Laio and F. L. Gervasio. Metadynamics: a method to simulate rare events and reconstruct the free energy in biophysics, chemistry and material science. *Reports on Progress in Physics*, 71(12):126601, 2008.

[87] A. Laio and M. Parrinello. Escaping free-energy minima. *Proceedings of the National Academy of Sciences*, 99(20):12562–12566, Jan. 2002.

[88] A. Laio, A. Rodriguez-Fortea, F. L. Gervasio, M. Ceccarelli, and M. Parrinello. Assessing the accuracy of metadynamics. *The Journal of Physical Chemistry B*, 109(14):6714–6721, Apr. 2005.

[89] J. K. Lanyi. Bacteriorhodopsin. *Annual Review of Physiology*, 66(1):665–688, Mar. 2004.

[90] H. Larsson and F. Elinder. A conserved glutamate is important for slow inactivation in K^+ channels. *Neuron*, 27(3):573–583, Sept. 2000.

[91] X. Li, G. Bett, X. Jiang, V. Bondarenko, M. Morales, and R. Rasmusson. Regulation of n- and c-type inactivation of kv1.4 by pH_o and K^+ Evidence for transmembrane communication. *American Journal of Physiology - Heart and Circulatory Physiology*, 284(1 53-1):H71–H80, 2003.

[92] Y. Li, O. S. Andersen, and B. Roux. Energetics of double-ion occupancy in the gramicidin a channel. *The Journal of Physical Chemistry B*, 114(43): 13881–13888, Nov. 2010.

[93] Y. Liu, M. E. Jurman, and G. Yellen. Dynamic rearrangement of the outer mouth of a K^+ channel during gating. *Neuron*, 16(4):859–867, Apr. 1996.

[94] S. B. Long, E. B. Campbell, and R. MacKinnon. Crystal structure of a mammalian voltage-dependent shaker family K^+ channel. *Science*, 309(5736):897–903, May 2005.

[95] S. B. Long, X. Tao, E. B. Campbell, and R. MacKinnon. Atomic structure of a voltage-dependent K^+ channel in a lipid membrane-like environment. *Nature*, 450(7168):376–382, Nov. 2007.

[96] H. Luecke. Structure of bacteriorhodopsin at 1.55 A resolution. *Journal of Molecular Biology*, 291(4):899–911, Aug. 1999.

[97] H. Luecke, B. Schobert, J.-P. Cartailler, H.-T. Richter, A. Rosengarth, R. Needleman, and J. K. Lanyi. Coupling photoisomerization of retinal to directional transport in bacteriorhodopsin1. *Journal of Molecular Biology*, 300 (5):1237–1255, July 2000.

[98] A. D. Mackerell. Empirical force fields for biological macromolecules: Overview and issues. *Journal of Computational Chemistry*, 25(13):1584–1604, Oct. 2004.

[99] A. D. MacKerell, J. Wiorkiewicz-Kuczera, and M. Karplus. An all-atom empirical energy function for the simulation of nucleic acids. *Journal of the American Chemical Society*, 117(48):11946–11975, Dec. 1995.

[100] A. D. MacKerell, D. Bashford, Bellott, R. L. Dunbrack, J. D. Evanseck, M. J. Field, S. Fischer, J. Gao, H. Guo, S. Ha, D. Joseph-McCarthy, L. Kuchnir, K. Kuczera, F. T. K. Lau, C. Mattos, S. Michnick, T. Ngo, D. T. Nguyen, B. Prodhom, W. E. Reiher, B. Roux, M. Schlenkrich, J. C. Smith, R. Stote, J. Straub, M. Watanabe, J. Wiórkiewicz-Kuczera, D. Yin, and M. Karplus. All-atom empirical potential for molecular modeling and dynamics studies of proteins. *The Journal of Physical Chemistry B*, 102(18):3586–3616, Apr. 1998.

[101] C. Maffeo, S. Bhattacharya, J. Yoo, D. Wells, and A. Aksimentiev. Modeling and simulation of ion channels. *Chemical Reviews*, 112(12):6250–6284, Dec. 2012.

[102] S. Mall, R. Broadbridge, R. P. Sharma, A. G. Lee, and J. M. East. Effects of aromatic residues at the ends of transmembrane alpha-helices on helix interactions with lipid bilayers. *Biochemistry*, 39(8):2071–2078, Feb. 2000.

[103] A. B. Mamonov, M. G. Kurnikova, and R. D. Coalson. Diffusion constant of K^+ inside gramicidin a: A comparative study of four computational methods. *Ion Hydration Special Issue*, 124(3):268–278, Dec. 2006.

[104] E. J. Mapes and M. F. Schumaker. Framework models of ion permeation through membrane channels and the generalized KingâĂŞAltman method. *Bulletin of Mathematical Biology*, 68(7):1429–1460, Oct. 2006.

[105] P. Marius, M. R. R. de Planque, and P. T. F. Williamson. Probing the interaction of lipids with the non-annular binding sites of the potassium channel KcsA by magic-angle spinning NMR. *Biochimica et Biophysica Acta (BBA) - Biomembranes*, 1818(1):90–96, Jan. 2012.

[106] G. V. Miloshevsky and P. C. Jordan. Conformational changes in the selectivity filter of the open-state KcsA channel: An energy minimization study. *Biophysical Journal*, 95:3239–3251, Oct. 2008.

[107] J. H. Morais-Cabral, Y. Zhou, and R. MacKinnon. Energetic optimization of ion conduction rate by the K^+ selectivity filter. *Nature*, 414(6859):37–42, Nov. 2001.

[108] L. J. Mullins. An analysis of conductance changes in squid axon. *The Journal of General Physiology*, 42(5):1013–1035, May 1959.

[109] M. Mustafa, D. J. Henderson, and D. D. Busath. Computational studies of gramicidin permeation: An entryway sulfonate enhances cation occupancy at entry sites. *Biochimica et Biophysica Acta (BBA) - Biomembranes*, 1788(6): 1404–1412, June 2009.

[110] C. M. Nimigean and T. W. Allen. Origins of ion selectivity in potassium channels from the perspective of channel block. *The Journal of General Physiology*, 137(5):405–413, Jan. 2011.

[111] C. M. Nimigean and C. Miller. Na^+ block and permeation in a K^+ channel of known structure. *The Journal of General Physiology*, 120(3):323–335, Sept. 2002.

[112] S. Y. Noskov, S. Bernèche, and B. Roux. Control of ion selectivity in potassium channels by electrostatic and dynamic properties of carbonyl ligands. *Nature*, 431(7010):830–834, Oct. 2004.

[113] R. A. Noulty and D. G. Leaist. Activity coefficients and diffusion coefficients of dilute aqueous solutions of lithium, sodium, and potassium hydroxides. *Journal of Solution Chemistry*, 13(11):767–778, Nov. 1984.

[114] E. M. Ogielska, W. N. Zagotta, T. Hoshi, S. H. Heinemann, J. Haab, and R. W. Aldrich. Cooperative subunit interactions in c-type inactivation of k channels. *Biophysical journal*, 69(6):2449–2457, Dec. 1995.

[115] C. Oostenbrink, A. Villa, A. E. Mark, and W. F. Van Gunsteren. A biomolecular force field based on the free enthalpy of hydration and solvation: The GROMOS force-field parameter sets 53A5 and 53A6. *Journal of Computational Chemistry*, 25(13):1656–1676, Oct. 2004.

[116] G. Panyi, Z. Sheng, and C. Deutsch. C-type inactivation of a voltage-gated K^+ channel occurs by a cooperative mechanism. *Biophysical journal*, 69(3): 896–903, Sept. 1995.

[117] S. Patel, A. D. Mackerell, and C. L. Brooks. Charmm fluctuating charge force field for proteins: Ii protein/solvent properties from molecular dynamics simulations using a nonadditive electrostatic model. *Journal of Computational Chemistry*, 25(12):1504–1514, 2004.

[118] J. Payandeh, T. Scheuer, N. Zheng, and W. A. Catterall. The crystal structure of a voltage-gated sodium channel. *Nature*, 475(7356):353–358, July 2011.

[119] E. Perozo, C. D. Marien, and L. G. Cuello. Structural rearrangements underlying K^+-channel activation gating. *Science*, 285(5424):73–78, July 1999.

[120] J. C. Phillips, R. Braun, W. Wang, J. Gumbart, E. Tajkhorshid, E. Villa, C. Chipot, R. D. Skeel, L. Kalé, and K. Schulten. Scalable molecular dynamics with NAMD. *Journal of Computational Chemistry*, 26(16):1781–1802, Dec. 2005.

[121] E. Piccinini, M. Ceccarelli, F. Affinito, R. Brunetti, and C. Jacoboni. Biased molecular simulations for free-energy mapping:Âă a comparison on the KcsA channel as a test case. *Journal of Chemical Theory and Computation*, 4(1): 173–183, Jan. 2008.

[122] R Core Team. *R: A Language and Environment for Statistical Computing*. R Foundation for Statistical Computing, Vienna, Austria, 2013. URL http://www.R-project.org.

[123] H. Risken. *The Fokker-Planck Equation*, volume 18 of *Springer Series in Synergetics*. Springer Berlin Heidelberg, Jan. 1996.

[124] M. A. Rogawski and W. Löscher. The neurobiology of antiepileptic drugs. *Nature Reviews Neuroscience*, 5(7):553–564, July 2004.

[125] D. Rotem, A. Mason, and H. Bayley. Inactivation of the KcsA potassium channel explored with heterotetramers. *The Journal of General Physiology*, 135(1):29–42, Jan. 2010.

[126] B. Roux. The calculation of the potential of mean force using computer simulations. *Computer Physics Communications*, 91(1-3):275–282, Sept. 1995.

[127] B. Roux. The membrane potential and its representation by a constant electric field in computer simulations. *Biophysical Journal*, 95(9):4205–4216, Nov. 2008.

[128] B. Roux, S. Bernèche, and W. Im. Ion channels, permeation, and electrostatics: Insight into the function of KcsA. *Biochemistry*, 39(44):13295–13306, Nov. 2000.

[129] B. Roux, T. Allen, S. Bernèche, and W. Im. Theoretical and computational models of biological ion channels. *Quarterly Reviews of Biophysics*, 37 (01):15–103, 2004.

[130] B. Roux, S. Bernèche, B. Egwolf, B. Lev, S. Y. Noskov, C. N. Rowley, and H. Yu. Ion selectivity in channels and transporters. *The Journal of General Physiology*, 137(5):415–426, Jan. 2011.

[131] C. N. Rowley and B. Roux. A computational study of barium blockades in the KcsA potassium channel based on multi-ion potential of mean force calculations and free energy perturbation. *The Journal of General Physiology*, 142 (4):451–463, Jan. 2013.

[132] M. S. Sansom, I. H. Shrivastava, J. N. Bright, J. Tate, C. E. Capener, and P. C. Biggin. Potassium channels: structures, models, simulations. *Biochimica et Biophysica Acta (BBA) - Biomembranes*, 1565(2):294–307, Oct. 2002.

[133] M. Schumaker and R. MacKinnon. A simple model for multi-ion permeation. single-vacancy conduction in a simple pore model. *Biophysical Journal*, 58(4): 975–984, Oct. 1990.

[134] I. H. Shrivastava and M. S. P. Sansom. Simulations of ion permeation through a potassium channel: Molecular dynamics of KcsA in a phospholipid bilayer. *Biophysical Journal*, 78(2):557–570, Feb. 2000.

[135] I. H. Shrivastava, D. Peter Tieleman, P. C. Biggin, and M. S. P. Sansom. K^+ versus Na^+ ions in a k channel selectivity filter: A simulation study. *Biophysical Journal*, 83(2):633–645, Aug. 2002.

[136] J. G. Starkus, L. Kuschel, M. D. Rayner, and S. H. Heinemann. Ion conduction through c-type inactivated shaker channels. *The Journal of General Physiology*, 110(5):539–550, Jan. 1997.

[137] L. Sutto, S. Marsili, and F. L. Gervasio. New advances in metadynamics. *Wiley Interdisciplinary Reviews: Computational Molecular Science*, 2(5):771–779, 2012.

[138] K. Takeuchi, H. Takahashi, S. Kawano, and I. Shimada. Identification and characterization of the slowly exchanging pH-dependent conformational rearrangement in KcsA. *Journal of Biological Chemistry*, 282(20):15179 –15186, May 2007.

[139] C. Tasserit, A. Koutsioubas, D. Lairez, G. Zalczer, and M.-C. Clochard. Pink noise of ionic conductance through single artificial nanopores revisited. *Physical Review Letters*, 105:260602, Dec 2010.

[140] A. N. Thompson, D. J. Posson, P. V. Parsa, and C. M. Nimigean. Molecular mechanism of pH sensing in KcsA potassium channels. *Proceedings of the National Academy of Sciences*, 105(19):6900–6905, May 2008.

[141] A. N. Thompson, I. Kim, T. D. Panosian, T. M. Iverson, T. W. Allen, and C. M. Nimigean. Mechanism of potassium-channel selectivity revealed by Na^+ and li^+ binding sites within the KcsA pore. *Nature Structural & Molecular Biology*, 16(12):1317–1324, Nov. 2009.

[142] D. Tieleman, S. Marrink, and H. Berendsen. A computer perspective of membranes: molecular dynamics studies of lipid bilayer systems. *Biochimica et Biophysica Acta (BBA) - Reviews on Biomembranes*, 1331(3):235–270, Nov. 1997.

[143] G. A. Tribello, M. Ceriotti, and M. Parrinello. A self-learning algorithm for biased molecular dynamics. *Proceedings of the National Academy of Sciences*, 107(41):17509 –17514, Oct. 2010.

[144] G. A. Tribello, M. Ceriotti, and M. Parrinello. Using sketch-map coordinates to analyze and bias molecular dynamics simulations. *Proceedings of the National Academy of Sciences*, 109(14):5196–5201, Mar. 2012.

[145] M. Tuckerman, B. J. Berne, and G. J. Martyna. Reversible multiple time scale molecular dynamics. *The Journal of Chemical Physics*, 97(3):1990–2001, 1992.

[146] S. Uysal, V. Vasquez, V. Tereshko, K. Esaki, F. A. Fellouse, S. S. Sidhu, S. Koide, E. Perozo, and A. Kossiakoff. Crystal structure of full-length KcsA in its closed conformation. *Proceedings of the National Academy of Sciences*, 106(16):6644–6649, Apr. 2009.

[147] S. Uysal, L. G. Cuello, D. M. Cortes, S. Koide, A. A. Kossiakoff, and E. Perozo. Mechanism of activation gating in the full-length KcsA K^+ channel. *Proceedings of the National Academy of Sciences of the United States of America*, 108 (29):11896–11899, July 2011.

[148] H. Wickham. *ggplot2: elegant graphics for data analysis*. Springer New York, 2009.

[149] W. Wojtas-Niziurski, Y. Meng, B. Roux, and S. Bernèche. Self-learning adaptive umbrella sampling method for the determination of free energy landscapes in multiple dimensions. *Journal of Chemical Theory and Computation*, 9(4): 1885–1895, Mar. 2013.

[150] G. Yellen. The voltage-gated potassium channels and their relatives. *Nature*, 419(6902):35–42, Sept. 2002.

[151] G. Yellen, D. Sodickson, T. Y. Chen, and M. E. Jurman. An engineered cysteine in the external mouth of a K^+ channel allows inactivation to be modulated by metal binding. *Biophysical Journal*, 66(4):1068–1075, Apr. 1994.

[152] L. Zhang and J. Hermans. Hydrophilicity of cavities in proteins. *Proteins: Structure, Function, and Bioinformatics*, 24(4):433–438, Apr. 1996.

[153] Y. Zhang and G. A. Voth. Combined metadynamics and umbrella sampling method for the calculation of ion permeation free energy profiles. *Journal of Chemical Theory and Computation*, 7(7):2277–2283, July 2011.

[154] M. Zhou and R. MacKinnon. A mutant KcsA K^+ channel with altered conduction properties and selectivity filter ion distribution. *Journal of Molecular Biology*, 338(4):839–846, May 2004.

[155] M. Zhou, J. H. Morais-Cabral, S. Mann, and R. MacKinnon. Potassium channel receptor site for the inactivation gate and quaternary amine inhibitors. *Nature*, 411(6838):657–661, June 2001.

[156] Y. Zhou and R. MacKinnon. The occupancy of ions in the K^+ selectivity filter: Charge balance and coupling of ion binding to a protein conformational change underlie high conduction rates. *Journal of Molecular Biology*, 333(5):965–975, Nov. 2003.

[157] Y. Zhou, J. H. Morais-Cabral, A. Kaufman, and R. MacKinnon. Chemistry of ion coordination and hydration revealed by a K^+ channel-fab complex at 2.0 A resolution. *Nature*, 414(6859):43–48, Nov. 2001.

[158] X. Zhu, P. E. M. Lopes, and A. D. MacKerell. Recent developments and applications of the charmm force fields. *Wiley Interdisciplinary Reviews: Computational Molecular Science*, 2(1):167–185, 2012.